Destabilization of lithium borohydride with additions of magnesium hydride

UNIVERSITY OF BIRMINGHAM

By

David Brampton

A thesis submitted to the University of Birmingham
for the degree of Master of Research (MRes)

Supervisor: Dr David Book

Metallurgy and Materials
School of Engineering
The University of Birmingham
2008

Contents **Page No.**

1. Introduction

As the world population continues to grow and the world's developing nations become more and more industrialised, the global energy demand is rapidly increasing. The International Energy Agency (IEA) has predicted that the world's energy demand will increase by approximately 60% between 2002 and 2030, reaching the equivalent of 16.5 billion tonnes of oil by the end of this period [1]. The projected rise in fuel use is illustrated below, but the projected rate of increase used in this model is 1.7%, which is less than the 2% increase which has actually been observed over the past three decades.

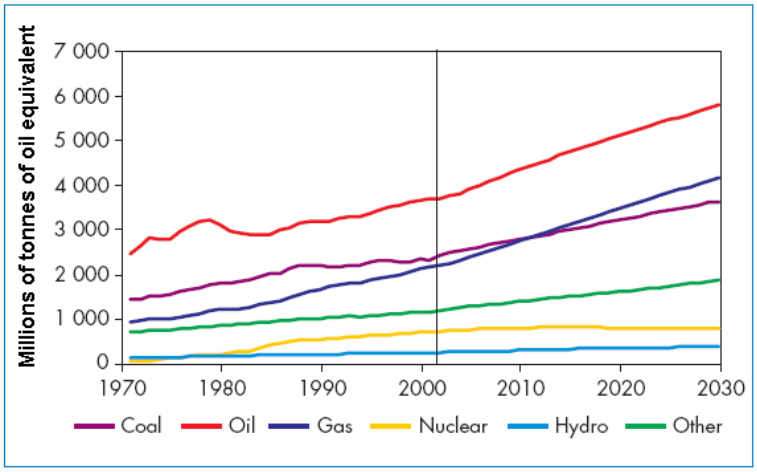

Figure 1) IEA Projected increase in energy demand from 2002 to 2030 by fuel [1]

This increase in energy consumption is accompanied by a need for more efficient, cleaner energy sources because our primary energy source (fossil fuels) can be both socially and environmentally damaging. Some countries have access to larger reserves of fossil fuels than others. Countries with smaller fossil fuel reserves will become more dependent on others as energy reserves begin to become depleted and fossil fuels become an increasingly scarce commodity. An important environmental concern of using fossil fuels is their carbon content, which upon combustion is released into the

atmosphere in the form of gases which include carbon dioxide (CO_2). Increased levels of atmospheric CO_2 are linked to increases in global temperature so high levels of this gas are highly undesirable. A warming effect has also been observed locally in recent years, with a sharp rise in average temperature anomalies occurring in central England since the 1990's (Figure 2) [2]. If fossil fuels maintain an 81% stronghold over our total primary energy supply, then CO_2 emissions are estimated to reach 40.4 Gt CO_2 / yr by 2030 [3]. This will bring further increases to the global temperature resulting in devastating effects to the whole ecosystem.

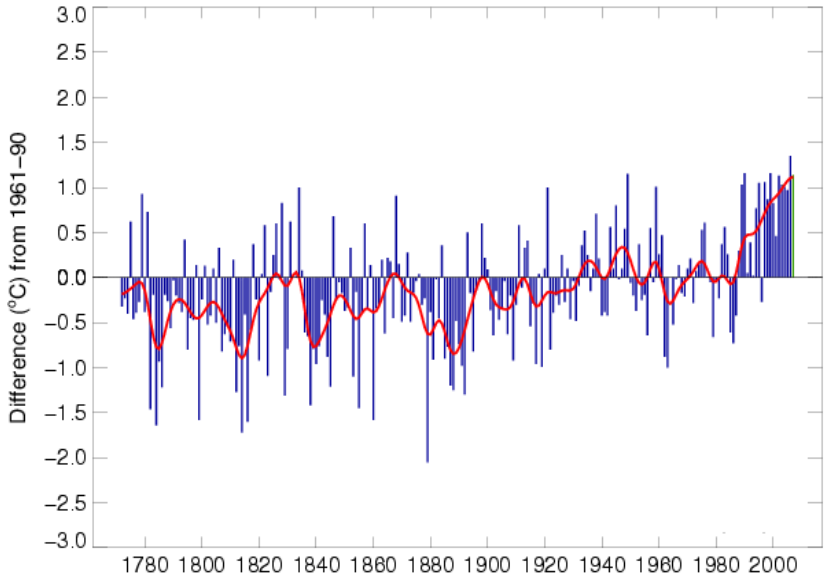

Figure 2) Mean Central England Temperature Anomalies from the Met Office [2]

These issues of environmental damage and energy security can be overcome with the use of cleaner and more sustainable energy technologies. Sustainable technologies utilise renewable energy sources such as wind [4], solar energy [5] and marine / wave energy [6]. Although these technologies allow for "in house" energy production, which would relieve some dependence upon foreign energy markets and pose less environmental damage than fossil fuels, they are not without problems. Firstly the

renewable resource (wind, sun or wave energy) must be abundantly present. Solar panels for instance would be of limited use to a country that did not see much sunlight. Other difficulties associated with sustainable energy technologies such as wind and solar energy, are they often require large areas of land and produce power intermittently. This sporadic production of energy is a significant problem because sometimes more energy will be produced than is actually required by the grid and at other times less. If sustainable energies were used to satisfy our energy requirements then any surplus energy produced would have to be stored and one method proposed for achieving this is with hydrogen. This would be done by using excess energy to produce hydrogen storing it chemically for times of high energy demand, but the efficiencies of storing energy in this way have caused great debate regarding its practicality.

Depending on its method of production hydrogen is a very environmentally friendly fuel when compared to fossil fuels, producing only water as a product of combustion. This property gives hydrogen a large application potential in the automotive industry where large quantities of CO_2 are produced each year as a result of combusting fossil fuels to support our transportation needs. A transition from combusting fossil fuels to using hydrogen in the modern automobile would therefore be a significant step in reducing anthropogenic global warming.

2. Literature Review

2.1 Hydrogen as an energy carrier

Hydrogen (H_2) has a lot of potential as a future energy carrier possessing 142 MJ of energy per kg compared to 47 MJ / kg for fossil fuels [7]. Unfortunately H_2 is not found as a free element on earth but is instead locked into compounds from which it must first be removed. Steam reforming hydrocarbons [8], [9] is one way of obtaining large volumes of hydrogen but unfortunately this produces carbon dioxide as a by-product due to the carbon content of the starting materials (equation 1 and 2).

$$C_x H_Y + 2x\ H_2O \rightarrow x\ CO_2 + (2x + \tfrac{1}{2}y)\ H_2 \qquad (1)$$

$$CH_4 + 2H_2O \rightarrow CO_2 + 4H_2 \qquad (2)$$

Other methods of hydrogen production include electrolysis [10] and thermochemical splitting of water [11] which both use, non-carbon based starting materials, reducing the amount of CO_2 released as a consequence of hydrogen production. The energy which has been used to create elemental hydrogen is now stored within this gas as chemical energy which must be retrievable again in order for it to become an efficient energy carrier. The chemical energy stored within hydrogen can be retrieved using a fuel cell or via combustion in a modified internal combustion engine.

Fuel cells recombine hydrogen and oxygen to create water and electrical energy, basically working on the opposite principal to an electrolyser. They are also relatively

simple in design with very few moving parts, and with only water and electricity as products of the reaction.

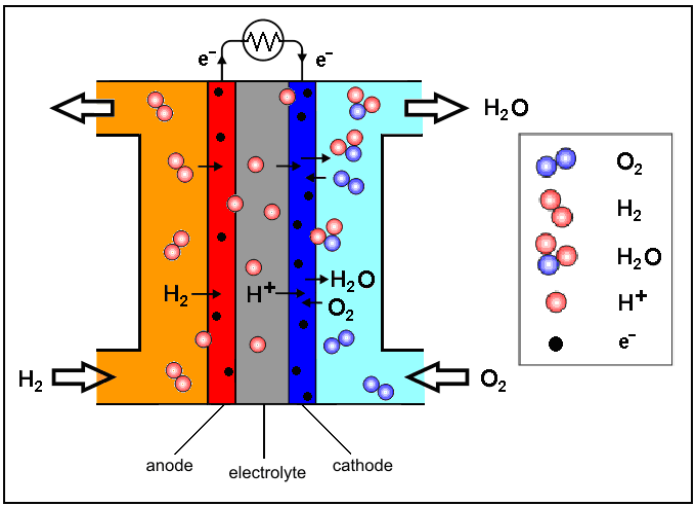

Figure 3) Schematic of a fuel cell converting H_2 and O_2 into electrical energy

$$\text{Anode:} \quad 2H_2 \rightarrow 4H^+ + 4e^- \qquad (3)$$

$$\text{Cathode:} \quad 4e^- + O_2 \rightarrow 2O^{2-} \qquad (4)$$

$$\text{Overall:} \quad 2H_2 + O_2 \rightarrow 2H_2O \qquad (5)$$

Table 1 highlights a few applications for which proton exchange membrane fuel cells (PEMFC's) can be employed due to the benefit of their quick start up times coupled with their relatively low operating temperatures and pressures [12], [13], [14]. A fuel cell powered bike for instance operated with a cell stack surface temperature of 40ºC and employed pressures of 1.5 and 1.2 bar on the hydrogen and oxygen sides of the cell respectively [13]. Higher temperatures can be used to run these fuel cells, as demonstrated by a hybrid powered bus which ran on a fuel cell operating between 50ºC and 75ºC whilst using a pressure of 1.3 bar on the air side of the cell and a 1.5 bar pressure on the hydrogen side of the cell [12]. The operating temperature of a PEMFC can depend largely on the membrane used to separate the two sides of the cell. The

standard membranes currently employed within PEMFC's, are sulfonated perfluoropolymer membranes such as Nafion whose proton conductivity is proportional to its degree of hydration [15]. If too high a temperature is used when operating a PEMFC then the proton exchange membrane may become dehydrated, reducing the efficiency of the stack and ultimately leading to the cells failure.

Application	Power (kW)	H_2 Storage Option
Hybrid Powered Bus [12]	50	Compressed Hydrogen
Powered Bicycle [13]	0.3	Metal Hydride
Stationary Generator [14]	5	Compressed Hydrogen

Table 1) Application tests on PEMFC's highlighting their electrical efficiencies

Hydrogen fuelled internal combustion engines (HICE) can also be used to convert the chemical energy of hydrogen to useful work. Like a fuel cell the only product produced by combusting hydrogen is water, but if the oxygen for this reaction is supplied from the air then nitrogen oxides (NO_x) can also be created. These nitrogen oxides can cause an acid rain effect when they react with water in our atmosphere [16] but measures can be taken to avoid their production. Reducing the operating temperature of a hydrogen engine or by supplying only pure oxygen will minimise these harmful emissions. Supplying pure oxygen to a combustion engine however places additional costs to the system and also takes up additional storage space within the vehicle, so ideally oxygen from the air would be used instead of this option. An advantage combustion engines have over fuel cells however is they're already a well established technology within the automotive industry and hydrogen could be slowly integrated into this field to ease the transition from one fuel type to another. Hydrogen can be combined directly with petrol and a proportion of ethanol to alter both the engine performance and its emission of

pollutants. A study using a mixture of hydrogen (4%), Ethanol (30%) and Petrol (66%) in a four stroke, single cylinder engine was observed reducing both the CO_2 output and the specific fuel consumption of the engine by 49% [17]. The use of petrol and ethanol is still highly undesirable due to their carbon content and issues regarding their sustainability but shows that there is more than one option for the use of hydrogen within internal combustion engines.

2.2 Hydrogen Storage

A major problem faced by both fuel cells and HICE technologies is to store enough hydrogen on board, so that hydrogen-powered vehicles can compete with the performance and cost of current petrol-ICE vehicles. The problems associated with hydrogen storage become more evident when we look at the volumes required to store fossil fuels compared to hydrogen. A kilogram of hydrogen contains 142 MJ of energy and at ambient temperature and pressure this amount of gas requires a volume of $11m^3$. Due to its lower energy density, to store 142 MJ of energy with petrol requires 3 kg of this fuel which would take up just 4 litres (~ 4×10^{-3} m^3) of the fuel tank [18]. This large volume requirement for hydrogen results in a poor volumetric density (kg H_2 / m^3) and in order to increase this density the molecules that make up the gas must be packed together more closely.

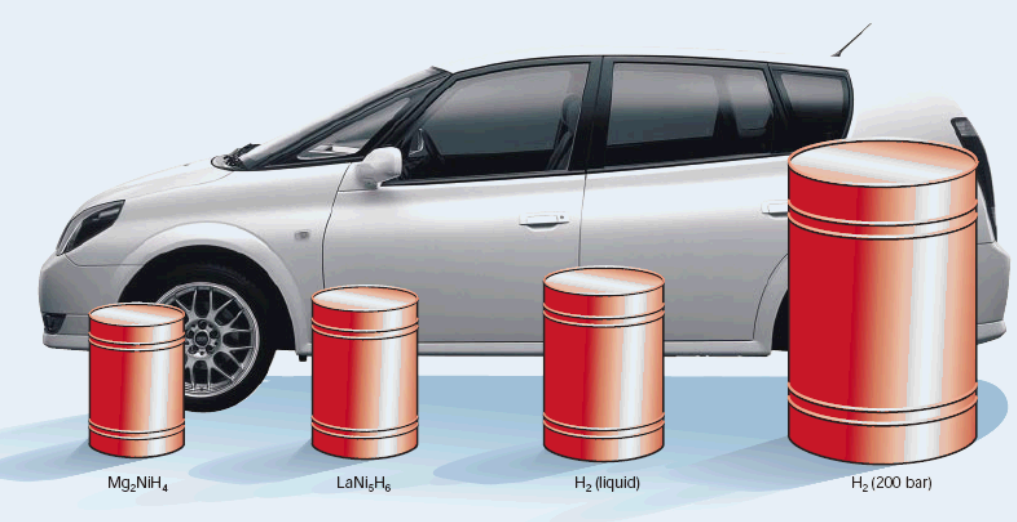

Figure 4) Relative volume for 4 kg of H_2 stored as a gas (200 bar), cryogenic liquid and in a solid state using $LaNi_5H_6$ and Mg_2NiH_4 compared to a family sized Toyota [19]

Decreasing the volume of hydrogen can be achieved in a number of ways, such as through extremely high compression of the gas or even chemically binding it with other elements in order to create an effective solid state hydrogen store. Figure 4 shows four examples of how researchers have tried to reduce this volumetric issue and how solid state stores are the most effective. The problem that arises from storing hydrogen within solids however is that although they now allow for more hydrogen to be stored by volume the weight of these materials used severely decreases the gravimetric density of the system (kg H_2 / kg system or wt% H_2). Because both the mass and volume of hydrogen storage systems are important considerations to be taken into account, the U.S Department of Energy (DOE) have set industry desired targets for both of these densities. The targets for 2007, 2010 and 2015 are shown in Table 2 [20].

Storage Parameter	Units	2007	2010	2015
Gravimetric Capacity	wt%	4.5	6	9
Volumetric Capacity	kg H_2 / m^3	36	45	81

Table 2) Hydrogen storage system targets set by the US DOE

Other variables to consider when gauging the potential of a hydrogen store include:

- Its operation within a suitable temperature and pressure range
- The reversibility of the store and its resistance to degradation after repeated cycling
- The possession of good reaction kinetics for both the dehydrogenation and recombination process
- Provide a high purity of hydrogen to prevent possible poisoning of PEM fuel cells
- Economic viability of the system

There are a number of materials under investigation today, some of which can satisfy a number of the above criteria but fail regarding others. The method employed for storing hydrogen also depends on the application for which the hydrogen will be used later. Applications which use hydrogen stored on site in large static units for example will place more emphasis on the initial cost, long term maintenance and efficiency of the store rather than the size and mass of the unit. When hydrogen fuelled transportation is considered however the volume and mass of the store becomes much more important than it does for a static store scenario.

2.2.1 Compressed Gas

Compressed hydrogen gas is currently the most commonly employed storage method for automotive applications, and involves holding hydrogen at high pressures in carefully engineered pressure vessels. These tanks must be as light as possible but at the same time strong enough to withstand the internal forces exerted on the walls of the vessel by the high pressure hydrogen. The materials employed must also be resistant to hydrogen absorption firstly to prevent any leakage of hydrogen and secondly because the introduction of hydrogen to materials can cause embrittlement (also known as hydrogen assisted cracking) [21]. Hydrogen tanks should also be thermally insulated to prevent any heat transfer to the hydrogen as this will create a pressure increase, which in turn increases the stresses exerted on the walls of the tank.

Advances in this field of hydrogen storage came with breakthroughs using composite materials which have allowed for stronger, lighter pressure tanks to be produced capable of supporting much greater pressures. Honda, a leading car manufacturer, has produced a fuel cell vehicle (Honda ZC1 FCX) in 2002 which used compressed hydrogen stored in high pressure tanks. These tanks are constructed from an inner layer of aluminium, a carbon fibre layer and an outside glass fibre material resistant to impacts and corrosion. The storage tank had a total mass of 56.91 kg and is capable of holding 3.75 kg of hydrogen in 157 litres (6.2 wt%, ~24 kg H_2 / m^3) of space at 5000 psi (≈350 bar), which gives the vehicle a driving range of approximately 355 km [22]. Using hydrogen in its gaseous state means it can be delivered for conversion to power with relative ease, just releasing hydrogen from the tank with the necessary equipment as and when it is needed.

2.2.2 Cryogenic Liquid H_2

Liquid hydrogen can be used in order to increase the volumetric density of hydrogen stored in vehicles but still has a rather low gravimetric density (70.8 kg / m^3). Challenges associated with using liquid hydrogen include lowering the energy required to get hydrogen into its liquid form and boil-off which occurs when liquid hydrogen absorbs heat from its surroundings.

Hydrogen is typically liquefied using the Joule – Thomson cycle which compresses hydrogen gas, cools it with a heat exchanger and then expands the gas rapidly to create liquid hydrogen. The liquefaction of hydrogen consumes approximately 30% of its heating value, creating a huge energy cost to this type of storage system [23]. Boil-off occurs due to hydrogen's low critical temperature (33 K), above which no liquid phase exists and is the reason why liquid hydrogen storage vessels must be open and isolated from any external heat. When liquid hydrogen absorbs heat from its surroundings a build up of pressure is created within the storage vessel. If this pressure build up becomes too much the stresses placed on the walls of the storage tank would result in failure. This can be prevented by venting some of the gaseous hydrogen formed during heat transfer to the atmosphere in order to reduce the pressure inside of the vessel. This is highly undesirable especially if a car is left parked in the sun for a long period. The problem of boil off can be minimised by surrounding the pressure vessel with insulation with the hope of maintaining a temperature below that of hydrogen's boiling point (20 K) [23]. It is due to this existing problem of boil-off, that liquid hydrogen is generally used in applications where the fuel will be used quickly and not stand idle for very long. Unfortunately cars are sometimes left standing idle for a number of days, and even weeks if the owner was to take a vacation. High-rise car parks would also

encounter problems with this type of storage option because if lots of vehicles were to vent their hydrogen on a hot day, a large build up of the explosive gas could occur posing a risk to the general public.

2.2.3 Hydrolysis / Alcoholysis Reactions

A number of solid state compounds will release hydrogen as a product of reaction when combined with water and one strong candidate for this type of system is sodium borohydride ($NaBH_4$). $NaBH_4$ is capable of supplying a high wt% of H_2, even when the mass of the water is taken into account. Highly alkaline solutions of $NaBH_4$ are quite stable and will release almost no hydrogen when left in this state, however when this highly alkaline solution comes into contact with a catalyst (such as ruthenium [24]) it will then liberate appreciable quantities of hydrogen (equation 6).

$$NaBH_4 + 2H_2O \rightarrow NaBO_2 + 4H_2 \qquad (6)$$

Unfortunately this reaction is not reversible, which means refuelling a vehicle run on this type of system would mean replacing the entire fuel tank to replenish both the borohydride fuel and the water used. A significant disadvantage in using water in a fuel system is during the winter months or in places of extreme cold, the water may freeze. This can be overcome by replacing water with ethylene glycol ($C_2H_4(OH)_2$) which is commonly used in antifreeze and is readily reduced by $NaBH_4$. However this transition to alcoholysis has a penalty in the form of a reduction to the gravimetric density of the system. The alcoholysis reaction proceeds as follows [24].

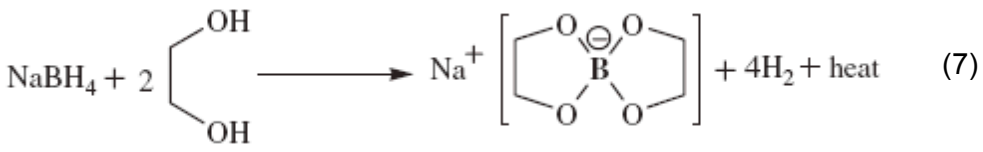

(7)

Even pure metals such as lithium, sodium and potassium have the ability to strip water of its hydrogen, but all of these materials fail to meet the readily reversible criteria required for an economically viable hydrogen store. One more aspect of these reactions which must be considered is that they are highly exothermic, evolving large quantities of heat as they proceed. To prevent any overheating which may occur some level of heat transfer technology will be needed and will inevitably add mass to the overall system reducing its gravimetric density.

2.2.4 Porous Storage Materials

Another method of storing hydrogen involves placing hydrogen onto the surface of materials which have very high surface areas per unit weight, either by physisorption or chemisorption. The difference between these two techniques is that physisorption involves hydrogen bonding to the surface of a solid via weak van der Waal's forces, while for chemisorption hydrogen is secured to a surface with much stronger chemical bonds. Physisorption is the preferred mechanism because van der Waals forces are more easily broken than the stronger chemical bonds formed by chemisorption, giving rise to lower dehydrogenation temperatures. Although the use of van der Waals forces is more desirable than the use of chemisorption, these forces are too weak for practical application at room temperature, requiring liquid nitrogen temperatures in order to keep the hydrogen on the surface.

B. Panella et al. have studied a number of carbon materials which included activated carbon with a surface area of 2564 m^2 / g and single walled nanotubes with a surface area of 124 m^2 / g. Their analysis of these materials found that high porosity activated carbon possessed the highest gravimetric densities. Activated carbon which had been prepared in Canada held the most amount of hydrogen, storing 4.5 wt% H_2 at 77 K. The highest adsorption figure observed at room temperature for these materials however was less than 1 wt% H_2 even at very high hydrogen pressures [25].

Zeolites are another group of materials under study for this type of hydrogen storage and are found occurring naturally, but can also be synthesised in a lab to create various novel structures. They store hydrogen reversibly within cavities created chemically throughout the structure of these materials. Control over the size of these cavities is achieved by exchanging cations which occupy certain sites within the zeolite framework, with others cations from the alkali and alkali earth metal groups [25]. The results obtained by Langmi et al. concluded that zeolite X with Ca^{2+} exchange replacing Si or Al at the cation sites was capable of storing 2.19 wt% H_2 (31 kg of H_2 / m^3) at 77 K and 15 bar of hydrogen [26].

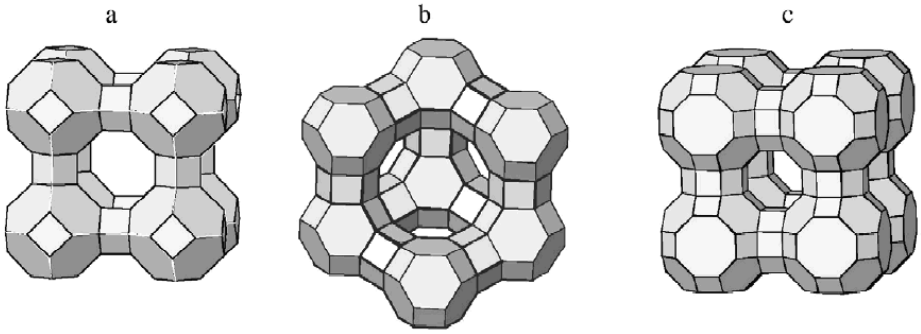

Figure 5) Zeolite structures: (a) A, (b) X and Y, (c) Rho. The corners represent Si or Al and these are linked by oxygen bridges represented by the lines on the frameworks[26]

Metal organic frameworks (MOF's) such as that in Figure 6, consist of metal atoms bridged together with organic ligands and have also received a lot of interest recently. The adsorption figures calculated for MOF-5 revealed a storage capacity of 4 wt% H_2 at 77K under 15 bar of H_2 [27], [28].

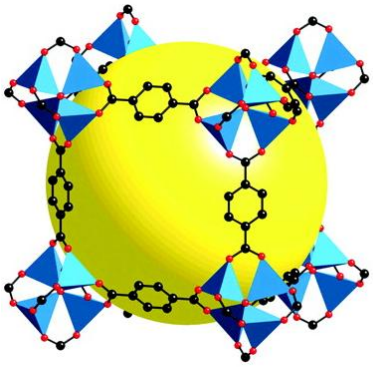

Figure 6) Each corner is a $[OZn_4(CO_2)_6]$ cluster which is bridged by six carboxylate groups. (Zn, blue polyhedron; O, red spheres; C, black spheres). The large yellow sphere in the middle of the picture indicates the volume of the cavity [28].

In spite of their lower than desired storage densities, porous materials will continue to be a highly researched storage option due a number of factors which include

- Porous materials operate at relatively low pressures
- They possess relatively rapid sorption kinetics when compared to other means of storing hydrogen
- Their low cost of manufacture
- And the degree of control that can be exercised over their structure

2.2.5 Hydrides

Hydrides come in many forms ranging from metallic elements which can interstitially store hydrogen within their metallic lattice e.g. ($PdH_{0.6}$), to those which chemically react

with hydrogen e.g. (CH_4). The advantage of packing hydrogen within metals is that it allows the hydrogen atoms to be stored much closer together than they would in their molecular form as a compressed gas or as a liquid. This closer packing results in higher volumetric hydrogen storage densities (as shown in terms of the y-axis of Figure 7).

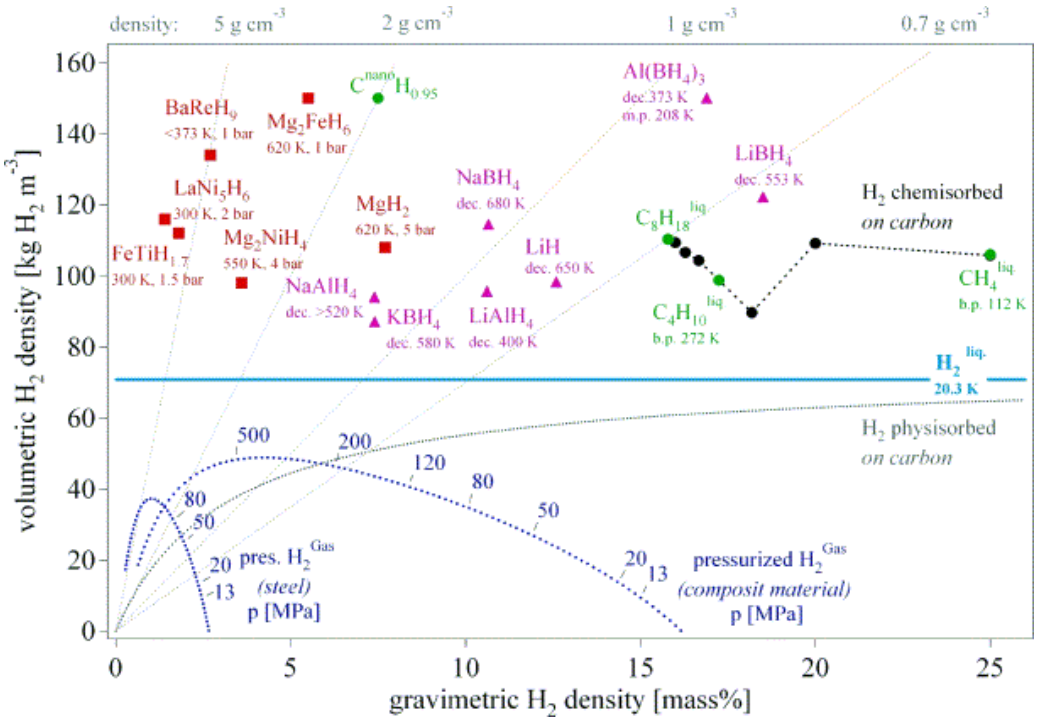

Figure 7) Hydrogen storage media plotted using their gravimetric (wt%) and volumetric storage (kg H_2 / m^3) densities [29]

Utilizing certain metals for hydrogen storage becomes problematic when we consider their mass. Metals can be relatively heavy which is undesirable for hydrogen storage applications because it results in poor gravimetric storage densities. The cost of certain metals can also hinder their economical practicalities for use as hydrogen storage materials. Researchers have therefore explored using light, inexpensive metals such as magnesium, which is capable of storing 7.6 wt% H_2 when converted to MgH_2. Despite its adequate storage density, MgH_2 is not widely used as a hydrogen store due its high

stability (ΔH_f = -75 kJ / mol) which results in a high dehydrogenation temperature (> 300ºC) [30].

$$MgH_2 \rightarrow Mg + H_2 \quad (8)$$

As received MgH_2 has been observed fully dehydrogenating at a temperature of 350ºC but required a time period of over 3000 seconds to do so [31]. The slow kinetics of this reaction results in dehydrogenation times being too long when large volumes of hydrogen are rapidly required, but the reaction kinetics can be improved with milling. Mechanically ball milling MgH_2 decreases the particle and grain size of the material while increasing the number of grain boundaries. This increased volume in the number of grain boundaries present provides a larger area over which hydrogen can diffuse increasing the likelihood of a reaction. The milling of MgH_2 has been shown to reduce the molar heat capacity of this material, from 156 kJ / mol K for unmilled MgH_2 to 120 kJ / mol K for the milled sample [31]. Reducing the heat capacity of this material means that less energy is required to raise the temperature of one mole of this material by 1 K. This means that the milled material will heat up quicker than the unmilled material for a given amount of energy input which can also affect the materials sorption kinetics. The effect of lowering the heat capacity with milling, reduces the dehydrogenation time of milled MgH_2 to 700 seconds, a significant reduction on the 3000 seconds observed for unmilled MgH_2 [31].

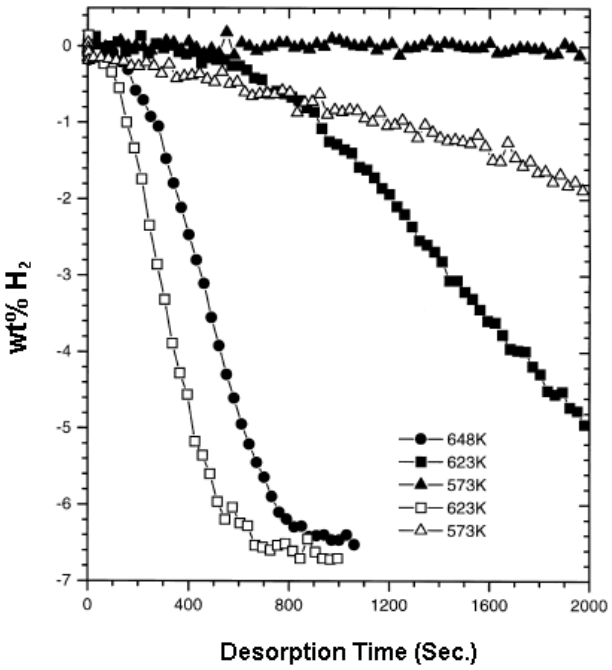

Figure 8) Hydrogen dehydrogenation curves of unmilled MgH_2 (solid marks) and MgH_2 which has been ball milled for 20 hrs (hollow marks) [31]

Catalysis is another method used to increase the sorption kinetics of hydrides. As mentioned above MgH_2 requires temperatures above 300ºC to fully dehydrogenate but this can be improved with catalytic additions. Hanada et al. has mechanically milled just 1 mol% of Nb_2O_5 with MgH_2 to successfully catalyze the sorption kinetics giving a hydrogen release of ~6 wt% H_2 between 200 - 250ºC for this material [32]. After dehydrogenation at 200ºC the catalytic activity of Nb_2O_5 on MgH_2 increased the sorption kinetics of this material to such a degree that the material was observed to hydride in less than 15 seconds with ~4.5 wt% H_2 at room temperature under a hydrogen pressure of 10 bar [32].

Alloying metals together has also been shown to improve the overall hydrogen storage properties compared to the single element hydrides. La and Ni for example can be alloyed together to create a $LaNi_5$ alloy which can rapidly and reversibly absorb and

desorb hydrogen at ambient temperatures. Due to the mass of La and Ni however, $LaNi_5$ is not a viable hydrogen store for mobile applications as it can only hold 1.28 wt% H_2 [33]. A number of alloys are known which will release hydrogen within the temperature range required for use with a fuel cell (Table 3) however their gravimetric densities are too low for practical mobile applications.

Alloy	ΔH (kJ / mol)	Temp. (ºC) for 1atm	Reversible H_2 (wt%)	\$ kg^{-1} of hydride
TiFe	28.1	-8	1.5	4.68
$TiMn_{1.5}$	28.7	-21	1.15	4.99
$ZrFe_{1.5}Cr_{0.5}$	25.6	-10	0.9	10.90
$CaNi_5$	31.9	43	0.99	7.56
$LaNi_5$	30.8	12	1.28	9.87

Table 3) Metallic hydrides dehydrogenating in the range, 1 – 10 atm and 0 - 100ºC [33]

2.2.6 Complex Hydrides

Complex hydrides are mixed ionic - covalent compounds which amongst other groups, contains the alanates (AlH_4^-) and the isostructural borohydrides (BH_4^-). Figure 9 illustrates the bonding found within lithium borohydride revealing that the hydrogen atoms are covalently bound in a tetrahedral fashion around a central metal atom which is then ionically bound to a cation.

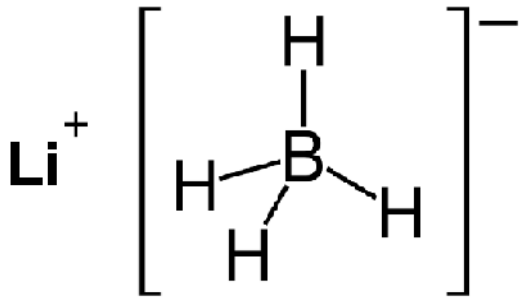

Figure 9) Schematic of a Lithium Borohydride unit

Borohydrides possess greater gravimetric storage densities than their alanate counterparts because boron is a lighter element than aluminium. To demonstrate this more clearly lithium aluminium hydride ($LiAlH_4$) contains 10.5 wt% H_2 but when the Al atom is replaced with B we get 18.5 wt% H_2 stored in lithium borohydride ($LiBH_4$), a significant rise. Au et al. observed commercially produced $LiBH_4$ initially releasing hydrogen at a slow rate around 325ºC, but the kinetics of the reaction greatly increased at 500ºC, and after heating to 600ºC, 9 wt% H_2 had been evolved [34].

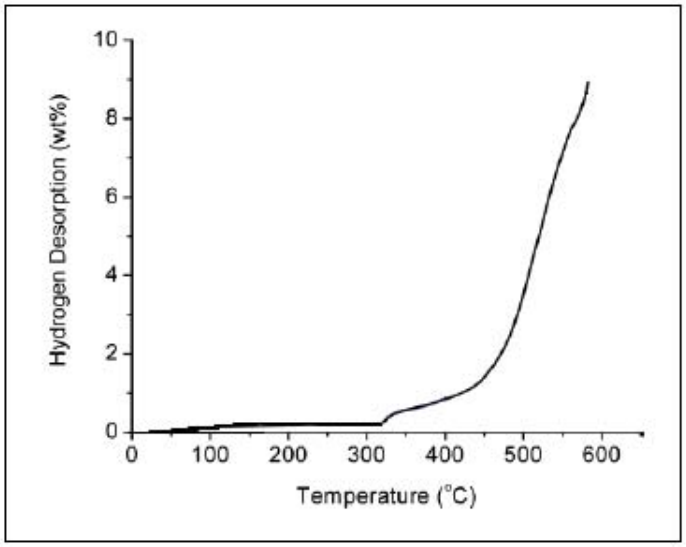

Figure 10) TGA analysis of pure $LiBH_4$ carried out by Au et al [35]. Carried out under vacuum and heated from ambient temperature to 600ºC at 5 ºC / min.

Even above temperatures of 600ºC, some of the 18.5 wt% H_2 available from this compound is retained within the system because lithium hydride is produced as a decomposition product which reduces the storage potential of this material from 18.5 wt% H_2 to 13.8 wt% H_2.

$$LiBH_4 \rightarrow LiH + B + 1½H_2 \qquad (13.8\ wt\%\ H_2) \qquad (9)$$

The US DOE targets (Table 2) are for an entire hydrogen storage system, which includes the vessel used to house the storage medium, the adjoining pipe work and any control systems used within the system such as gas flow controllers and heat management devices. With this in mind even when LiH formation is taken into account and $LiBH_4$'s gravimetric density is reduced to 13.8 wt% H_2, the material still shows great potential for meeting the 2010 US DOE target (6 wt% H_2). The enthalpy of reaction for equation 9 is reported to be 67 kJ / mol H_2 [36] and it is this relatively high enthalpy value that results in its high dehydrogenation temperature. However, different approaches have been used to reduce the dehydrogenation temperature of $LiBH_4$, such as ball milling and the addition of catalysts [34], [35].

As received $LiBH_4$ has also been analysed by Orimo et al. who found that hydrogen dehydrogenation from this material began at approximately 380ºC on TGA equipment, which is slightly higher than that found by Au et al. Orimo et al. also observed more hydrogen being released from this material (14 wt% H_2) than Au et al. but higher temperatures were used during this investigation (630ºC) [37]. DTA data was also obtained by Orimo et al. and revealed four endothermic peaks occurring between, 30 – 630ºC. Two distinct endothermic peaks were observed at 110ºC and 280ºC, which result from the phase change and melting point of this material respectively. The room

temperature crystal structure of this material is orthorhombic (with a Pnma space group) however at approximately 110ºC, contraction occurs along the orthorhombic a direction and an expansion takes place in the b and c direction yielding a hexagonal crystal structure ($P6_3mc$) [38]. Heating past 280ºC produces two more peaks which are superimposed, beginning at approximately 430ºC and 530ºC which are assigned to a loss of hydrogen from this material (Figure 11 below).

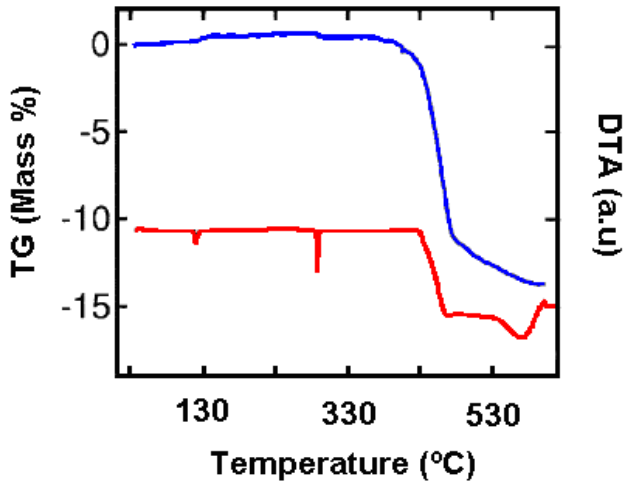

Figure 11) TGA (top) and DTA profile (bottom) of pure $LiBH_4$. Both sets of data were obtained by heating to 630ºC at 5ºC / min under He flowing at 150 ml / min [37]

2.3 Destabilization reactions

Destabilization is different to simply creating new alloys which can reversibly hold hydrogen because the decomposition products of a destabilized system will reversibly react with hydrogen to reform the starting materials used. This technique was first demonstrated in 1967 when Mg_2Cu was reversibly hydrogenated to MgH_2 + $MgCu_2$ [39] (equation 10).

$$MgCu_2 + 3MgH_2 \rightarrow 2Mg_2Cu + 3H_2 \quad (10)$$

Vajo et al. have investigated several such systems including the destabilization of LiH and MgH_2 with silicon (Si) [40] and also destabilizing $LiBH_4$ with MgH_2 [36]. These types of system could prove to be very useful in the search for a more viable H_2 storage medium because when destabilizing species are present within a material they can offer lower energy pathways for the removal of hydrogen from other materials present within the sample. They do this by providing alternative reaction pathways for the removal of hydrogen from the sample, which may be kinetically and/or more thermodynamically favourable than when using the starting materials alone.

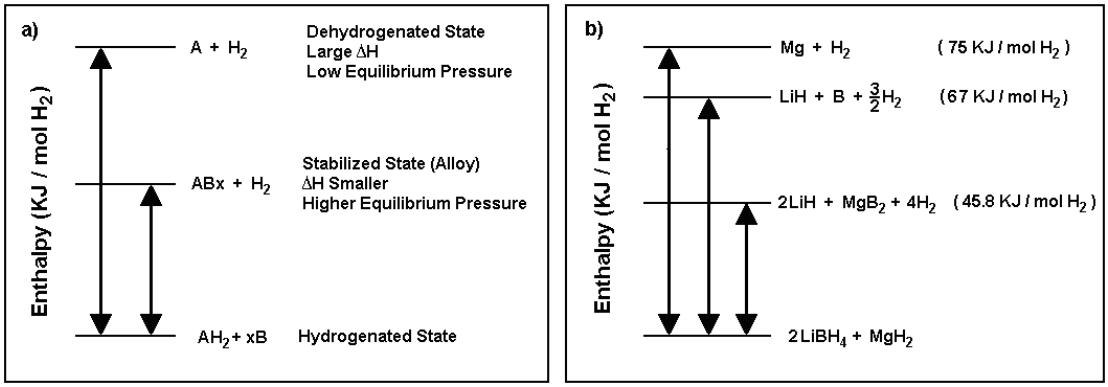

Figure12 a) General Destabilization case b) Comparison of the decomposition enthalpy for pure Mg, pure $LiBH_4$ and a mixed $LiBH_4$ + MgH_2 system [41].

Combining $LiBH_4$ with MgH_2 changes the chemical pathway by which these two materials individually lose their hydrogen, the result of which is that less energy is required to remove their hydrogen. The dehydrogenation mechanism of these two materials changes from equations 8 and 9, to now follow the chemical pathway expressed by equation 11 which has a reported reaction enthalpy of 45.8 kJ / mol H_2 [41]. This enthalpy value is approximately 20 kJ / mol H_2 lower than that required for the

decomposition of pure $LiBH_4$ (equation 9) (~67 kJ / mol H_2) [36], [41] and approximately 30 kJ / mol H_2 lower than the enthalpy required to remove hydrogen from pure MgH_2 (~75 kJ / mol H_2) [42] [43].

$$2LiBH_4 + MgH_2 \rightarrow 2LiH + MgB_2 + 4H_2 \quad (11.45\ wt\%\ H_2) \qquad (11)$$

The $LiBH_4$ + MgH_2 mixed hydride systems have aroused a lot of interest recently due to its high gravimetric density and the possibility of further destabilizing the system with the addition of dopants. This increased interest however has led to a number of reported hypotheses regarding the underlying mechanism of destabilization. It was Vajo et al. who first suggested equation 11, as a possible decomposition route for mixtures of $LiBH_4$ and MgH_2 concluding that it was the formation of MgB_2 which made the dehydrogenated state more energetically favourable than the starting materials [36]. Vajo et al. milled samples with a composition of $2LiBH_4$ + MgH_2 + 0.04 $TiCl_3$ for one hour at 400 rpm after which they were then dehydrogenated up to 450ºC at 2ºC / min. Samples were initially desorbed into an evacuated volume but the hydrogen released was allowed to build up creating a pressure of hydrogen above the sample. It was concluded from this investigation that a dehydrogenation atmosphere of hydrogen was necessary for decomposition to occur via equation 11 because under a dynamic vacuum the MgH_2 constituent of these samples was found to dehydrogenate to Mg rather than MgB_2.

Bosenberg et al. have also studied this $2LiBH_4$ + MgH_2 system using in situ XRD analysis and produced results that support the reaction mechanism proposed by Vajo (equation 11).

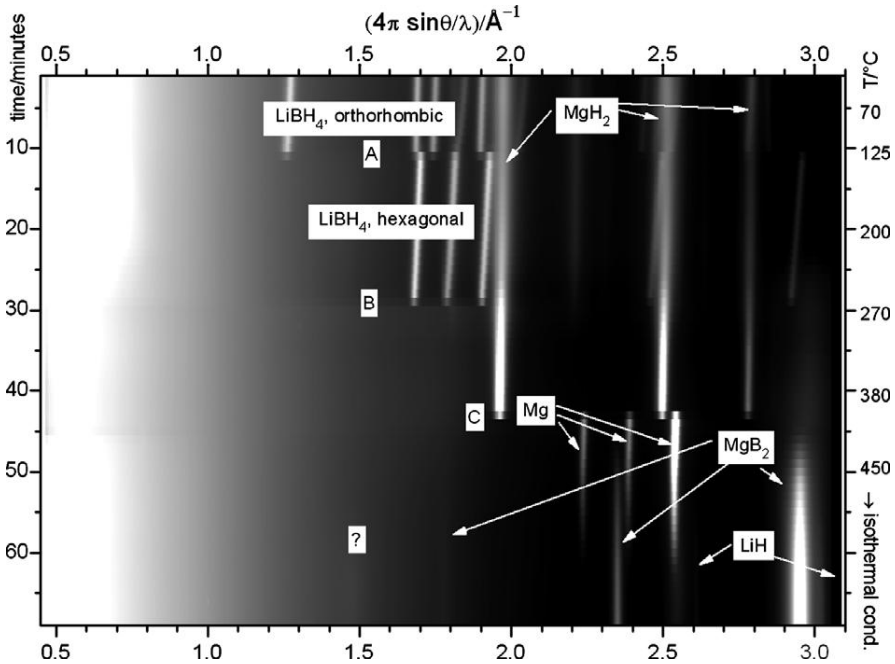

Figure 13) In situ XRD measurement for the decomposition of a $2LiBH_4 + MgH_2$ composite doped with 5 at.% titanium isopropoxide using 5 bar hydrogen with a heating rate of 5 K min^{-1} to 450ºC. A and B correspond to the polymorphic transformation and to the melting of LiBH4, respectively. C is where MgH_2 loses its hydrogen to form Mg [44].

Bosenberg et al. used conditions that differed slightly to those used by Vajo. Bosenberg milled MgH_2 for five hours using a ball to powder ratio of 4:1 after which samples were then milled for another five hours once the $LiBH_4$ and any dopants had been added. The in situ XRD data for dehydrogenation was obtained using a sample with the composition $2LiBH_4 + MgH_2$ + 5at% $Ti(OCH(CH_3)_2)_4$ and conducted under 5 bar H_2 up to 450ºC at 5ºC / min. From this in situ XRD work it was found that MgH_2 released hydrogen to form elemental Mg at 390ºC, which was then closely followed by the formation of MgB_2 at 400ºC. LiH, the other product of the reaction occurring in equation 11 was also observed by Bosenbergs in situ XRD analysis but appeared after the production of MgB_2 [44].

Yu et al., another group to have studied this mixed hydride system used both different conditions and a different stoichiometry compared to the two groups mentioned above. During this investigation $LiBH_4 – MgH_2$ (1:4 mass ratio) samples were milled for one hour

under an atmosphere of N_2 after which they were then dehydrogenated with a thermogravimetric analyser. Samples were dehydrogenated on the TG up to 600ºC with a heating rate of 10ºC / min using a 1 atm over pressure of argon flowing at 200 ml / min. The decomposition products obtained from heating this stoichiometry up to different temperatures were then analysed with XRD to try and decipher the mechanism by which these samples lost their hydrogen. This group found that under an Ar atmosphere $LiBH_4$ – MgH_2 samples (1:4 mass ratio) first released hydrogen due to the dehydrogenation of MgH_2 at 360ºC to give Mg and H_2. At 405ºC the $LiBH_4$ constituent of these samples began to lose hydrogen yielding LiH and B but no change was observed for the XRD peaks produced by elemental Mg suggesting that the metal had acted as a catalyst. Upon heating to 440ºC the LiH now present within the samples began to react with the Mg present producing hydrogen and a Li – Mg alloy. With further heating to 600ºC the formation of a MgB_2 phase was observed but this happens at a much higher temperature than that observed by Vajo et al. The overall reaction proposed by Yu et al. can be observed below in equation 12 [45].

$$MgH_2 + 0.3\ LiBH_4 \rightarrow 0.37\ Li_{0.184}Mg_{0.816} + 0.15\ MgB_2 + 0.78\ Li_{0.3}Mg_{0.7} + 1.6\ H_2 \quad (12)$$

Johnson et al. have also worked on the activation of MgH_2 with 10 mol% $LiBH_4$ additions but did not report on the presence of either MgB_2 or a Li-Mg alloy, instead suggesting that $LiBH_4$ simply served as a means of introducing Li^+ ions into the lattice of MgH_2 [46]. The dehydrogenation of samples studied by this group occurred under vacuum and temperatures no higher than 300ºC were reached which would explain why neither, MgB_2 nor a Li – Mg phase was observed during this investigation. What was observed however was an increase in the hydrogen sorption kinetics of MgH_2 which was concluded to be a result of lattice defects introduced into the crystal structure of MgH_2

due to the presence of Li^+. It has also been reported that the charge transfer between the metallic cation (M^+) and the borohydride unit (BH_4^-) is integral to the stability of metallic borohydrides [47], [48], [49]. Partial substitution of this cation could therefore potentially suppress some of the charge transfer between cation and borohydride unit ultimately decreasing the stability of these complex hydrides, reducing their dehydrogenation temperatures.

3. Aims and Objectives

The aim of this project is to assess the potential of destabilizing lithium borohydride with the addition of magnesium hydride for the purpose of hydrogen storage. Analyses of the reaction products produced by dehydrogenation (under Ar) will be carried out to try and clarify the mechanisms by which this system loses hydrogen. The reverse reaction of samples with hydrogen will also be assessed in order to establish how much hydrogen can be retrieved from these mixed hydride systems after recombination has been carried out.

In order to accomplish these aims, lithium borohydride will be ball milled with magnesium hydride in varying molar ratios to create an intimate mixture of the two compounds. The samples will then be dehydrogenated and recombined twice with the aid of DSC equipment to gauge how much energy is required for the removal and recombination of hydrogen with these mixed hydride systems. Thermogravimetric analysis will be used to measure the amount of hydrogen released during the dehydrogenation cycles. Thermogravimetric analysis will also give an indication as to how successful the recombination reaction has been, under the conditions used for this process.

The three $LiBH_4$ – MgH_2 samples to be studied have molar ratios of

- $2LiBH_4 + MgH_2$
- $LiBH_4 + 2MgH_2$
- $LiBH_4 + 5MgH_2$

The first of these stoichiometries ($2LiBH_4 + MgH_2$) was picked for the ratio of Mg to B which is suited to the formation of MgB_2. The other two samples contain excess MgH_2, in order to assess the destabilization effect of increasing MgH_2 additions on $LiBH_4$.

4. Experimental

4.1 Sample Processing

All samples were prepared using lithium borohydride (95%) from Sigma Aldrich and magnesium hydride (95% MgH_2, 5% Mg) from Goldschmidt. Each powder was weighed out in an argon glovebox, due to the sensitivity of both materials to air and moisture.

After each powder had been weighed out to give 6g sample batches, they were then placed in a 50 cm^3 stainless steel milling pot which was sealed under argon and milled at 250 rpm for one hour using a Retsch PM400 planetary ball mill. The ball to powder ratio used was 60:1, and the balls and pot were made of stainless steel. The diameter of the balls was 14 mm. The samples were not milled continuously for one hour, but were instead milled for ten minutes with rest periods of ten minutes, giving a total milling time of two hours. A resting period of 10 minutes was employed to minimise the amount of heat transferred to the material as a result of the friction occurring during the milling process. After one hour of milling (30 mins on; 30 mins off) the milling pot was warm and reopened in the glove box to relieve a pressure build-up which was observed whilst milling this material and to dislodge any material fixed to the walls of the pot. The pressure that built up in the pot during milling is most likely a build up of hydrogen released from the material as a result of this process.

4.2 Heating Tests

In order to determine what temperatures these samples could be taken up to during dehydrogenation, pan testing was carried out in a vacuum to simulate heating with an

overpressure of argon. Aluminium differential scanning calorimeter (DSC) pans and alumina thermo gravimetric analysis (TGA) pots were loaded with small amounts of sample then placed on an alumina boat which was then loaded into a furnace tube ready for heating. These pan tests revealed 450ºC to be a safe temperature for the dehydrogenation of these samples because above this temperature samples began to foam over the sides of the containers. Above 550ºC the TGA pots used showed signs of degradation due to chemical attack by these mixtures and at 600ºC the alumina pots were reduced to an ash-like state.

4.3 Sample Characterisation

The thermal stability of samples was studied by measuring the energy required for various processes to occur during their dehydrogenation and this was done using a Netzsch DSC204HP. The DSC was used to heat between 5 – 14 mg of sample housed in an aluminium DSC pan, from 30ºC to 450ºC with a heating rate of 2ºC / min. Decomposition of the samples occurred under an argon atmosphere of 3 bar(g), flowing at a rate of 100 ml / min. The maximum temperature samples could have been subjected to under this 3 bar(g) atmosphere is 600ºC. Before runs the DSC was calibrated with the melting point of known metals such as indium and bismuth.

The recombination of desorbed samples with hydrogen was also investigated using the DSC which was again run from 30ºC to 450ºC at 2ºC / min, but this time with a 100 bar(g) hydrogen pressure flowing at 100 ml min^{-1}. The maximum temperature at which samples could have been heated for recombination under a 100 bar(g) H_2 atmosphere is 550ºC.

Thermogravimetric analysis (TGA) was conducted on samples with the aid of a Netzsch TG209, which monitors the mass changes that occur during heating. The TGA like the DSC was also taken up to a temperature of 450ºC from 30ºC, at a heating rate of 2ºC / min however the atmosphere into which dehydrogenation took place was 0.5 bar(g) argon flowing at 40 ml / min. The maximum temperature the TGA is capable of under these conditions is 1000ºC. The TGA was also used in conjunction with a Hiden Analytical HAL IV quadropole mass spectrometer to measure any evolved chemical species, such as hydrogen or diborane.

Characterisation of the crystal structures present was performed using a Philips X'pert X-ray diffractometer (XRD), which scanned a 2θ range of 20 – 100º using Cu K_α radiation (λ = 1.54Å) at a scanning rate of 1º / min. Again due to their air sensitive nature, XRD samples were prepared in a glovebox by placing the powder onto a slide and then secured with sticky tape, to isolate the sample from air during its run.

A Nicolet 8600 Fourier Transform – Infrared (FTIR) spectrometer with a DTGS detector was used with the aid of a golden gate attenuated total reflectance (ATR) attachment to facilitate inert loading of the samples. This analytical technique was used to measure IR activity of the bonds within the samples at various stages of their cycling, providing evidence for the reversibility of the reaction and to identify the presence of any new IR bonds developed.

5. Results and Discussion

5.1 Starting Materials

MgH_2 is capable of storing a maximum of 7.6 wt% H_2 when fully hydrided but TGA analysis carried out on this material revealed that only 6.5 wt% is released when heated under half a bar(g) of Ar up to 450ºC. Although the maximum theoretical hydrogen capacity of MgH_2 is 7.6 wt% H_2, when the purity of this material (95%) is taken into consideration this figure then becomes 7.22 wt% H_2. Our observed mass loss from this material (6.5 wt% H_2) is still lower than expected (7.22 wt% H_2) and may be due to a loss of hydrogen resulting from the milling process. The MgH_2 material began to release hydrogen at approximately 310ºC and had stopped at 370ºC. As the graph levels off toward the latter stages of its heating run, it would appear that all of the available hydrogen has desorbed before 370ºC.

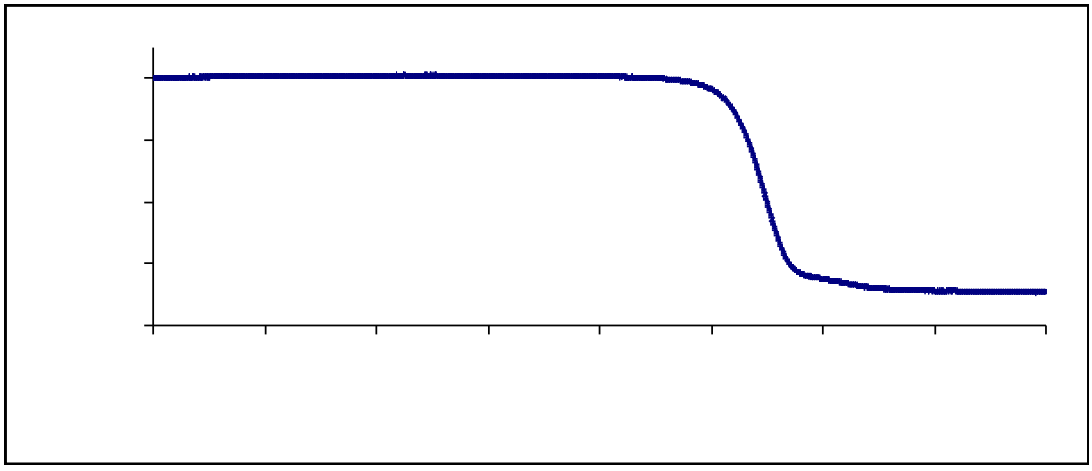

Figure 14) Goldschmidt MgH_2 (95%) milled for one hour at 250 rpm. Sample was dehydrogenated under 0.5 bar(g) of Ar flowing at 40 ml / min whilst heating to 450ºC at 2ºC / min.

Gennari et al. observed magnesium hydride, which had been formed by milling >99.9% magnesium under half a bar of 99.995% H_2 for 50 hours, desorbing at approximately 350ºC but found only 5 wt% H_2 was released by the time 500ºC had been reached [50]. The DSC and TGA data obtained under an argon atmosphere for the MgH_2 used in Gennari's investigation shows that the energy change associated with hydrogen removal from this compound levels off by 360ºC suggesting that MgH_2 had released all of its available hydrogen by 450ºC.

The reaction enthalpy for removing hydrogen from this compound up to 450ºC was calculated from the DSC profile below (Figure 15) and measured 65.91 kJ / mol H_2. This enthalpy value is lower than that used by Gennari et al. (75 kJ / mol MgH_2) [50]. Energy absorbed by MgH_2 through ball milling can lead to the introduction of stresses within its structure and may even result in some decomposition of the material, which would explain the lower than expected wt% H_2 figure obtained from TGA experiments [31].

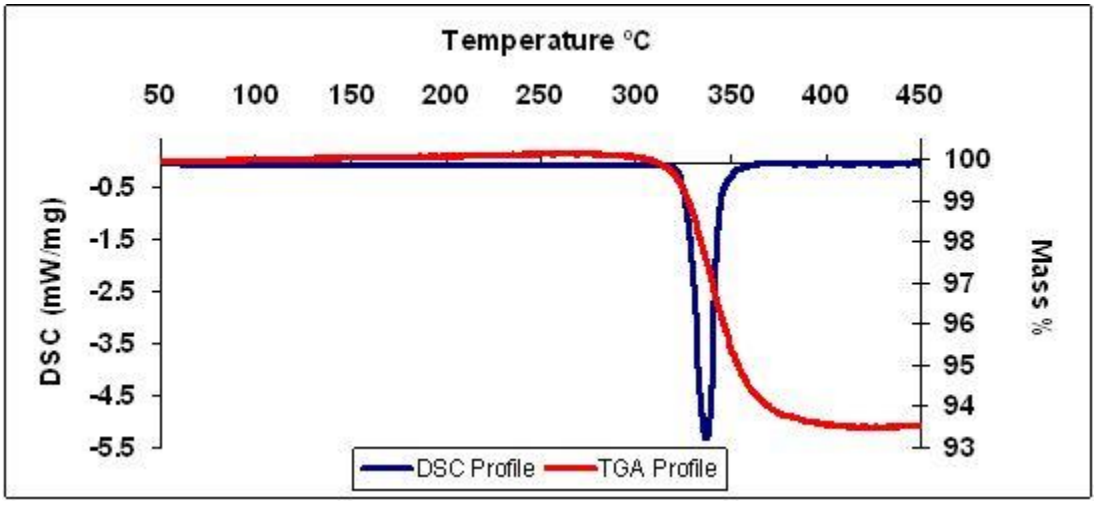

Figure 15) DSC and TGA data for MgH_2 (95%). TGA data was obtained by dehydrogenating the sample under 0.5 bar(g) of Ar flowing at 40 ml / min whilst heating to 450ºC at 2ºC/min. DSC data for MgH_2 was obtained by dehydrogenating into 3 bar(g) of Ar flowing at 100 ml / min whilst heating up to 450ºC at 2ºC/min.

Due to the volatile boiling observed during heat testing, it was not possible to measure as received $LiBH_4$ on either the TGA or the DSC, for fear of damaging the equipment. Therefore, data obtained by Orimo et al. [37] and Ming et al. [34], [35] presented in the literature review, will be used for comparing as received $LiBH_4$ and the mixed hydride systems.

Infrared spectroscopy of MgH_2 revealed IR active bonds were present, with a large broad signal at the start of the profile ranging from 790 – 1400 cm^{-1} (Figure 16). This broad IR signal observed for MgH_2 has also been seen occurring between 800 and 1400 cm^{-1} by Wang et al [51]. $LiBH_4$ exhibited two sets of IR peaks: one between 1000 and 1500 cm^{-1} (close to the range of MgH_2); and another between 2000 and 2500 cm^{-1}, producing a large peak which on closer inspection appears to be composed of four separate peaks (Figure 17).

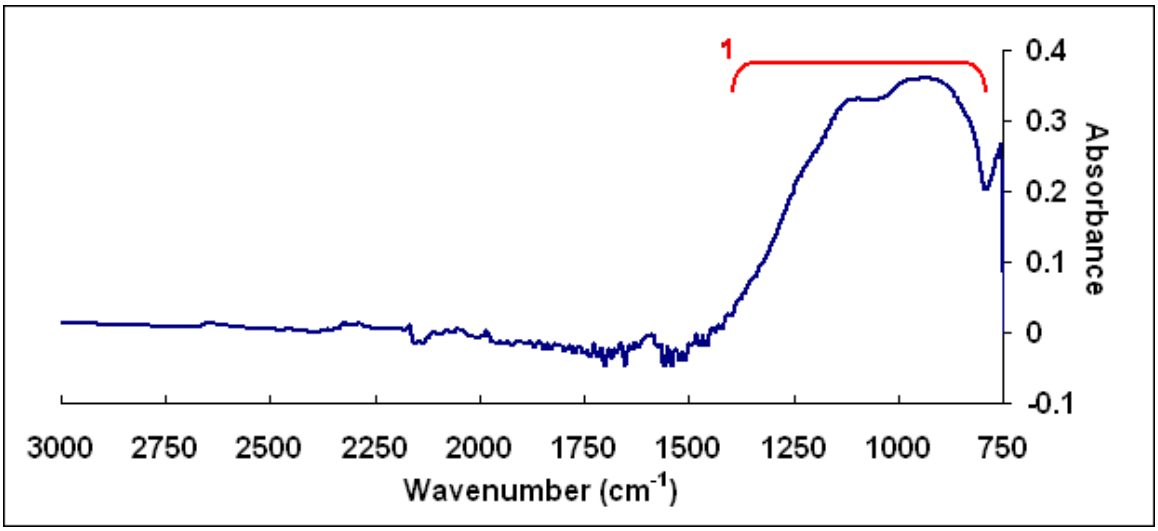

Figure 16) FTIR spectra of as received MgH_2

Peak	Wavenumber (cm^{-1})	Internal change
1	790 – 1400	Mg – H stretch

Table 4) FTIR table for as received MgH_2

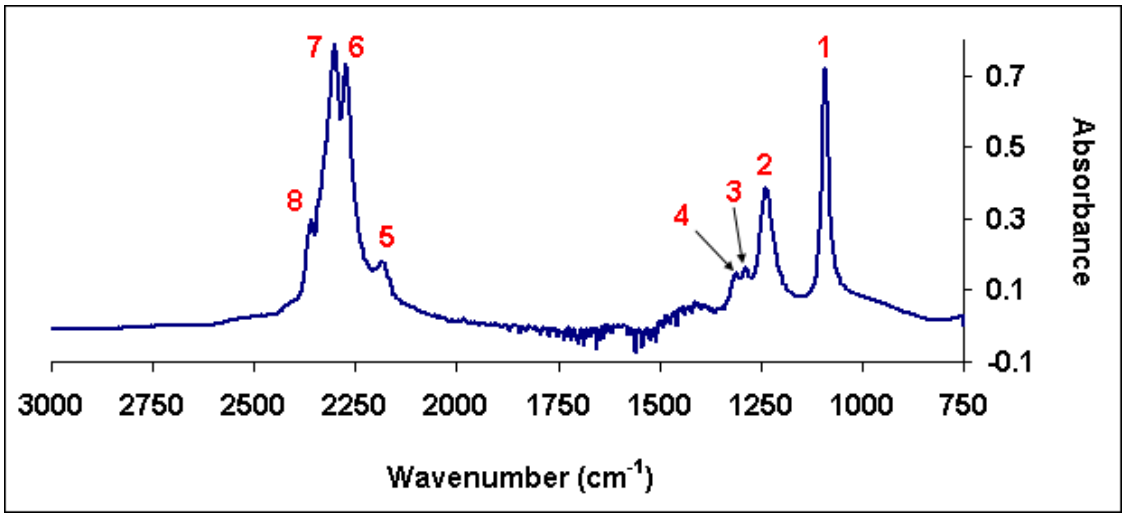

Figure 17) FTIR spectra of as received $LiBH_4$

Peak	Wavenumber (cm^{-1})	Internal Change	Assignment [52]
1	1090	B – H Bending	υ_4
2	1240		$3\upsilon_L$
3	1285		υ_2
4	1320		υ_2'
5	2190	B – H Stretching	$2^{10}\upsilon_4$
6	2270		υ_3
7	2300		υ_3'
8	2360		υ_3''

Table 5) FTIR table for as received $LiBH_4$

XRD analyses was also carried out on the as received MgH_2 and $LiBH_4$ to evaluate the purity of the starting materials and the XRD patterns for these can be seen below in Figures 18 and 19.

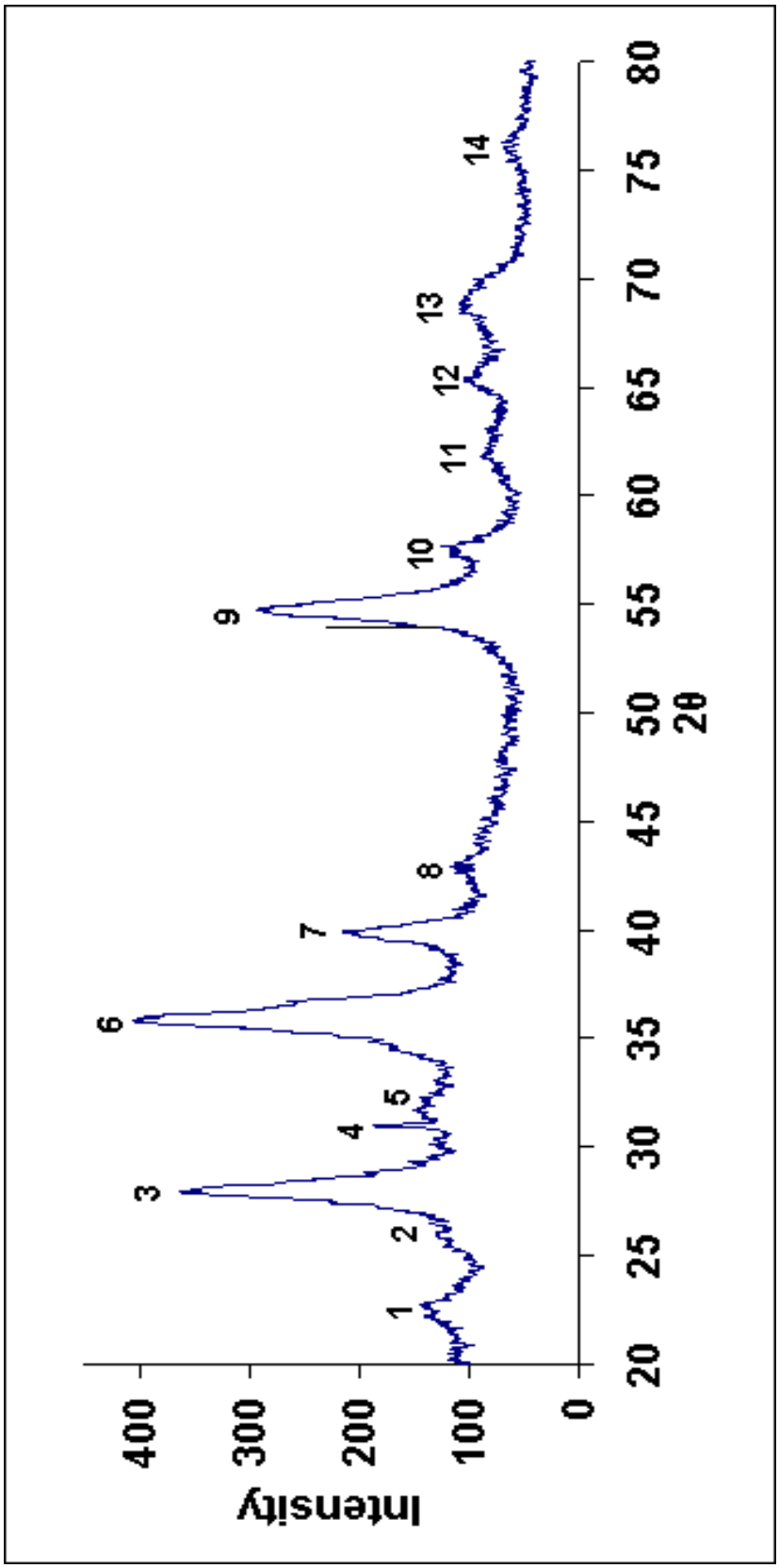

Figure 18) XRD pattern of as received MgH_2

Peak Number	2θ value	d Spacing (Å)	Assignment
1	22.71	3.92	MgH_2
2	25.69	3.47	Tape
3	27.99	3.19	MgH_2
4	30.95	2.89	MgH_2
5	31.88	2.81	$\gamma - MgH_2$
6	35.84	2.51	MgH_2
7	39.87	2.26	MgH_2
8	42.88	2.11	MgO
9	54.79	1.68	MgH_2
10	57.48	1.60	MgH_2
11	61.97	1.50	MgO
12	65.30	1.43	MgH_2
13	68.76	1.37	MgH_2
14	76.08	1.25	MgH_2

Table 6) XRD table for as received MgH_2

The XRD pattern produced for MgH_2 reveals that the most intense peaks occur with 2θ values of 27.99°, 35.84°, 39.87° and 54.79°. Peaks arising at 42.88° and 61.97° indicate that the as received MgH_2 has oxidised to some extent as these are MgO peaks. A gamma phase of magnesium hydride ($\gamma - MgH_2$) was found but no trace of magnesium metal was seen.

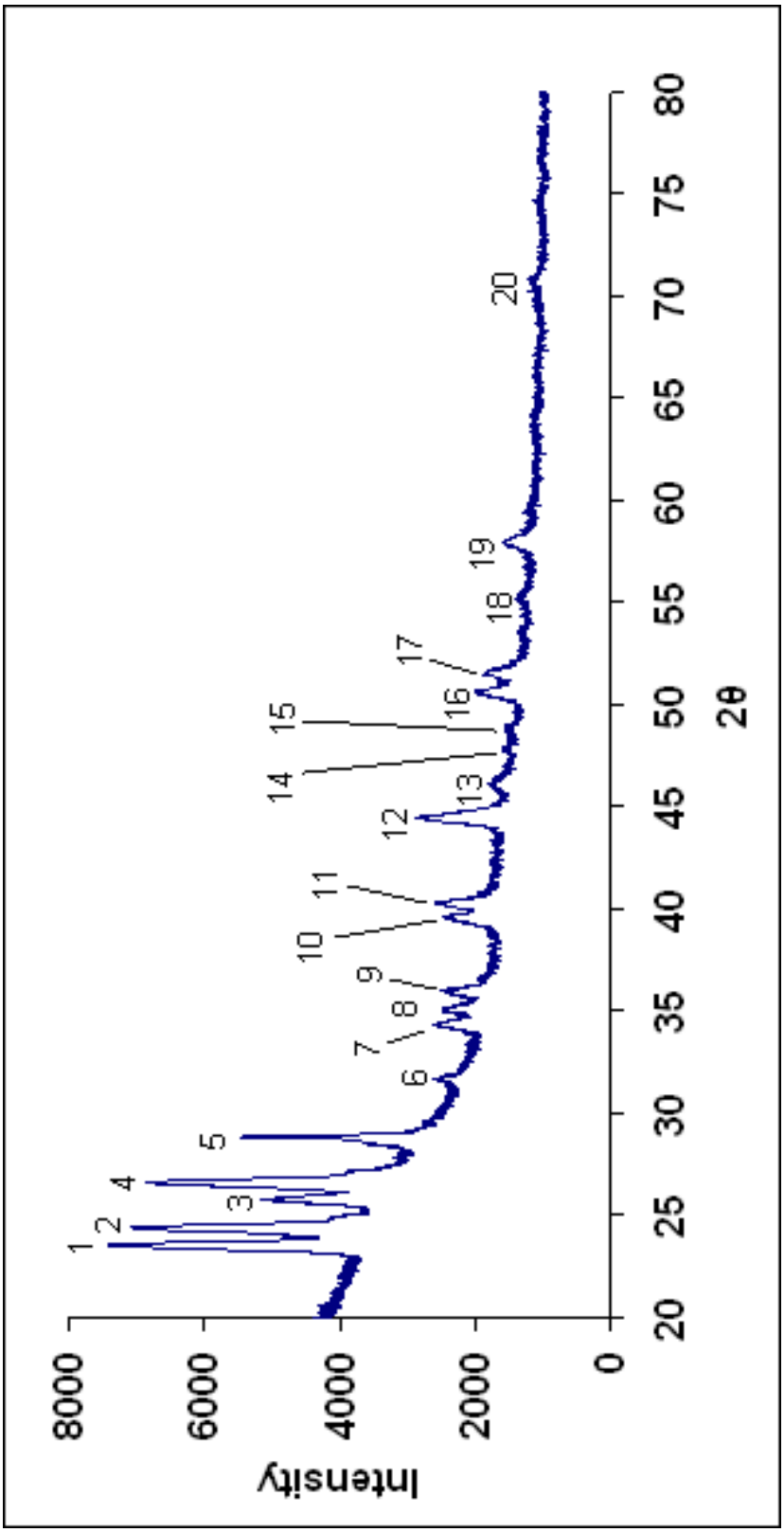

Figure 19) XRD pattern of as received $LiBH_4$

Peak Number	2θ value	d Spacing (Å)	Assignment
1	23.55	3.78	$LiBH_4$
2	24.41	3.65	$LiBH_4$
3	25.82	3.45	$LiBH_4$
4	26.64	3.35	$LiBH_4$
5	28.87	3.09	$LiBH_4$
6	31.71	2.82	$LiBH_4$
7	34.37	2.61	$LiBH_4$
8	35.06	2.56	$LiBH_4$
9	36.03	2.49	$LiBH_4$
10	39.59	2.28	$LiBH_4$
11	40.30	2.24	$LiBH_4$
12	44.49	2.04	$LiBH_4$
13	46.12	1.97	$LiBH_4$
14	47.87	1.90	$LiBH_4$
15	48.88	1.86	$LiBH_4$
16	50.64	1.80	$LiBH_4$
17	51.56	1.77	$LiBH_4$
18	55.25	1.66	$LiBH_4$
19	57.99	1.59	$LiBH_4$
20	70.81	1.33	$LiBH_4$

Table 7) XRD table for as received $LiBH_4$

The XRD pattern obtained for the as received $LiBH_4$ material reveals that there is no lithium hydroxide present, no presence lithium hydride or lithium metal.

5.2 $2LiBH_4 + MgH_2$

5.2.1 As milled $2LiBH_4 + MgH_2$

IR and XRD techniques were used on the as milled material to determine if any reaction products had been produced or structural changes induced as a result of the milling process. For the $2LiBH_4 + MgH_2$ sample the IR active site for MgH_2 (790 – 1400 cm^{-1}) was superimposed onto the first IR active region of $LiBH_4$ which was then followed by a second phase of IR peaks which was only observed for the $LiBH_4$ material.

The fourth IR peak produced by pure $LiBH_4$ which occurred at 1320 cm^{-1} (see Figure 17 and Table 5) is no longer observed in the as-milled material, being overshadowed by the stronger MgH_2 signal. Other than the non-visibility of the 1320 cm^{-1} peak, all peaks observed for the starting materials are observed in the $2LiBH_4 + MgH_2$ sample, and there is no evidence for the formation of new IR active bonds.

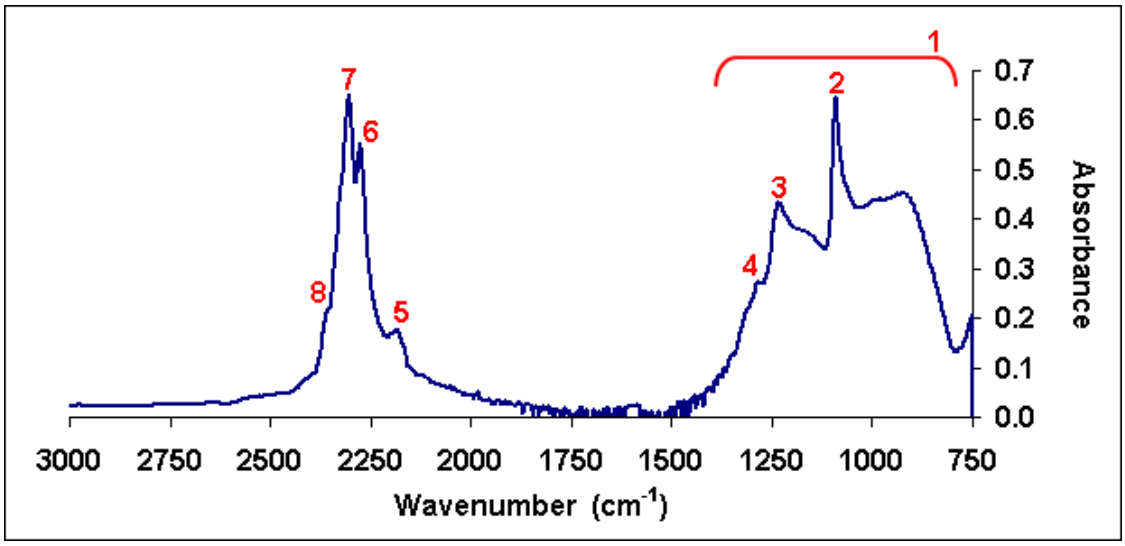

Figure 20) FTIR spectra of $2LiBH_4 + MgH_2$ milled at 250 rpm for 1 hr under Ar

Peak	Wavenumber (cm^{-1})	Assignment [52]	Internal Change	Material
1	790 - 1400		Mg – H stretch	MgH_2
2	1090	υ_4	B – H Bending	$LiBH_4$
3	1220	$3\upsilon_L$		$LiBH_4$
4	1265	υ_2		$LiBH_4$
5	2170	$2^{10}\upsilon_4$	B – H Stretching	$LiBH_4$
6	2270	υ_3		$LiBH_4$
7	2300	υ_3'		$LiBH_4$
8	2345	υ_3''		$LiBH_4$

Table 8) FTIR table for $2LiBH_4 + MgH_2$ milled at 250 rpm for 1 hr under Ar.

Results obtained through XRD analysis of $2LiBH_4 + MgH_2$ revealed a mixture of peaks which were found when analysing both MgH_2 and $LiBH_4$ alone, with no new peaks observed. The number and intensity of 2θ peaks produced by an as-milled sample is significantly less than those produced by the as-received materials, due to a loss in crystallographic long-range order that can occur as a result of milling. The lack of any new XRD peaks further suggests that no new phases have formed between these two materials as a result of milling. If any reaction has occurred during milling then the

products of this are X-ray amorphous and IR inactive, or they occur in too small a quantity under these conditions to be detected with these techniques.

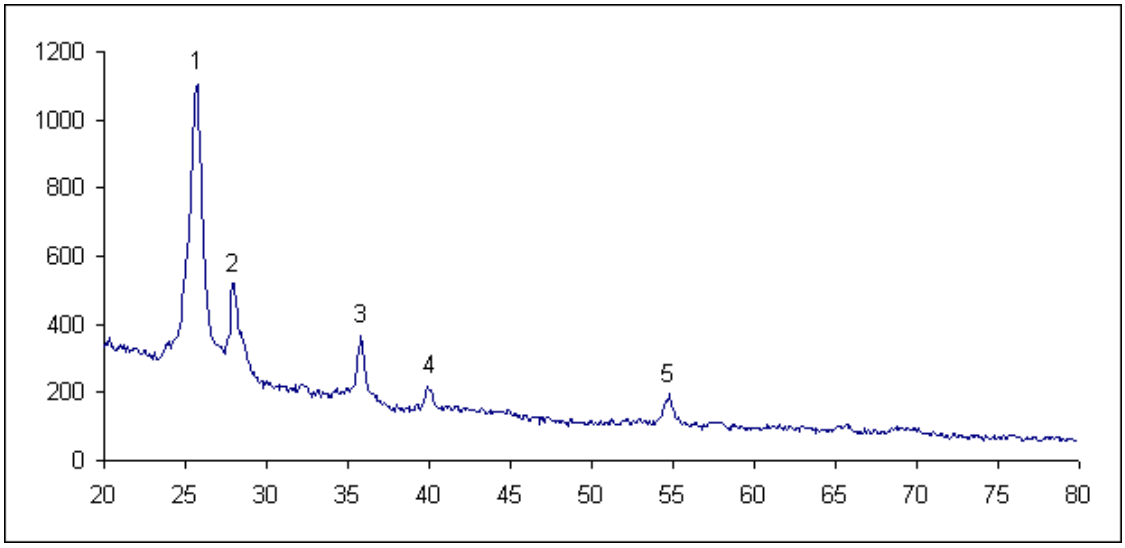

Figure 21) XRD analysis of $2LiBH_4 + MgH_2$ milled at 250 rpm for 1 hr under Ar

Peak Number	2θ value	d Spacing (Å)	Assignment
1	25.59	3.48	Tape
2	28.05	3.18	MgH_2
3	35.91	2.50	MgH_2
4	40.02	2.25	MgH_2
5	54.82	1.68	MgH_2

Table 9) XRD table for $2LiBH_4 + MgH_2$ milled at 250 rpm for 1 hr under Ar

5.2.2 First Dehydrogenation of $2LiBH_4 + MgH_2$

A mixed hydride system with this stoichiometry is capable of holding a maximum of 11.45 wt% H_2 when the formation of lithium hydride is taken into account. When the purity of the starting materials is considered the maximum theoretical storage capacity is reduced to a value of 10.88 wt% H_2. TGA analysis of the first dehydrogenations show that up to 450ºC, these samples release less mass than their theoretical maximum

predicts. At 450ºC a total of 9.25 wt% was lost by samples of this stoichiometry, which is 2.2 wt% less than their absolute theoretical maximum and 1.63 wt% lower than their maximum when the purity of the materials is considered.

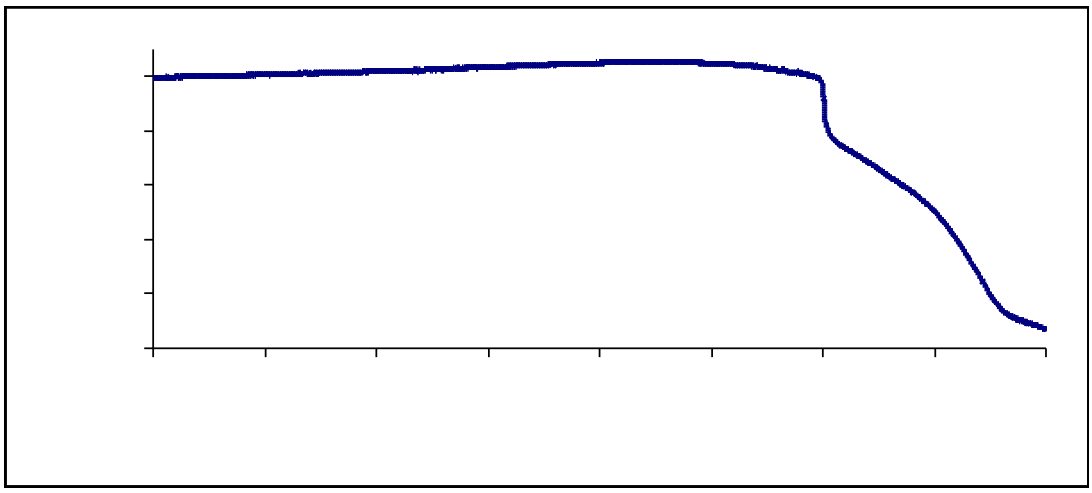

Figure 22) TGA profile of $2LiBH_4 + MgH_2$ dehydrogenated into 0.5 bar(g) of Ar flowing at 40 ml / min by heating up to 450ºC at 2ºC / min.

From the TGA data obtained it appears that these samples lose mass in two stages. The first loss of mass occurs rapidly at 350ºC releasing 2.5 wt% which is then almost immediately followed by a slower release of 6.75 wt%. The first loss of mass coincides well with what has been observed before for the dehydrogenation of MgH_2 (Figure 14). If the MgH_2 (95% purity) retained all of its hydrogen after the milling process of these samples it would be expected to release 2.72 wt%. If $LiBH_4$ (95%) was to do the same and retain all of its hydrogen during milling then you'd expect to see a loss of 8.15 wt% upon complete dehydrogenation. This calculated release of 8.15 wt% H_2 is higher than the 6.75 wt% value observed for the second TGA loss in Figure 22. Fedneva et al. who used DTA to investigate the decomposition of $LiBH_4$ found that 2 wt% of the hydrogen contained within $LiBH_4$ was liberated upon melting this complex hydride [53]. TGA analysis of $LiBH_4$ (95%, Aldrich) conducted by Orimo et al. (Figure 11) also revealed a

small loss in mass around the melting point but only <0.2 wt% [37]. Although the above TGA profile appears to lose a small amount of mass beginning at approximately 300ºC this result was not repeatable with subsequent TGA runs.

Mass spectrometry data for these samples was obtained from their gas stream released during dehydrogenation on the TGA. The mass spectrometry data like the TGA profile indicates that hydrogen is being released in just a two stage process. The first release of hydrogen appears to come from MgH_2 and produces a large sharp signal on the mass spectrometer. This signal is then followed by a smaller, broader signal due to a less rapid release of hydrogen from $LiBH_4$.

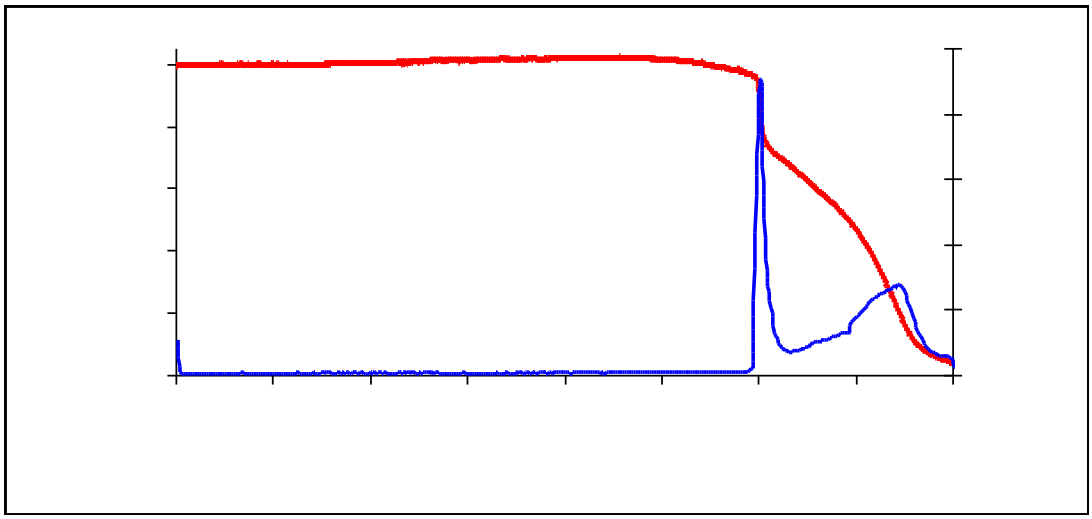

Figure 23) TGA and mass spec. (m/z = 2) data produced by $2LiBH_4 + MgH_2$. TGA data obtained by dehydrogenating under 0.5 bar(g) of Ar flowing at 40 ml / min up to 450ºC at a heating rate of 2ºC / min.

The mass spectroscopy data from these samples also revealed the presence of some diborane (B_2H_6) in the gas stream of one dehydrogenating $2LiBH_4 + MgH_2$ sample (Figure 24), however in three other runs carried out on this stoichiometry no diborane signal was observed. The signal produced by the presence of diborane was only very

small and may have only just reached the limits of detection for our mass spec. equipment. Another reason for only producing this result once may be due to some diborane condensing within the pipework of the mass spectrometer from a previous experiment that somebody else had run, and was then liberated again when I ran my sample. As this result has not proved repeatable it must be assumed that this is an anomalous result which could have been due to some form of contamination within the line between the TGA and mass spectrometer. This result can not be dismissed completely though due to the presence of boron and hydrogen within my sample that may combine to form this product. Au et al. has reported the detection of borane (BH_3) from a 75% $LiBH_4$ + 25% TiO_2 sample [34] and $Zn(BH_4)_2$ has also been shown to decompose with the production of diborane [54] suggesting that borane production from borohydrides is not uncommon.

The presence of even minute traces of B_2H_6, are undesirable from a hydrogen store for a number of reasons. Firstly the production of diborane will deplete the sample of some of its boron which in turn will affect both the dehydrogenation and recombination kinetics of this material. Finding diborane in the gas stream also tells us that the hydrogen produced by this system is not entirely pure. Impure hydrogen means a purification step would be required if the hydrogen from this system were to be used for certain applications such as a PEMFC.

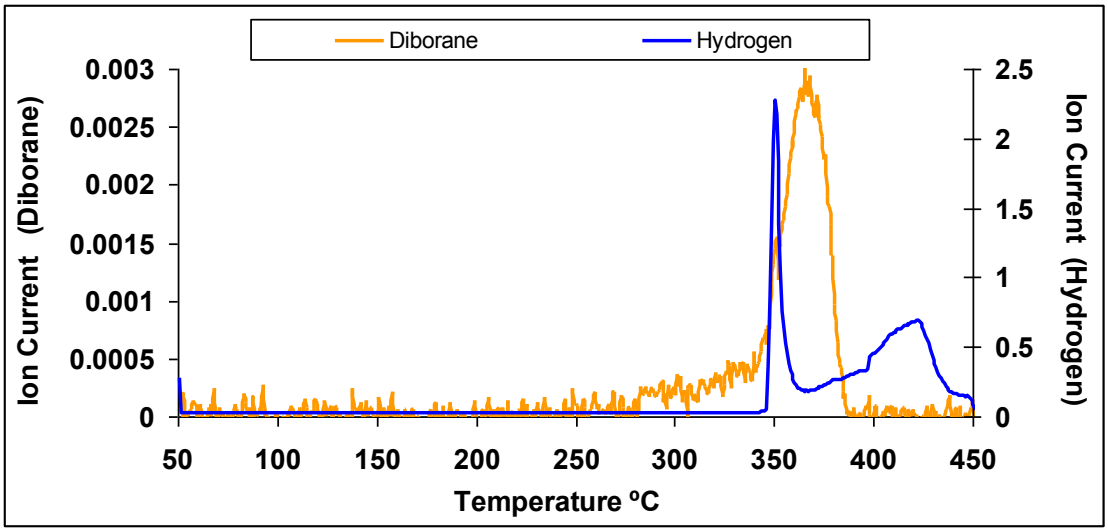

Figure 24) Hydrogen and Diborane signal produced by one of the $2LiBH_4 + MgH_2$ samples during dehydrogenation under 0.5 bar(g) of Ar flowing at 40 ml / min whilst heating up to 450ºC at 2ºC / min.

DSC data resulting from the analysis of this material shows four endothermic peaks, the first two of which occur due to the phase change and melting point of the $LiBH_4$ material respectively. The third peak occurs due to the removal of hydrogen from MgH_2 and occurs at the same temperature the TGA recorded a 2.5 wt% loss in mass from this sample. The fourth and final peak is actually two peaks which appear as one and is the energy requirement for removing the available hydrogen from $LiBH_4$. In Figure 11 these two peaks can be seen occurring at peak temperatures of 475ºC and 580ºC, which is much later and further apart than when they occur in Figure 25 and Figure 26, peaking at 395ºC and 425ºC. The final two peaks at the end of the DSC profile were also observed by Orimo et al. who believed that the reason these two peaks occurred was due to an intermediate compound ($Li_2B_{12}H_{12}$) being formed upon dehydrogenation of $LiBH_4$ [37].

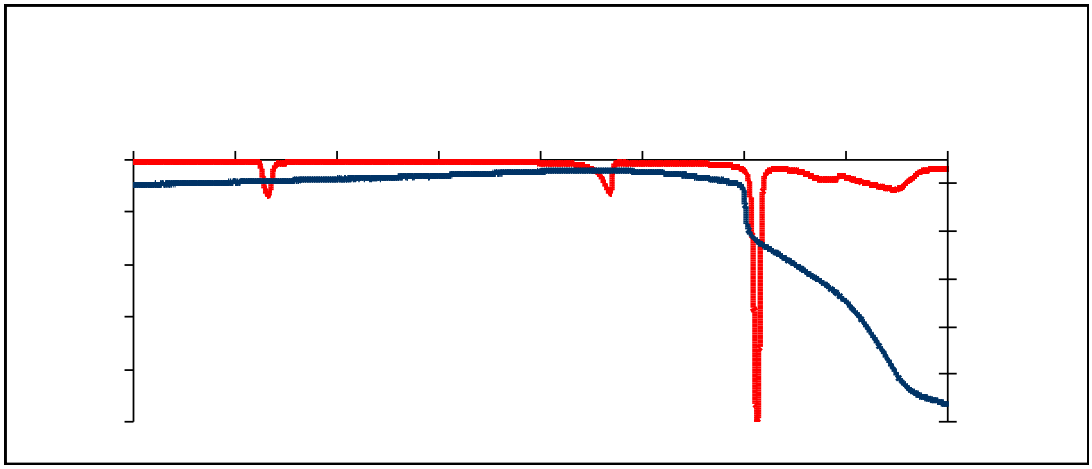

Figure 25) DSC and TGA profile of $2LiBH_4 + MgH_2$. TGA data was obtained by dehydrogenating under 0.5 bar(g) of Ar flowing at 40 ml / min up to 450ºC at 2ºC / min. DSC data was obtained by dehydrogenating into 3 bar(g) of Ar flowing at 100 ml / min up to 450ºC at a heating rate of 2ºC/min.

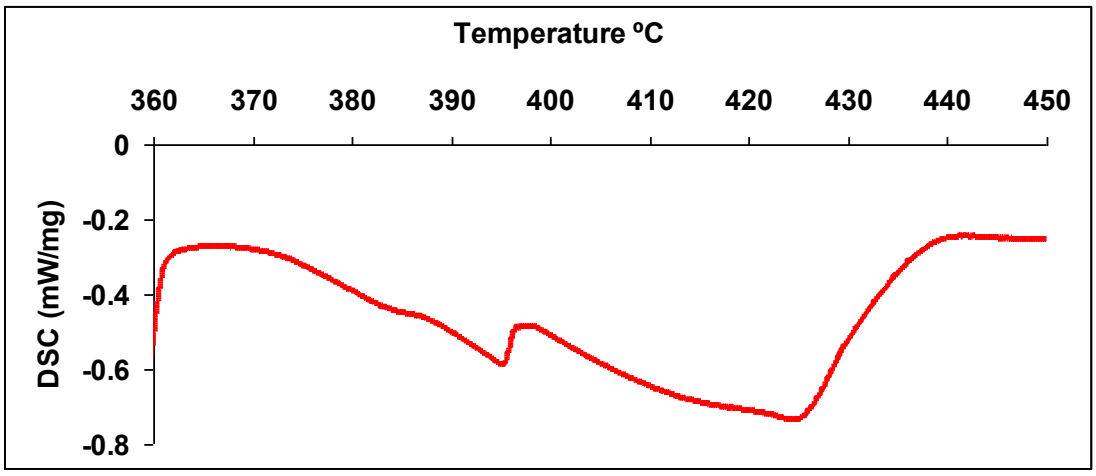

Figure 26) Expanded View of the final DSC peak from $2LiBH_4 + MgH_2$. Taken from Figure 25.

Enthalpy values for these endothermic processes have been calculated from the DSC data obtained and tabulated below (Table 10). Zuttel et al. who has also worked with pure $LiBH_4$ found the phase change to occur at 118ºC with an enthalpy value of 4.18 kJ / mol $LiBH_4$, and the melting point to occur at 287ºC with an enthalpy of 7.56 kJ / mol $LiBH_4$ [55]. The DSC trace from Figure 25 reveals that the phase change occurred at 117ºC with an average enthalpy of 4.40 kJ / mol $LiBH_4$ and the melting point

peaked at 286ºC with an average enthalpy of 6.72 kJ / mol $LiBH_4$. The average enthalpy of dehydrogenation for this reaction, per mole of hydrogen released (33.09 kJ / mol H_2) is around half that stated in the literature for pure $LiBH_4$ which is reported to be around 66.7 kJ / mol H_2 [36], [55]. The MgH_2 DSC peak, which is the third peak present in the DSC trace of Figure 25, has an onset temperature of 350ºC which would be expected from the onset data revealed by TGA analysis (Figure 22). The near vertical slope of the first mass loss shown by the TGA, suggests a rapid mass loss over a short temperature range, which is supported by the DSC as the MgH_2 peak starts at 350ºC and ends at 365ºC. The fourth peak begins at 365ºC and levels off by the time 450ºC is reached.

Sample Mass (mg)	9.40	8.06	7.52	9.12	12.02	7.92	**Average**
Phase Change (kJ / mol $LiBH_4$)	4.10	4.42	4.53	4.33	5.03	3.98	**4.40**
Melting Point (kJ / mol $LiBH_4$)	6.18	6.78	7.19	6.72	7.25	6.17	**6.72**
MgH_2 dehydrogenation (kJ / mol H_2)	13.74	14.69	15.35	14.72	17.00	14.36	**14.98**
$LiBH_4$ dehydrogenation (kJ / mol H_2)	10.75	11.91	14.23	12.58	9.08	10.98	**11.59**
Total KJ / mol H_2 (Assuming 9.25 wt.% H_2 released)	30.53	33.18	36.47	33.80	33.29	31.30	**33.09**

Table 10) Enthalpy values obtained for the first dehydrogenation of $2LiBH_4 + MgH_2$. Calculated from DSC data obtained under 3 bar(g) of Ar flowing at 100 ml / min whilst heating up to 450ºC at 2ºC / min.

After dehydrogenation, FTIR analysis of a $2LiBH_4 + MgH_2$ sample revealed that the IR activity between 790 and 1400 cm^{-1}, which occurred due to the IR active bonds of both MgH_2 and $LiBH_4$, can no longer be observed. Three small peaks do however remain occurring at values of 2162 cm^{-1}, 2320 cm^{-1} and 2360 cm^{-1} providing some evidence to

suggest that not all of the $LiBH_4$ present within this sample has been decomposed after heating up to 450ºC.

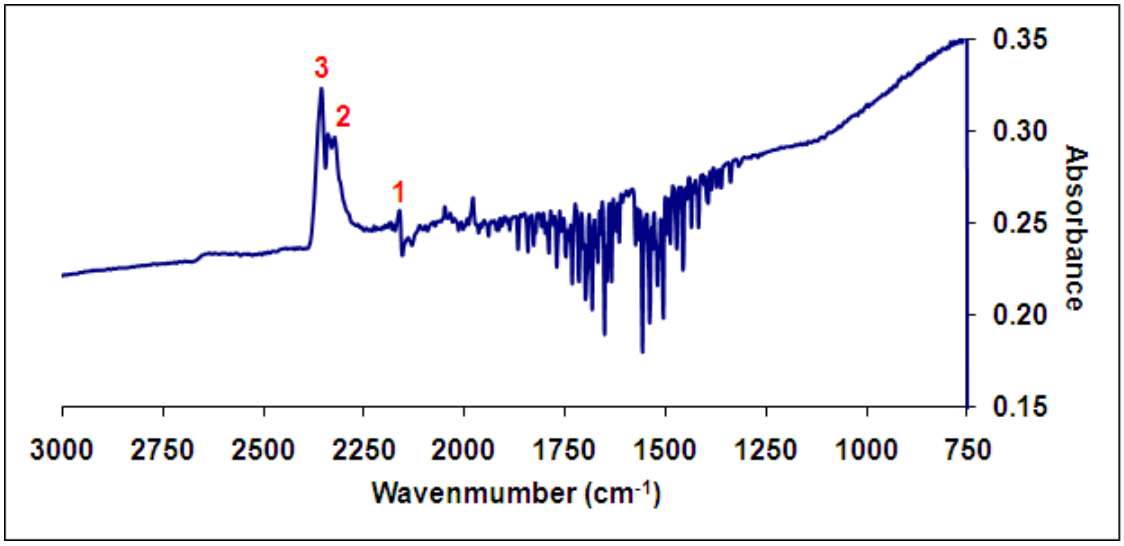

Figure 27) FTIR spectra produced by a desorbed sample of $2LiBH_4 + MgH_2$. Dehydrogenated under 3 bar(g) of Ar flowing at 100 ml / min whilst heating up to 450ºC at a rate of 2ºC / min.

Peak	Wavenumber (cm^{-1})	Assignment [52]	Internal Change	Material
1	2162	$2^{10}\upsilon_4$	B – H Streching	$LiBH_4$
2	2320	υ_3'		$LiBH_4$
3	2360	υ_3''		$LiBH_4$

Table 11) FTIR table for dehydrogenated of $2LiBH_4 + MgH_2$. Dehydrogenated under 3 bar(g) of Ar flowing at 100 ml / min whilst heating up to 450ºC at a rate of 2ºC / min.

According to Vajo et al. a mixed hydride system with this stoichiometry should dehydrogenate according to equation 11, giving lithium hydride (LiH) as a product of reaction. LiH is an ionic compound with a crystalline structure which should give relatively intense 2θ peaks at 38.2º, 44.4º and 64.5º in an XRD pattern. These peaks were not observed in the XRD pattern obtained for dehydrogenated samples of $2LiBH_4 + MgH_2$ (Figure 28). There is also an absence of MgB_2 peaks within Figure 28

which would be expected if dehydrogenation proceeded via equation 11 however because dehydrogenation took place under Ar rather than H_2, MgB_2 formation is unlikely to have occurred. The first and most intense peak produced occurs at 25.62° and is not due to either of the starting materials or a product of reaction. Peak number 1 at 25.62° is actually due to the tape used to secure the sample within its holder to avoid exposure to air and moisture. There is still a trace of MgH_2 present within the dehydrogenated sample indicated by peaks at 27.97° and 35.82°. Magnesium oxide is also still present within the dehydrogenated sample giving rise to the two peaks at 42.57° and 62.20°.

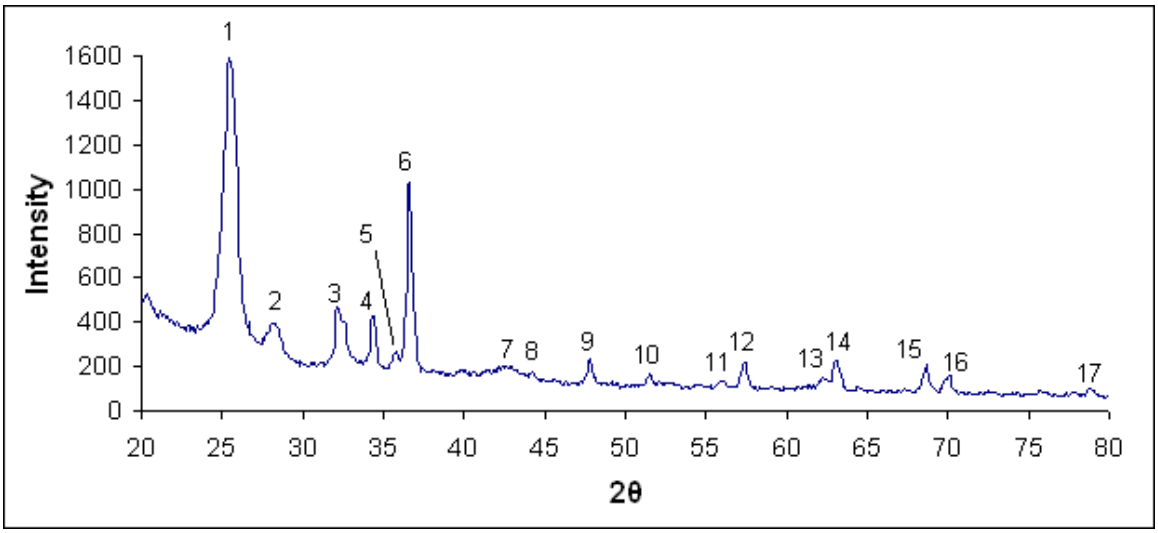

Figure 28) XRD analysis of dehydrogenated $2LiBH_4 + MgH_2$. Dehydrogenated under 3 bar(g) of Ar flowing at 100 ml / min whilst heating up to 450ºC at a rate of 2ºC / min.

Peak number	2θ value	d Spacing (Á)	Assignment
1	25.62	3.48	Tape
2	27.97	3.19	MgH_2
3	32.36	2.77	$Li_{0.184}Mg_{0.816}$
4	34.76	2.58	$Li_{0.184}Mg_{0.816}$
5	35.82	2.52	MgH_2
6	36.86	2.44	$Li_{0.184}Mg_{0.816}$
7	42.57	2.12	MgO
8	44.30	2.05	Unassigned
9	47.80	1.90	$Li_{0.184}Mg_{0.816}$
10	51.56	1.77	Unassigned
11	56.05	1.64	Unassigned
12	57.67	1.60	$Li_{0.184}Mg_{0.816}$
13	62.20	1.49	MgO
14	63.72	1.46	$Li_{0.184}Mg_{0.816}$
15	68.63	1.37	$Li_{0.184}Mg_{0.816}$
16	70.40	1.34	$Li_{0.184}Mg_{0.816}$
17	78.46	1.22	$Li_{0.184}Mg_{0.816}$

Table 12) XRD table for the first dehydrogenation of $2LiBH_4 + MgH_2$. Dehydrogenated under 3 bar(g) of Ar flowing at 100 ml / min whilst heating up to 450ºC at a rate of 2ºC / min.

There are two unassigned peaks at 51.56° and 56.05° but the remaining 2θ values are due to the formation of a $Li_{0.184}Mg_{0.816}$ alloy. The values obtained for the $Li_{0.184}Mg_{0.816}$

alloy coincide well with those obtained by Yu et al. X.Yu et al. produced a series of XRD patterns for the dehydrogenation of a $LiBH_4$ – MgH_2 sample (1:4 mass ratio) and suggested the presence of a $Li_{0.184}Mg_{0.816}$ alloy [45]. Yu et al commented that the 2θ values produced by the $Li_{0.184}Mg_{0.816}$ alloy formed during his investigation lie close to 2θ theta values expected for Mg but are dismissed as being the metal because the alloy peaks actually occur at slightly higher values of 2θ [45].

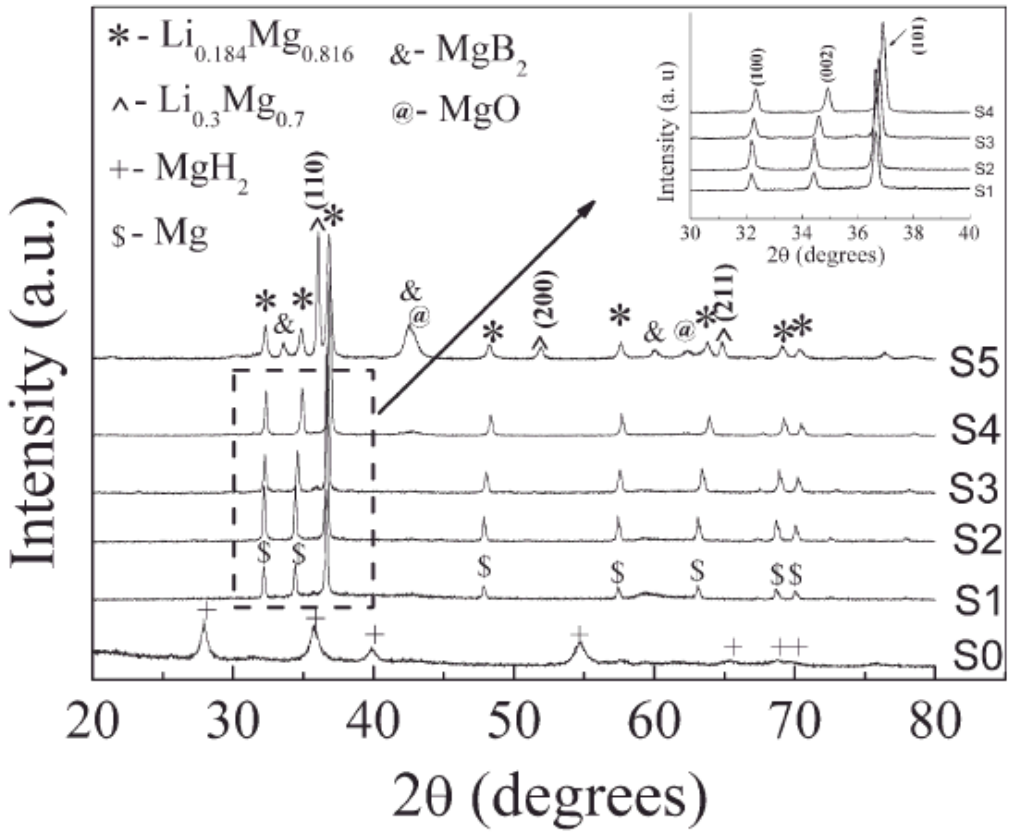

Figure 29) XRD pattern for $LiBH_4$ - MgH_2 (1:4 mass ratio) desorbed under 1 atm of Ar, up to 600ºC at 10ºC / min. Before dehydrogenation (S0), dehydrogenation up to 360ºC (S1), 405ºC (S2), 440ºC (S3), 500ºC (S4) and 600ºC (S5) [45]

5.2.3 Cycling of $2LiBH_4 + MgH_2$

$2LiBH_4$ + MgH_2 samples which were cycled through two dehydrogenations behaved differently to the first dehydrogenations in a number of ways. The largest difference

when compared to the first dehydrogenation is the amount of hydrogen released during the second attempted dehydrogenation. After milling $2LiBH_4$ + MgH_2 samples lose approximately 9.75 wt% when subjected to temperatures of up to 450ºC but after a recombination with hydrogen they only lost 2.2 wt% during dehydrogenation. This shows that the material does not recombine completely in 100 bar(g) of H_2 up to 450ºC, releasing just a fifth of the hydrogen it did for the first dehydrogenation for the same temperature range (Figure 30). It must be noted however that the second TGA data hadn't completely levelled off by the time 450°C had been reached indicating that more hydrogen may have been left within the system (Figure 31).

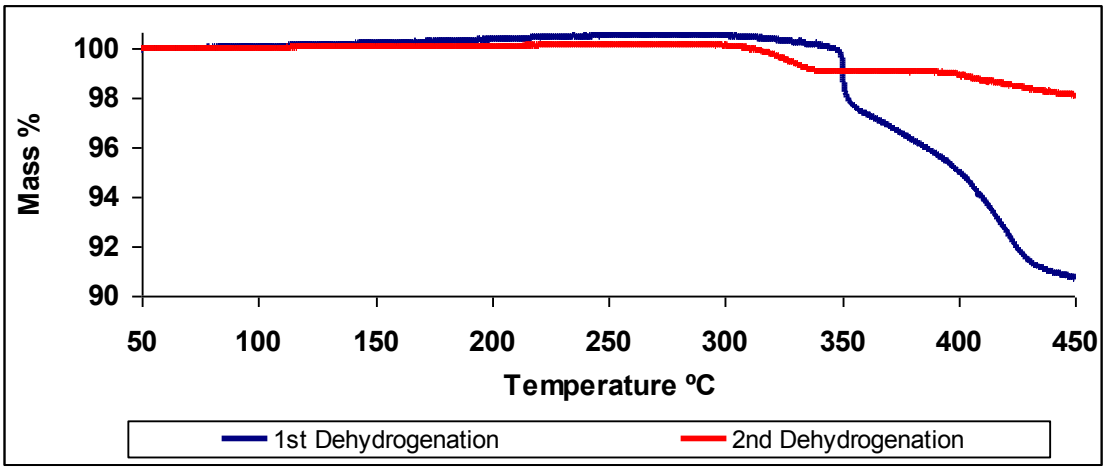

Figure 30) First and second TGA profiles for $2LiBH_4$ + MgH_2. First decomposition was obtained by dehydrogenating the sample under 0.5 bar(g) of Ar flowing at 40 ml / min whilst heating up to 450ºC. The second decomposition was then obtained by dehydrogenating a sample on the DSC under 3 bar(g) of Ar flowing at 100 ml / min up to 450ºC. After dehydrogenation the sample was then recombined on the DSC using 100 bar(g) of H_2 flowing at 100 ml / min whilst being heated to 450ºC. After recombination the sample was dehydrogenated again but this time on the TGA under 0.5 bar(g) of Ar flowing at 40 ml / min up to 450ºC. All heating was at 2ºC / min.

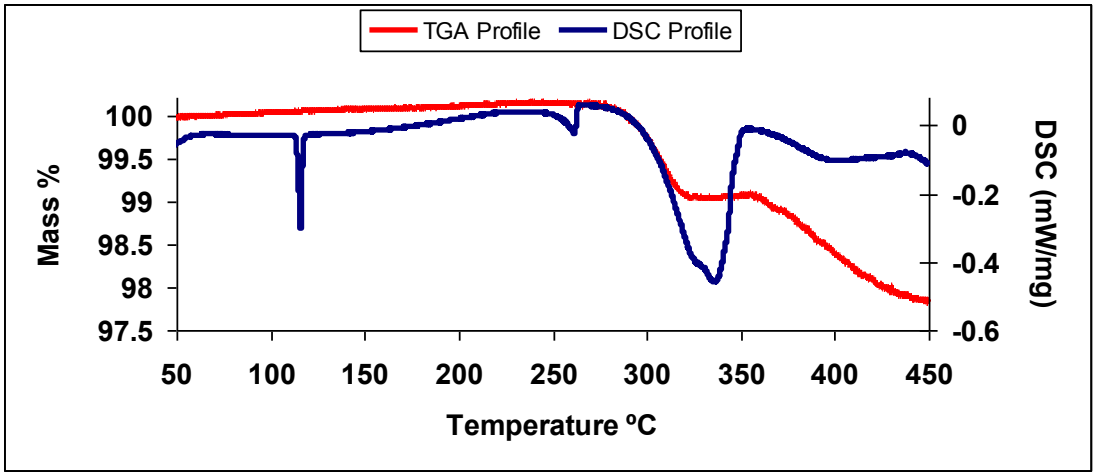

Figure 31) TGA and DSC data for the second dehydrogenation of $2LiBH_4 + MgH_2$. Two samples were firstly dehydrogenated on the DSC under 3 bar(g) of Ar flowing at 100 ml / min up to 450ºC, then recombined on the DSC using 100 bar(g) of H_2 flowing at 100 ml / min up to 450ºC. The second dehydrogenations for these samples were then carried out on the TGA under 0.5 bar(g) of Ar flowing at 40 ml / min up to 450ºC and on the DSC under 3 bar(g) of Ar flowing at 100 ml / min up to 450ºC. All heating was at 2ºC/min.

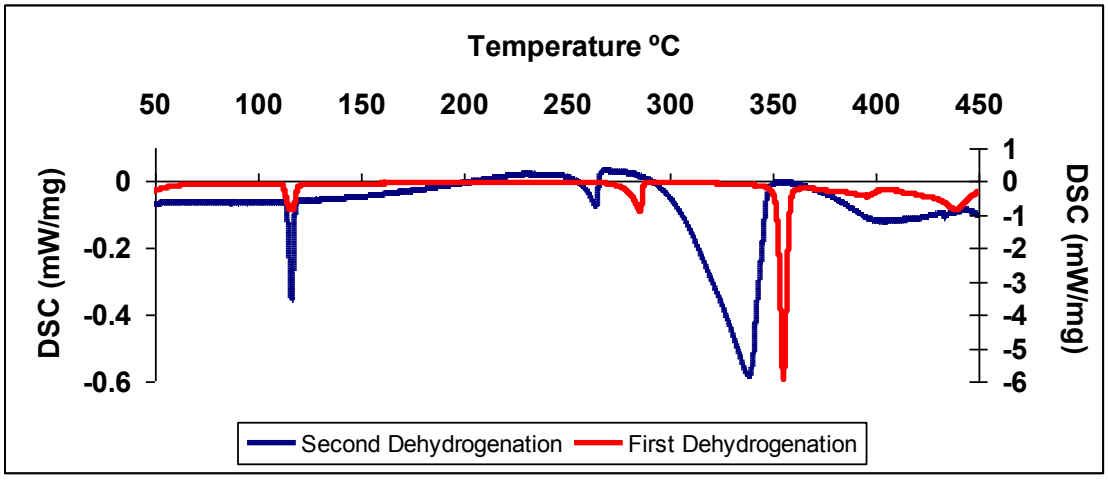

Figure 32) DSC profile of the first and second dehydrogenations of $2LiBH_4 + MgH_2$. Samples were firstly desorbed on the DSC under 3 bar(g) of Ar flowing at 100 ml / min up to 450ºC. The dehydrogenated sample was then recombined on the DSC with 100 bar(g) of H_2 flowing at 100 ml / min whilst heating to 450ºC. The sample was then dehydrogenated again on the DSC under 3 bar(g) of Ar flowing at 100 ml / min to 450ºC to yield the second decomposition profile. All heating was at 2ºC/min.

The DSC profile for the second dehydrogenations has also changed (Figure 32), with the peak associated with MgH_2 during the first decomposition, becoming much broader and starting at a lower temperature. The peak attributed to hydrogen release from MgH_2 begins almost instantly after $LiBH_4$ has melted, which as with the MgH_2 peak occurs at a lower temperature during the second run than it did in the first. The melting point of $LiBH_4$ peaks at 262ºC and MgH_2 decomposition begins shortly after this at approximately 275ºC. Hydrogen release from MgH_2 began at approximately 350ºC during the first run, which means a reduction of 75ºC in the dehydrogenation temperature of MgH_2 has been achieved. Although the removal of hydrogen from MgH_2 appears to now take longer than it did during its first dehydrogenation, the kinetics of the reaction appear improved, indicated by the reaction now beginning at a lower temperature during its second dehydrogenation.

The DSC peak associated with a release of hydrogen from $LiBH_4$ has also broadened, with only one peak apparently observed during the second dehydrogenations instead of the two observed during its first decomposition. Dehydrogenation from $LiBH_4$ begins after the decomposition of MgH_2 has finished at approximately 360ºC and therefore also begins slightly earlier during the second dehydrogenation.

Calculations have been made for the second dehydrogenations (Table 13) and show that these samples required significantly lower quantities of energy for the phase change and melting point of $LiBH_4$, when compared to the first decompositions. The amount of energy required to release one mole of hydrogen from the system however has increased by approximately 20 kJ when compared to the first set of dehydrogenations.

As the phase change of a material shouldn't differ by very much the phase change of $LiBH_4$ can be used to evaluate how much $LiBH_4$ has reformed during the recombination attempt of the decomposition products. We know from work carried out by Zuttel [55] that the phase change of $LiBH_4$ should be 4.18 KJ / mol $LiBH_4$ and by using this figure in conjunction with the enthalpy value obtained for the second dehydrogenation (0.73 kJ / mol $LiBH_4$) we can approximate recombination figures. The same is true for the enthalpy of fusion for $LiBH_4$ (7.56 KJ / mol $LiBH_4$).

Using the enthalpy values obtained for the phase change of the first and second dehydrogenations a figure of 16.59% is obtained. This means that 16.59% of the $LiBH_4$ we start with gets recombined during the first recombination attempt. The enthalpy of fusion data obtained for the first (6.72 kJ / mol H_2) and second dehydrogenation (0.90 kJ / mol H_2) results in a figure of 13.39% recombined during the first recombination attempt. These two values derived from the phase change and melting point of $LiBH_4$ are in good agreement and by taking the average of these two figures suggests that an average of 14.99% of the $LiBH_4$ started with gets recombined during the first recombination attempt.

Sample Mass (mg)	9.12	9.40	**Average**
Phase Change ($kJ / mol\ LiBH_4$)	0.70	0.76	**0.73**
Melting Point ($kJ / mol\ LiBH_4$)	0.86	0.93	**0.90**
MgH_2 Dehydrogenation ($kJ / mol\ H_2$)	44.59	41.81	**43.20**
$LiBH_4$ Dehydrogenation ($kJ / mol\ H_2$)	4.15	7.11	**5.63**
$kJ / mol\ H_2$ (2.2 wt.% H_2 released)	52.59	53.10	**52.85**

Table 13) Enthalpy values calculated from the DSC for the second dehydrogenations of $2LiBH_4 + MgH_2$. Samples were dehydrogenated on the DSC under 3 bar(g) of Ar flowing at 100 ml / min with heating up to 450ºC. Samples were then recombined under 100 bar(g) of H_2 flowing at 100 ml / min with heating up to 450ºC. Samples were then dehydrogenated for a second time on the DSC under 3 bar(g) of Ar flowing at 100 ml / min with heating up to 450ºC. All heating was done at a rate of 2ºC / min.

Recombination of the desorbed samples with hydrogen was also conducted and analysed with the aid of the DSC revealing that the first recombination has two exothermic peaks, one occurring at 267ºC and the other at 440ºC. These two exothermic peaks are likely due to the recombination of MgH_2 and $LiBH_4$ respectively. A second recombination attempt on this $2LiBH_2 + MgH_2$ material shows the first recombination peak is no longer present, suggesting that the recombination mechanism may have changed or that the reaction no longer takes place.

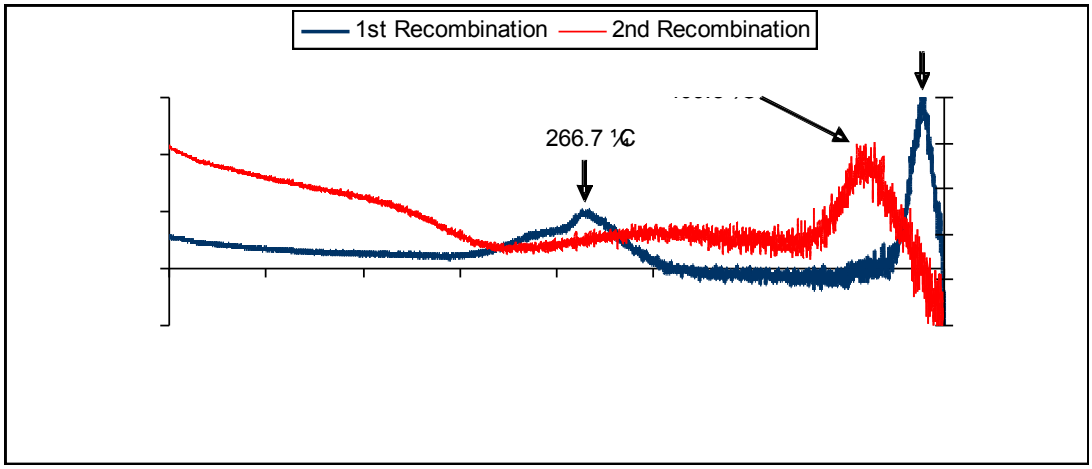

Figure 33) DSC data for the first and second recombinations of $2LiBH_4 + MgH_2$. For the first recombination samples were dehydrogenated on the DSC using 3 bar(g) of Ar flowing at 100 ml / min whilst heating up to 450ºC. The sample was then recombined under 100 bar(g) of H_2 flowing at 100 ml / min by heating up to 450 ºC. For the second recombination the sample was dehydrogenated and recombined again using the same conditions employed for the first dehydrogenation and recombination. All heating was at 2ºC / min.

Recombined samples were also studied with both FTIR and XRD to determine if any structural changes resulted from the samples being dehydrogenated and then recombined with hydrogen. Reversibly reacting, the dehydrogenation products with hydrogen back to the starting materials is an important requirement of a destabilized system and the reformation of IR peaks found in the as milled material, suggests that the starting materials have in fact been reformed to some degree.

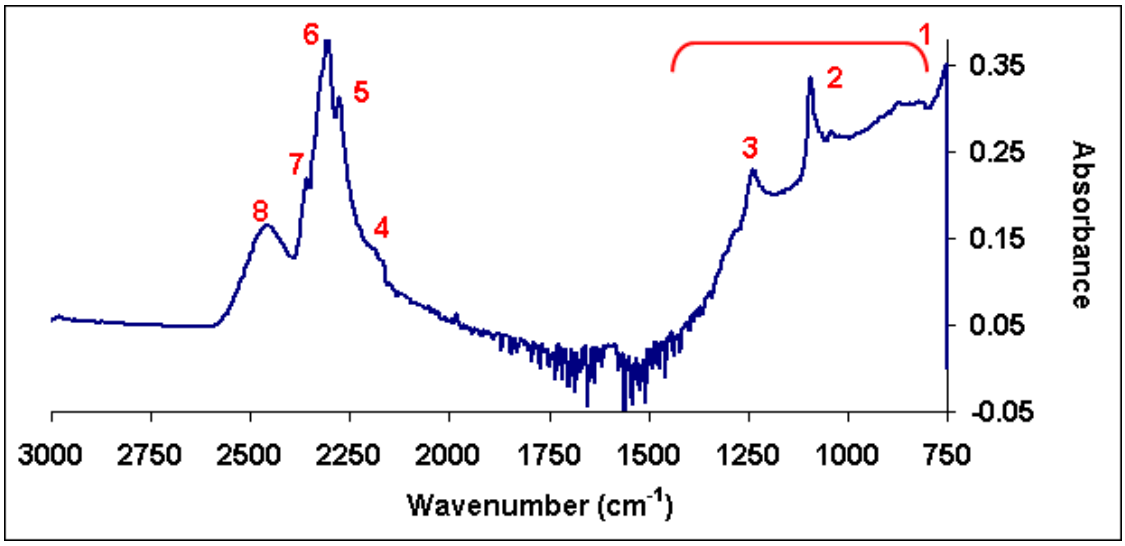

Figure 34) FTIR profile of the first recombination for $2LiBH_4 + MgH_2$. Samples were dehydrogenated on the DSC under 3 bar(g) of Ar flowing at 100 ml/min with heating to 450ºC. Samples were then recombined using 100 bar(g) of H_2 flowing at 100 ml / min with heating up to 450ºC. All heating was done at a rate of 2ºC / min.

Peak	Wavenumber (cm^{-1})	Assignment [52]	Internal Change	Material
1	790 - 1400		Mg – H Stretch	MgH_2
2	1090	υ_4	B – H Bending	$LiBH_4$
3	1230	$3\upsilon_L$		$LiBH_4$
4	2165	$2^{10}\upsilon_4$	B – H Stretching	$LiBH_4$
5	2275	υ_3		$LiBH_4$
6	2300	υ_3'		$LiBH_4$
7	2345	υ_3''		$LiBH_4$
8	2440		In Phase Breathing	$Li_2B_{12}H_{12}$

Table 14) FTIR table for the first recombination of $2LiBH_4 + MgH_2$. Samples were dehydrogenated on the DSC under 3 bar(g) of Ar flowing at 100 ml/min with heating to 450ºC. Samples were then recombined using 100 bar(g) of H_2 flowing at 100 ml / min with heating up to 450ºC. All heating was done at a rate of 2ºC / min.

In addition to the IR peaks which have resulted from reforming the starting materials, there is a new IR peak present within the spectra occurring at 2440 cm^{-1} (compare with Figure 20). Cycling the $2LiBH_4 + MgH_2$ material through two dehydrogenations and two

recombinations again produces this IR peak at 2445 cm^{-1} indicating that this could be a permanent change occurring within the material after the first dehydrogenation.

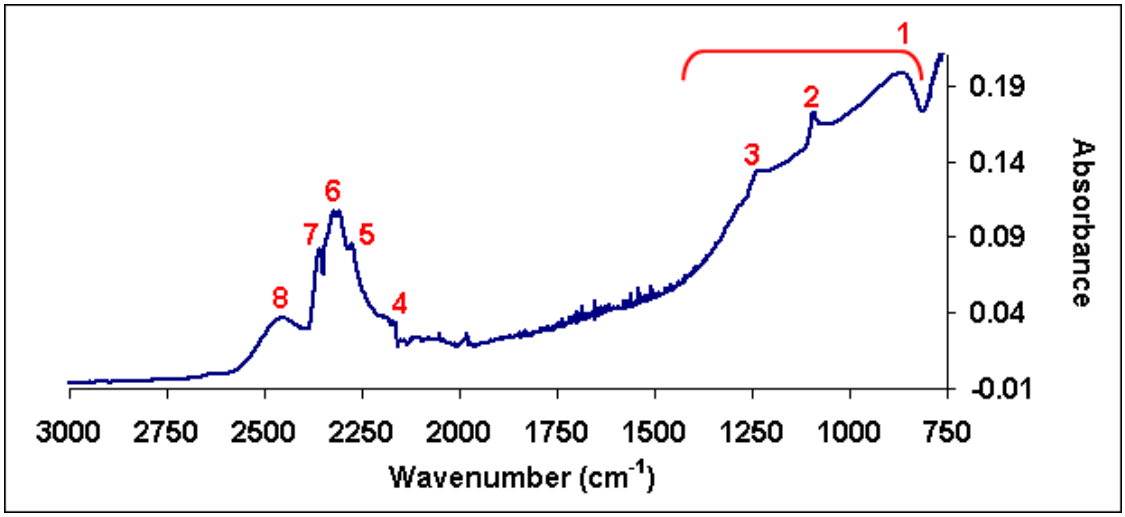

Figure 35) FTIR profile of twice recombined $2LiBH_4 + MgH_2$. The sample was dehydrogenated twice on the DSC under 3 bar(g) of Ar flowing at 100 ml / min with heating up to 450ºC. After the dehydrogenations samples were recombined using 100 bar(g) of H_2 flowing at 100 ml / min up to 450ºC. All heating was at 2ºC / min.

Peak	Wavenumber (cm^{-1})	Assignment [52]	Internal Change	Material
1	790 - 1400		Mg – H Stretch	MgH_2
2	1085	υ_4	B – H Bending	$LiBH_4$
3	1225	$3\upsilon_L$		$LiBH_4$
4	2160	$2^{10}\upsilon_4$	B – H Stretching	$LiBH_4$
5	2275	υ_3		$LiBH_4$
6	2305	υ_3'		$LiBH_4$
7	2355	υ_3''		$LiBH_4$
8	2445		In phase Breathing	$Li_2B_{12}H_{12}$

Table 15) FTIR table for twice recombined $2LiBH_4 + MgH_2$. The sample was dehydrogenated twice on the DSC under 3 bar(g) of Ar flowing at 100 ml / min with heating up to 450ºC. After the dehydrogenations samples were recombined using 100 bar(g) of H_2 flowing at 100 ml / min up to 450ºC. All heating was at 2ºC / min.

The IR peak occurring at 2440 cm^{-1} and 2445 cm^{-1} has been seen by researchers studying the decomposition products of pure $LiBH_4$ and concluded that this IR activity was due to a $Li_2B_{12}H_{12}$ complex [56]. During the investigation carried out by Muetterties et al. this peak was observed during decomposition of $LiBH_4$ however the IR peak observed at ~2445 cm^{-1} during this study was only seen during the recombination attempts. A peak should also be present at 1070 cm^{-1} according to Muetterties et al if $Li_2B_{12}H_{12}$ is present but due to the position of the MgH_2 signal (790 – 1400 cm^{-1}) this 1070 cm^{-1} peak would be overshadowed if present.

If the new IR peaks which arise for the recombined and twice cycled samples are due to the formation of a crystalline phase then evidence for this would be expected in the XRD data of the recombined samples. The XRD data for the first recombination (Figure 36) reveals a 2θ value occurring at 25.88º which arises due to the presence of the tape used to secure the recombined sample within its sample holder during analysis. MgH_2 and MgO peaks are shown to be present providing evidence to support the FTIR results which suggest successful reformation of the starting materials. No evidence was found within the XRD pattern however for the reformation of $LiBH_4$. There are two small unassigned peaks occurring at 38.02° and 44.20° but other than these the remaining peaks can be attributed to the $Li_{0.184}Mg_{0.816}$ alloy that was formed during dehydrogenation. As all but two small signals can be identified in the XRD pattern it is unlikely that the material responsible for the IR peak at 2445 cm^{-1} is crystalline.

For the twice cycled sample (Figure 37) the large peak at 25.73° is again due to the tape that has been used to secure the sample. Magnesium hydride and oxide are once again present suggesting recombination of the starting materials has occurred but no evidence for the reformation of $LiBH_4$ is present. The two peaks that arise at 32.51° and 36.63°

occur due to left over $Li_{0.184}Mg_{0.816}$ alloy. It should be noted that there are less $Li_{0.184}Mg_{0.816}$ alloy peaks remaining during the second recombination than there was during the first. As with the first recombination effort, because all of the peaks can be assigned to compounds other than $Li_2B_{12}H_{12}$, if the IR peak is due to this material it is unlikely that $Li_2B_{12}H_{12}$ is highly crystalline in nature.

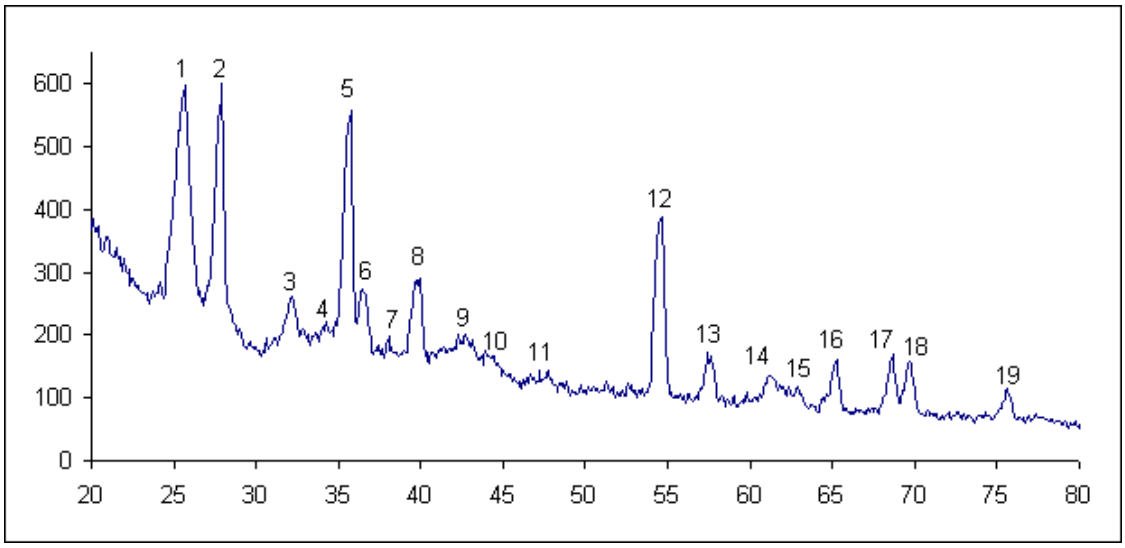

Figure 36) XRD analysis of the first recombination for $2LiBH_4 + MgH_2$. The sample was dehydrogenated under 3 bar(g) of Ar flowing at 100 ml / min whilst heating up to 450ºC and then recombined under 100 bar(g) of H_2 flowing at 100 ml / min whilst heating up to 450ºC. Heating was carried out at a rate of 2ºC / min.

Peak number	2θ value	d Spacing (Å)	Assignment
1	25.88	3.44	Tape
2	27.98	3.19	MgH_2
3	32.16	2.78	$Li_{0.184}Mg_{0.816}$
4	34.25	2.62	$Li_{0.184}Mg_{0.816}$
5	35.81	2.51	MgH_2
6	36.35	2.47	$Li_{0.184}Mg_{0.816}$
7	38.02	2.37	Unassigned
8	40.00	2.25	MgH_2
9	42.66	2.12	MgO
10	44.20	2.05	Unassigned
11	47.77	1.90	$Li_{0.184}Mg_{0.816}$
12	54.65	1.68	MgH_2
13	57.78	1.60	MgH_2
14	61.24	1.51	MgO
15	63.02	1.48	MgH_2
16	65.22	1.43	MgH_2
17	68.67	1.37	MgH_2
18	69.66	1.35	MgH_2
19	75.67	1.26	MgH_2

Table 16) XRD table for the first recombination effort of $2LiBH_4 + MgH_2$. The sample was dehydrogenated under 3 bar(g) of Ar flowing at 100 ml / min whilst heating up to 450ºC and then recombined under 100 bar(g) of H_2 flowing at 100 ml / min whilst heating up to 450ºC. Heating was carried out at a rate of 2ºC / min.

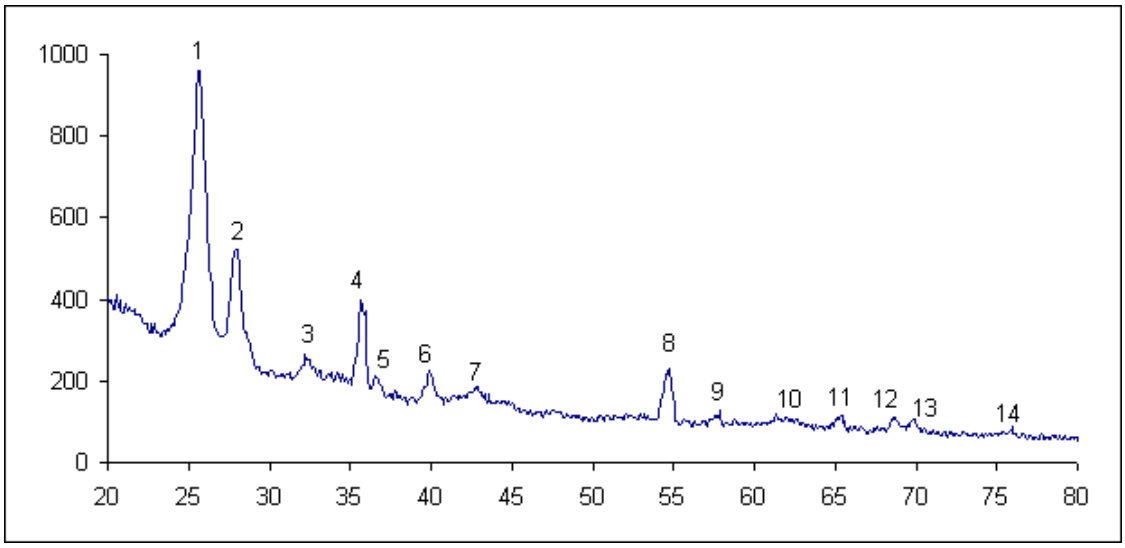

Figure 37) XRD analysis of twice recombined $2LiBH_4 + MgH_2$. The sample was dehydrogenated twice on the DSC under 3 bar(g) of Ar flowing at 100 ml / min with heating up to 450ºC and recombined twice under 100 bar(g) of H_2 flowing at 100 ml / min up to 450ºC. All heating was done at 2ºC / min.

Peak number	2θ value	d Spacing (Å)	Assignment
1	25.73	3.45	Tape
2	28.00	3.21	MgH_2
3	32.51	2.77	$Li_{0.184}Mg_{0.816}$
4	35.82	2.50	MgH_2
5	36.63	2.46	$Li_{0.184}Mg_{0.816}$
6	39.99	2.26	MgH_2
7	42.68	2.11	MgO
8	54.45	1.68	MgH_2
9	57.57	1.59	MgH_2
10	62.07	1.50	MgO
11	65.33	1.43	MgH_2
12	68.74	1.37	MgH_2
13	69.80	1.35	MgH_2
14	75.76	1.25	MgH_2

Table 17) XRD table for the second recombination of $2LiBH_4 + MgH_2$. The sample was dehydrogenated twice on the DSC under 3 bar(g) of Ar flowing at 100 ml / min with heating up to 450ºC and recombined twice under 100 bar(g) of H_2 flowing at 100 ml / min up to 450ºC. All heating was done at 2ºC / min.

5.3 $LiBH_4 + 2MgH_2$

5.3.1 As milled $LiBH_4 + 2MgH_2$

In the as milled $LiBH_4 + 2MgH_2$ material, the FTIR peaks associated with $LiBH_4$ are not as sharp as for the $2LiBH_4 + MgH_2$ material, due to the reduced amount of $LiBH_4$ within the sample. The IR activity of MgH_2 is still noticeably present with its peak beginning at 790 cm^{-1} and ending at 1400 cm^{-1}, which was also observed for as received MgH_2 (Figure 16) and as milled $2LiBH_4 + MgH_2$ (Figure 20).

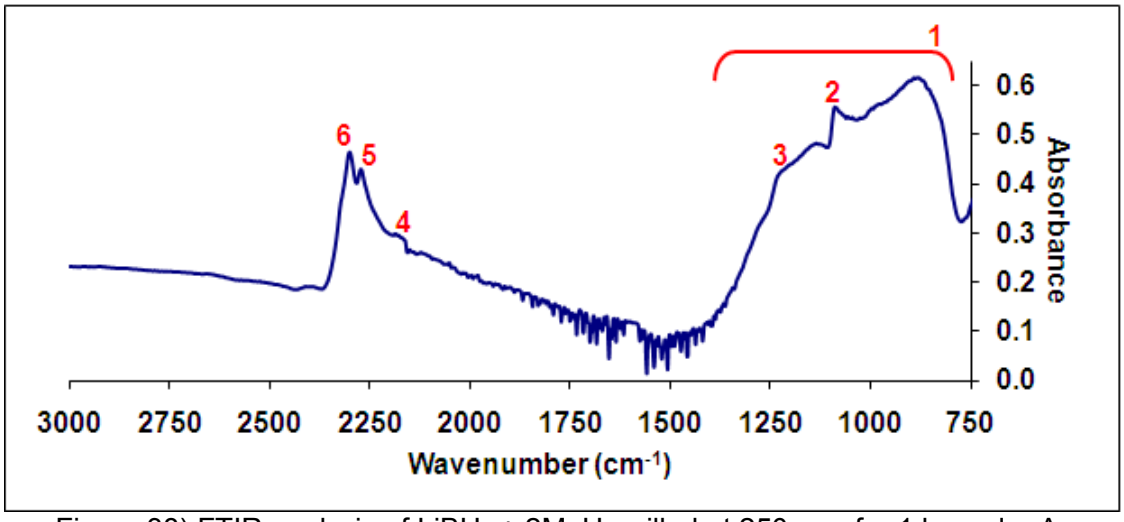

Figure 38) FTIR analysis of $LiBH_4 + 2MgH_2$ milled at 250 rpm for 1 hr under Ar

Peak	Wavenumber (cm^{-1})	Assignment [52]	Internal Change	Material
1	790 – 1400		Mg – H Stretch	MgH_2
2	1070	υ_4	B – H Bending	$LiBH_4$
3	1205	$3\upsilon_L$		$LiBH_4$
4	2160	$2^{10}\upsilon_4$	B – H Stretching	$LiBH_4$
5	2265	υ_3		$LiBH_4$
6	2295	υ_3'		$LiBH_4$

Table 18) FTIR table for $LiBH_4 + 2MgH_2$ milled at 250 rpm for 1 hr under Ar

The first peak observed in the XRD pattern of $LiBH_4$ + $2MgH_2$ is again due to the tape that was employed to secure the sample and ensure it did not get exposed to any air or moisture before it was analysed. The majority of the peaks can be assigned to the presence of MgH_2 but there are three peaks which arise that are not linked to this material. Those three peaks occur at 2θ values of 32.20°, 34.47° and 36.61° and arise due to the formation of a $Li_{0.184}Mg_{0.816}$ alloy during the milling process. This was not observed during the milling process of $2LiBH_4$ + MgH_2 (Figure 21).

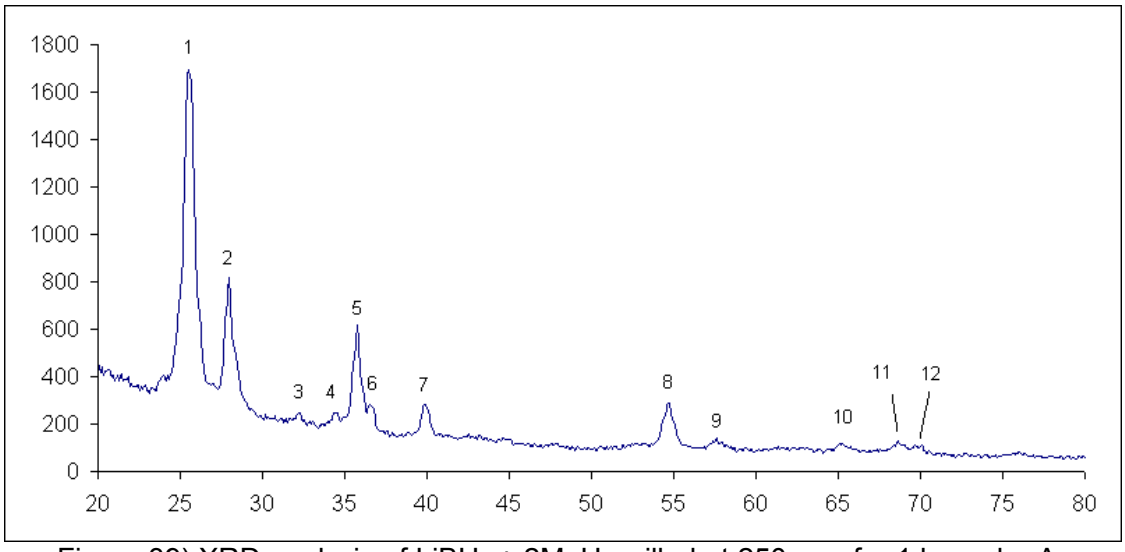

Figure 39) XRD analysis of $LiBH_4$ + $2MgH_2$ milled at 250 rpm for 1 hr under Ar

Peak number	2θ value	D Spacing (Å)	Assignment
1	25.53	3.49	Tape
2	27.94	3.19	MgH_2
3	32.20	2.78	$Li_{0.184}Mg_{0.816}$
4	34.47	2.60	$Li_{0.184}Mg_{0.816}$
5	35.75	2.51	MgH_2
6	36.61	2.46	$Li_{0.184}Mg_{0.816}$
7	39.89	2.26	MgH_2
8	54.67	1.68	MgH_2
9	57.59	1.60	MgH_2
10	65.25	1.43	MgH_2
11	68.69	1.37	MgH_2
12	69.77	1.35	MgH_2

Table 19) XRD table for $LiBH_4$ +$2MgH_2$ milled at 250 rpm for 1 hr under Ar

5.3.2 First Dehydrogenation of $LiBH_4 + 2MgH_2$

A $LiBH_4 + 2MgH_2$ sample is capable of holding a maximum of 10.75 wt% H_2 which is reduced to 9.41 wt% H_2 with the assumption that LiH is formed as a product of dehydrogenation. TGA analysis for the first removal of hydrogen from this sample reveals that a total of 8 wt% H_2 is lost up to a temperature of 450ºC. The failure to release the remaining 1.41 wt% may be due to higher temperatures required for the dehydrogenation of $LiBH_4$ or it could be due to a loss of hydrogen occurring as a result of the milling process.

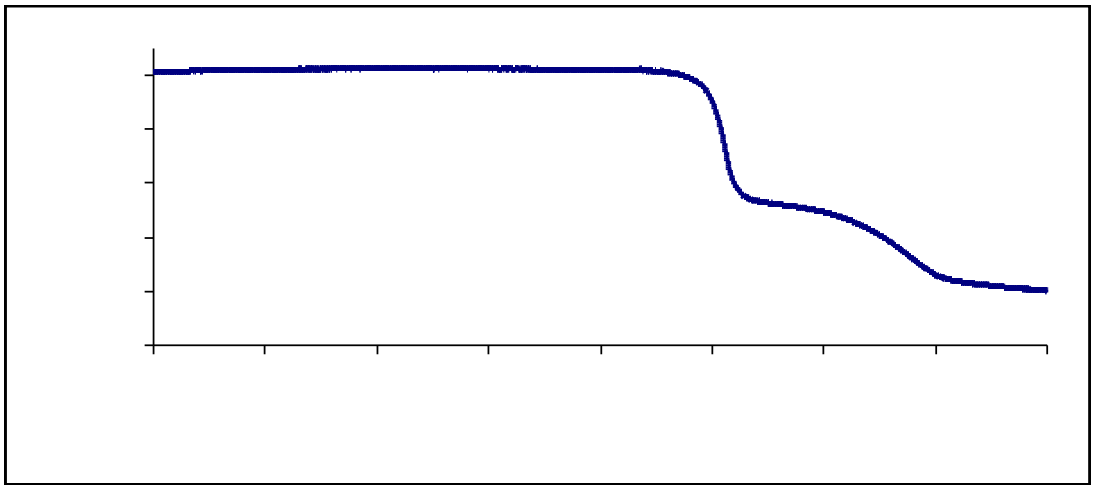

Figure 40) TGA analysis for the dehydrogenation of $LiBH_4 + 2MgH_2$. The sample was dehydrogenated under 0.5 bar(g) of Ar flowing at 40 ml / min while heating up to 450ºC at 2ºC / min.

The first loss of hydrogen begins at approximately 275ºC and corresponds to a mass loss of 4.5 wt% by the time 320ºC is reached. The MgH_2 portion of this sample is expected to account for 5.37 wt% of the hydrogen available and therefore indicates that less than 1 wt% H_2 remains unaccounted for (wrt the theoretical maximum). Increasing the MgH_2 content of this mixed hydride system has reduced the onset temperature for hydrogen release by 75ºC when compared to the $2LiBH_4 + MgH_2$ sample which began

desorbing hydrogen at 350ºC. The second loss of mass which released 3.5 wt% between 320ºC and 450ºC has also seen a reduction in the temperature at which hydrogen is released. The second release of mass from $2LiBH_4 + MgH_2$ began at approximately 365ºC while this samples' second release of mass begins at 320ºC, a reduction of 45ºC.

Mass spectrometry data obtained from the gas stream of a dehydrogenating $LiBH_4 + 2MgH_2$ sample supports the TGA results which indicate that this sample releases hydrogen in two stages. As with the mass spectroscopy data gained from the $2LiBH_4 + MgH_2$ sample, a sharp signal appears first, shortly followed by a smaller broader signal. No diborane was detected in the gas stream of this sample like it was for $2LiBH_4 + MgH_2$.

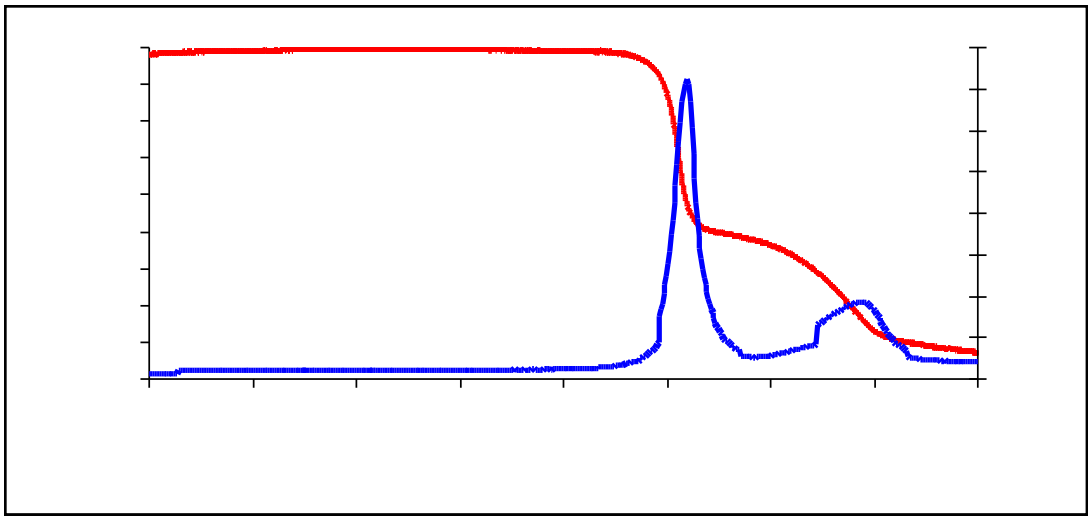

Figure 41) TGA and Hydrogen mass spectroscopy data for $LiBH_4 + 2MgH_2$. The sample was dehydrogenated under 0.5 bar(g) of Ar flowing at 40 ml / min whilst heating up to 450ºC at 2ºC / min

DSC analysis of this sample reveals four endothermic peaks (Figure 42), which were also observed during the dehydrogenation of $2LiBH_4 + MgH_2$. The first two peaks

correspond to the phase change (118ºC) and melting point (287ºC) of $LiBH_4$ respectively. The reduction in onset temperature of MgH_2 has caused the third DSC peak to become incorporated into the second DSC peak produced by the melting point of $LiBH_4$. The final DSC peak which arises due to a release of hydrogen from $LiBH_4$ appears to be just one peak but further analysis of this peak reveals that it is in fact composed of at least three endothermic events.

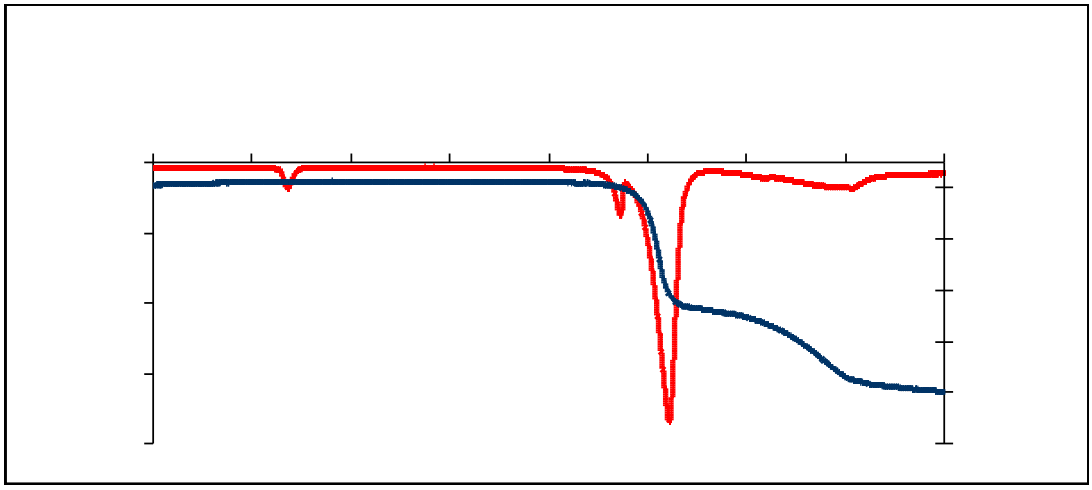

Figure 42) DSC and TGA profile of $LiBH_4$ + $2MgH_2$. TGA data was obtained by dehydrogenating under 0.5 bar(g) Ar flowing at 40 ml / min while heating up to 450ºC at 2ºC / min. DSC data was obtained by dehydrogenating into 3 bar(g) of Ar flowing at 100 ml / min whist heating to 450ºC at a heating rate of 2ºC/min

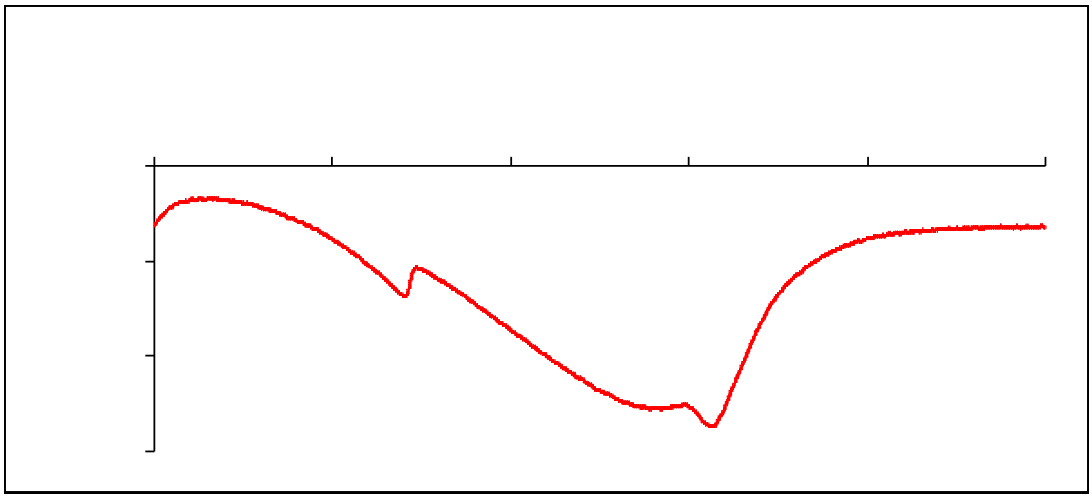

Figure 43) Expanded view of the fourth endothermic peak produced by dehydrogenating a $LiBH_4 + 2MgH_2$ sample. Taken from Figure 41

The energy required for these endothermic steps has been calculated (Table 20). These figures reveal that the energy required for the phase change and melting point of $LiBH_4$ are lower than energy values obtained during the first dehydrogenation of $2LiBH_4 + MgH_2$. The energy required to remove hydrogen from MgH_2 is also lower for this stoichiometry than it was for the first sample studied. In contrast to these reduced enthalpy values, the energy required for the removal of hydrogen from $LiBH_4$ has increased when compared to the first sample and so has the overall enthalpy of reaction.

Because the enthalpy value for the phase change and melting point of $LiBH_4$ wouldn't be expected to change just because of it's stoichiometry the difference between the value obtained (3.93 kJ / mol $LiBH_4$) and the expected value (4.18 kJ / mol $LiBH_4$) can be used to determine how much $LiBH_4$ remains within the sample up to 450°C. By factoring 3.93 kJ / mol $LiBH_4$ up to the expected 4.18 kJ / mol $LiBH_4$ it can be approximated that 5.98% of the $LiBH_4$ we started with is lost. This 5.98% may either still be in the sample unreacted or was lost during decomposition as a result of the milling process, or a combination of the two.

The same can be done for the enthalpy of fusion which would not be expected to deviate far from the value of 7.56 kJ / mol $LiBH_4$. When the average value for the enthalpy of fusion obtained from this investigation (4.83 kJ / mol $LiBH_4$) is factored up to the expected enthalpy change (7.56 kJ / mol $LiBH_4$) it can be estimated that only 63.89% of the $LiBH_4$ material we started with went through the phase change. This is means that 36.11% of the material is unaccounted for. This is a big difference to the 5.98% we found unaccounted for when using the phase change enthalpy to perform these calculations. One reason for this may be due to the melting point of $LiBH_4$ occurring at a higher temperature than the phase change and some of the $LiBH_4$ may react with MgH_2 during melting.

Sample Mass (mg)	13.90	5.90	6.25	8.91	12.13	11.00	11.30	9.70	**Average**
Phase Change (kJ / mol $LiBH_4$)	3.680	4.020	4.003	4.121	3.911	4.148	4.199	3.355	**3.93**
Melting Point (kJ / mol $LiBH_4$)	4.486	5.137	5.185	5.176	4.781	4.818	5.012	4.039	**4.83**
MgH_2 Dehydrogenation (kJ / mol H_2)	29.38	33.03	33.53	32.89	30.76	31.07	34.07	27.95	**31.58**
$LiBH_4$ Dehydrogenation (kJ / mol H_2)	6.65	6.52	6.36	7.58	7.14	6.99	7.58	6.54	**6.92**
kJ / mol H_2 (Assuming 8wt.% H_2)	38.63	42.47	42.82	43.44	40.67	40.92	44.59	36.85	**41.30**

Table 20) Enthalpy values calculated for the first dehydrogenation of $LiBH_4$ + $2MgH_2$. Calculated from DSC data obtained under 3 bar(g) of Ar flowing at 100 ml / min whilst heating up to 450ºC at 2ºC / min.

FTIR analysis of dehydrogenated $LiBH_4$ + $2MgH_2$ revealed that there were no IR active bonds present within the samples after heating the samples to 450ºC. This would suggest that dehydrogenation had occurred to completion releasing all of the available hydrogen from this sample.

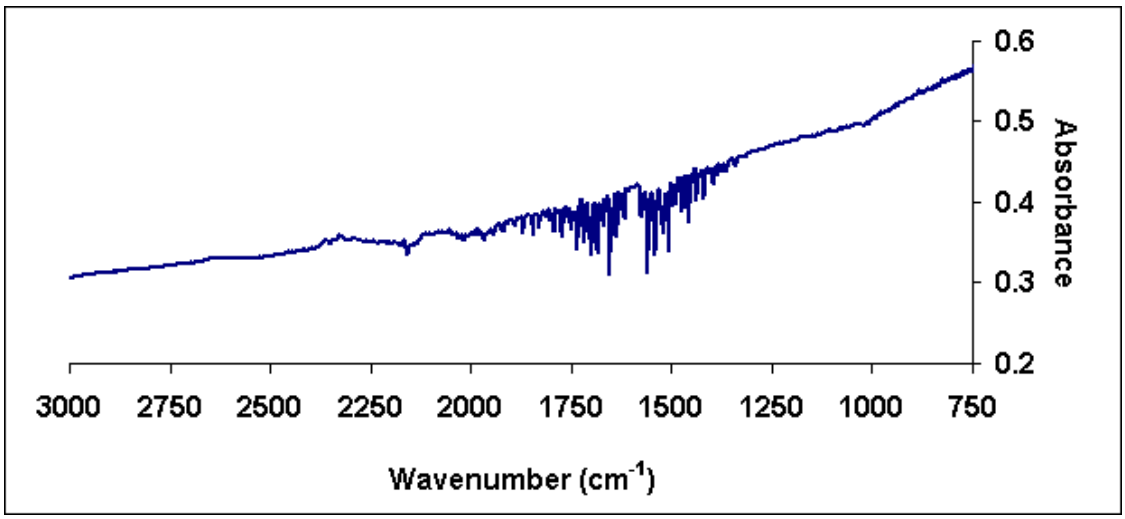

Figure 44) FTIR spectra produced by a dehydrogenated sample of $LiBH_4$ + $2MgH_2$. Dehydrogenated in 3 bar(g) of Ar flowing at 100 ml / min whilst heating up to 450ºC at a heating rate of 2ºC / min.

Wavenumber (cm^{-1})	Assignment
No Peaks	NA

Table 21) FTIR table for the dehydrogenation of $LiBH_4$ + MgH_2

Although the FTIR of the dehydrogenated sample reveals no presence of the starting materials the XRD pattern produced for the dehydrogenated of $LiBH_4$ + $2MgH_2$ reveals something different. The peak at 25.63° is due to the tape used to mount the sample but the remaining peaks can be assigned to traces of MgH_2, MgO and the formation of $Li_{0.184}Mg_{0.816}$. The presence of MgH_2 peaks would indicate that not all of the starting material has been dehydrogenated. One peak remains unassigned occurring at a 2θ value of 51.56°.

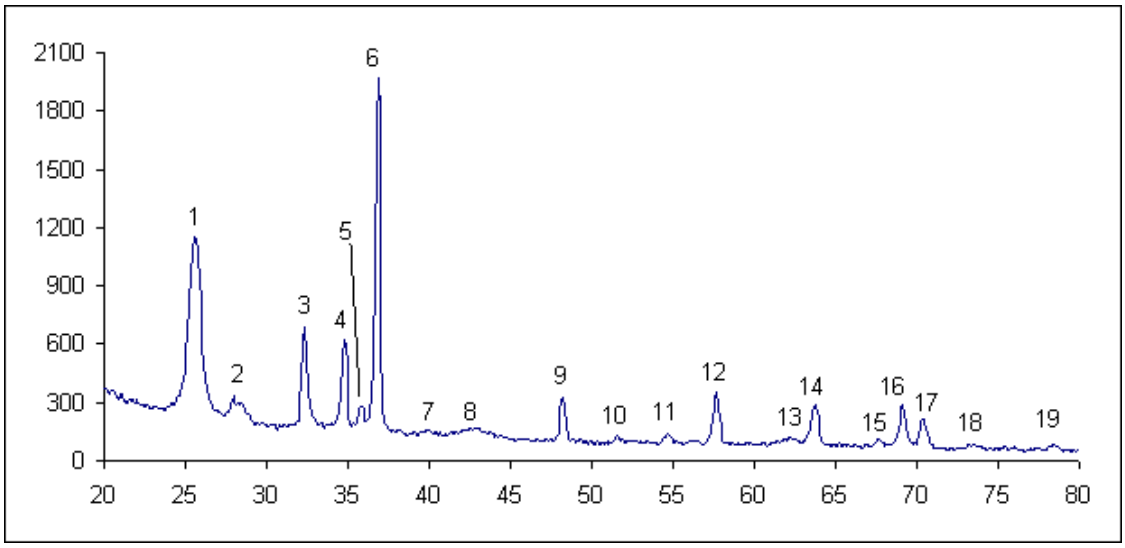

Figure 45) XRD data obtained for a dehydrogenated sample of $LiBH_4$ + $2MgH_2$. Sample was dehydrogenated under 3 bar(g) of Ar flowing at 100 ml / min whilst heating up to 450ºC at 2ºC / min.

Peak number	2θ value	d Spacing (Å)	Assignment
1	25.63	3.48	Tape
2	27.97	3.19	MgH_2
3	32.36	2.77	$Li_{0.184}Mg_{0.816}$
4	34.76	2.58	$Li_{0.184}Mg_{0.816}$
5	35.82	2.51	MgH_2
6	36.86	2.44	$Li_{0.184}Mg_{0.816}$
7	39.89	2.26	MgH_2
8	43.02	2.10	MgO
9	48.23	1.89	$Li_{0.184}Mg_{0.816}$
10	51.56	1.77	Unassigned
11	54.70	1.68	MgH_2
12	57.67	1.60	$Li_{0.184}Mg_{0.816}$
13	62.20	1.49	MgO
14	63.72	1.46	$Li_{0.184}Mg_{0.816}$
15	67.67	1.39	$Li_{0.184}Mg_{0.816}$
16	69.13	1.36	$Li_{0.184}Mg_{0.816}$
17	70.40	1.34	$Li_{0.184}Mg_{0.816}$
18	73.43	1.29	$Li_{0.184}Mg_{0.816}$
19	78.46	1.22	$Li_{0.184}Mg_{0.816}$

Table 22) XRD table for dehydrogenated $LiBH_4$ +$2MgH_2$. Sample was dehydrogenated under 3 bar(g) of Ar flowing at 100 ml / min whilst heating up to 450ºC at 2ºC / min.

5.3.3 Cycling of $LiBH_4 + 2MgH_2$

TGA analyses for the second dehydrogenations of $LiBH_4 + 2MgH_2$ revealed that this sample underwent cycling much better than the $2LiBH_4 + MgH_2$ samples studied (compare Figures 47 and 31). The first dehydrogenations for $LiBH_4 + 2MgH_2$ released approximately 8 wt% and the second dehydrogenations released a total of 5.5 wt%. The MgH_2 part of the TGA profile appears to have been unaffected by the recombination attempt made on this sample but the $LiBH_4$ part is significantly reduced suggesting incomplete recombination. As with the TGA profile for the second dehydrogenation of $2LiBH_4 + MgH_2$ it should be noted that the second TGA curve of $LiBH_4 + 2MgH_2$ has not levelled of by 450°C either. This again would suggest that there is further hydrogen left within the system available for dehydrogenation (Figure 47). The first mass loss recorded at 4.8 wt% is higher than the first loss of mass from the first decomposition making it closer to the theoretical amount of hydrogen that can be stored by Mg in this sample.

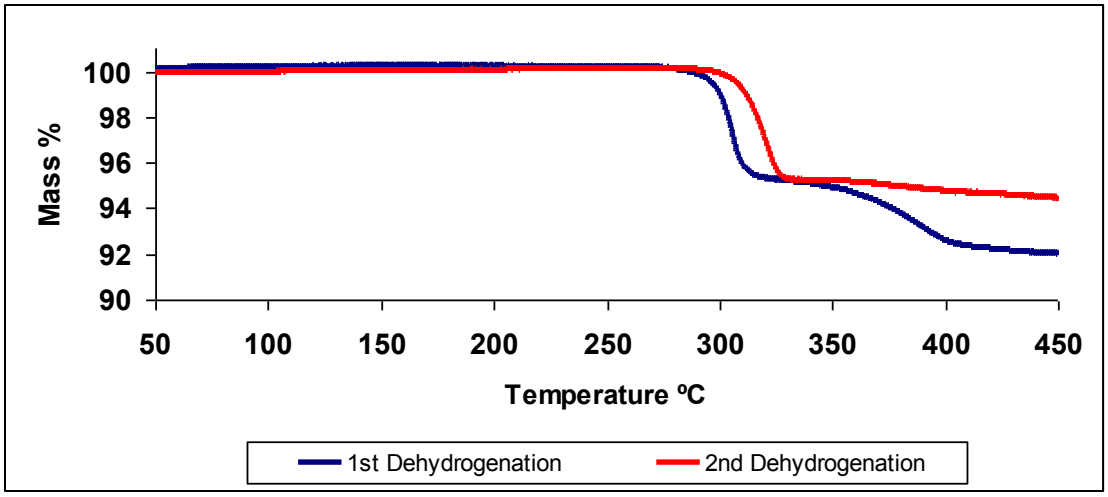

Figure 46) First and second TGA profiles for $LiBH_4$ + $2MgH_2$. First decomposition was obtained by dehydrogenating under 0.5 bar(g) of Ar flowing at 40 ml / min whilst heating up to 450ºC. The second decomposition was then obtained by dehydrogenating a sample on the DSC under 3 bar(g) of Ar flowing at 100 ml / min whilst heating up to 450ºC. The sample was then recombined using 100 bar(g) of H_2 flowing at 100 ml / min up to 450ºC on the DSC. After recombination the sample was then dehydrogenated again but this time on the TGA with 0.5 bar(g) of Ar flowing at 40 ml / min up to 450ºC. All heating was at 2ºC / min.

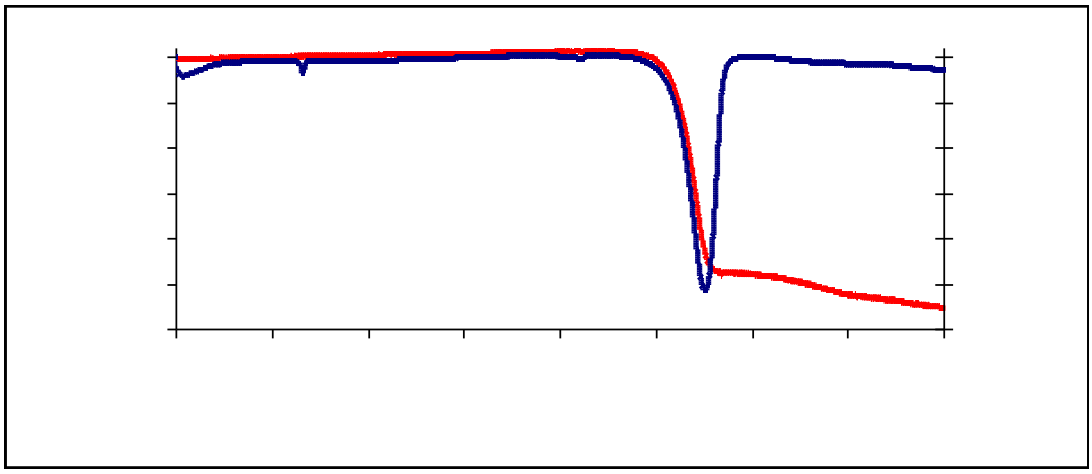

Figure 47) TGA and DSC data for the second dehydrogenations of $LiBH_4$ + $2MgH_2$. Two samples were firstly dehydrogenated on the DSC under 3 bar(g) of Ar flowing at 100 ml / min while heating up to 450ºC, then recombined on the DSC under 100 bar(g) of H_2 flowing at 100 ml / min while heating up to 450ºC. One of these samples was then dehydrogenated on the TGA under 0.5 bar(g) of Ar flowing at 40 ml / min whilst heating up to 450ºC and the other was dehydrogenated on the DSC using 3 bar(g) of Ar flowing at 100 ml / min while heating up to 450ºC. All heating was at 2ºC / min.

The second dehydrogenation of $LiBH_4$ + $2MgH_2$ results in the melting point of $LiBH_4$ occurring earlier than it did during the first dehydrogenation, separating it from the MgH_2 DSC peak. The onset of the MgH_2 DSC peak begins at approximately 295ºC which is slightly later than that observed during the first dehydrogenation and also finishes later at 350ºC. The suggestion that $LiBH_4$ may not have completely reformed while heated under 100 bar H_2, is supported by an expanded view of the second dehydrogenation DSC curve between 325ºC and 450ºC, which appears quite different when compared to the first (Figure 49).

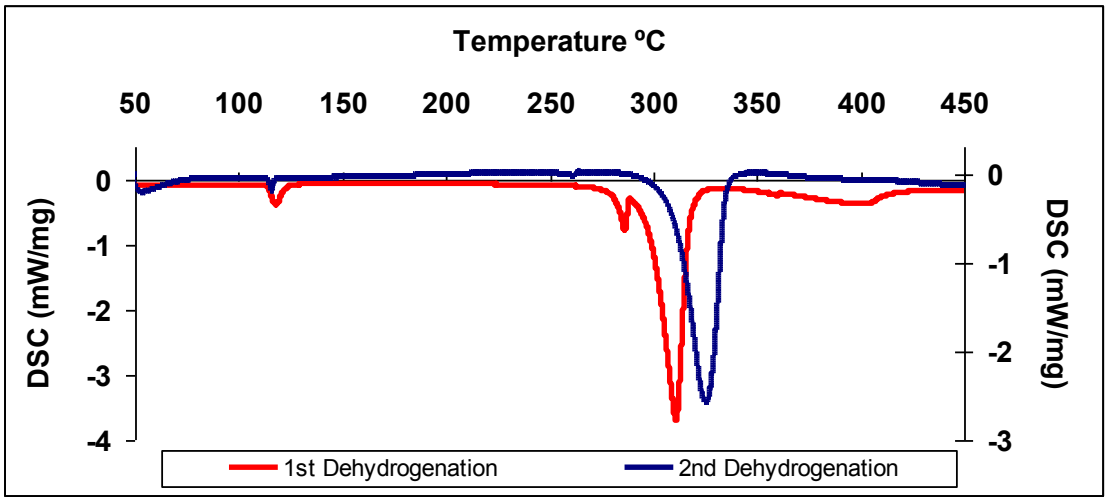

Figure 48) DSC profile of the first and second dehydrogenation of $LiBH_4$ + $2MgH_2$. Samples were firstly desorbed on the DSC under 3 bar(g) of Ar flowing at 100 ml / min while heating up to 450ºC. The dehydrogenated samples were then recombined on the DSC with 100 bar(g) H_2 flowing at 100 ml / min whilst heating to 450ºC.The sample was then dehydrogenated again on the DSC under 3 bar(g) of Ar flowing at 100 ml / min while heating to 450ºC to yield the second dehydrogenation profile. All heating was at 2ºC / min.

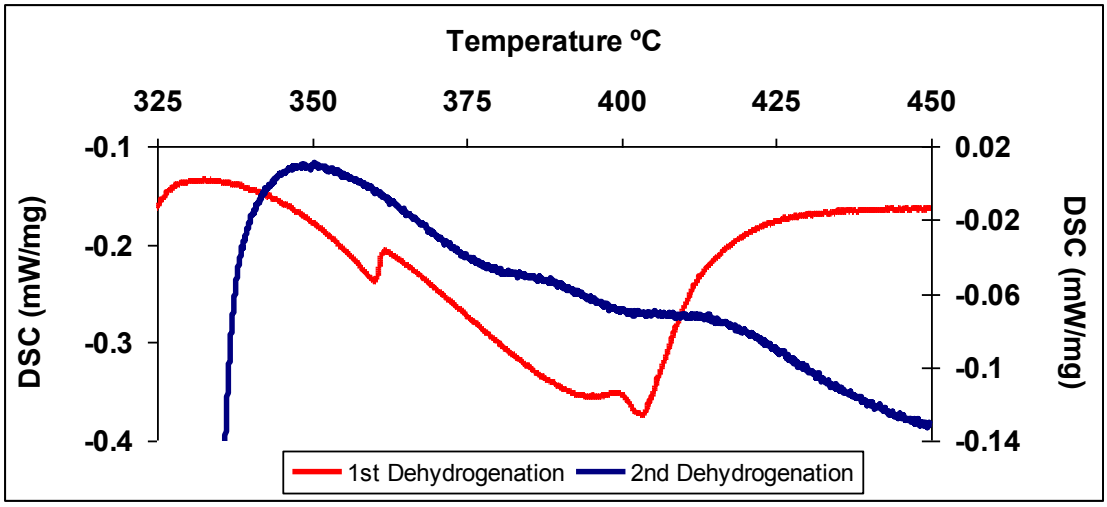

Figure 49) Expanded view of first and second dehydrogenations of $LiBH_4 + 2MgH_2$. Taken from Figure 48

The enthalpy values calculated from these second dehydrogenations are shown in Table 23. Despite the smaller amount of hydrogen stored by the $LiBH_4 + 2MgH_2$ sample (9.41 wt% H_2), when compared to the $2LiBH_4 + MgH_2$ samples (11.45 wt% H_2) it releases more hydrogen during the second dehydrogenations. In addition to releasing more H_2 during the second dehydrogenation than the $2LiBH_4 + MgH_2$ samples did, the second dehydrogenations of $LiBH_4 + 2MgH_2$ also requires 6 kJ / mol H_2 less energy than the $2LiBH_4 + MgH_2$ samples did for releasing this H_2. As with the $2LiBH_4 + MgH_2$ samples you would not expect the phase change or enthalpy of fusion to differ from the first dehydrogenation. Using the same method employed for $2LiBH_4 + MgH_2$ an approximation about how much $LiBH_4$ has been recombined can be made by using the difference of these two values.

When the value of 0.69 kJ / mol $LiBH_4$ obtained for the phase change of the second is factored up to the expected value of 4.18 kJ / mol $LiBH_4$ it can be approximated that 16.51% of the $LiBH_4$ we started with gets reformed during the first recombination. The

enthalpy of fusion for the second (0.76 kJ / mol $LiBH_4$) dehydrogenation indicates that 10.05% of the $LiBH_4$ started with gets reformed during the first recombination. These two figures are not drastically different and the average of these two figures suggests that on average of 13.28% recombination of $LiBH_4$ occurs during the first recombination attempt.

Sample Mass (mg)	9.70	8.91	13.90	**Average**
Phase Change (kJ / mol $LiBH_4$)	0.74	0.61	0.73	**0.69**
Melting Point (kJ / mol $LiBH_4$)	0.79	0.65	0.83	**0.76**
MgH_2 Dehydrogenation (kJ / mol H_2)	48.02	40.94	47.50	**45.49**
$LiBH_4$ Dehydrogenation (kJ / mol H_2)	0.41	0.02	0.89	**0.44**
kJ / mol H_2 (5.5 wt.% H_2)	49.14	41.54	49.11	**46.60**

Table 23) Enthalpy values obtained for the 2nd dehydrogenations of $LiBH_4$ + $2MgH_2$. Samples were dehydrogenated on the DSC under 3 bar(g) of Ar flowing at 100 ml / min with heating up to 450ºC. Samples were then recombined under 100 bar(g) of H_2 flowing at 100 ml / min with heating up to 450ºC. Samples were then dehydrogenated for a second time on the DSC under 3 bar(g) of Ar flowing at 100 ml / min with heating up to 450ºC. All heating was at 2ºC / min.

The recombination of $LiBH_4$ + $2MgH_2$ samples was also studied with the aid of DSC and produced results different to those obtained by recombining $2LiBH_4$ + MgH_2 samples with hydrogen. The first recombination of $2LiBH_4$ + MgH_2 produced two exothermic peaks but the first recombination of $LiBH_4$ + $2MgH_2$ produced just one (compare Figures 33 and 50). The peak produced by the first recombination of $LiBH_4$ + $2MgH_2$ also occurs, approximately 57ºC earlier than the first peak produced by $2LiBH_4$ + MgH_2. The peak produced by recombining this material a second time occurs at a higher

temperature than for the first recombination indicating that recombining these samples with hydrogen becomes more difficult under cycling. The absence of a second recombination peak could also be evidence for $LiBH_4$ failing to completely recombine, with the single peak due to the recombination of only MgH_2.

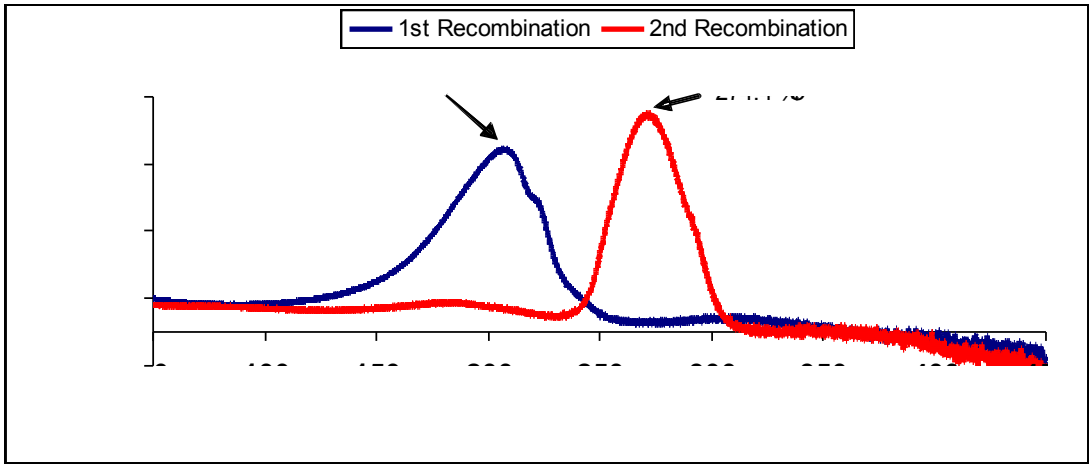

Figure 50) DSC data for first and second recombination data of $LiBH_4 + 2MgH_2$. For the first recombination samples were dehydrogenated on the DSC up to 450ºC then recombined under 100 bar(g) of H_2 flowing at 100 ml / min by heating up to 450 ºC. For the second recombination the sample used for the first recombination was dehydrogenated and recombined again using the same conditions employed for the first dehydrogenation and recombination. All heating was at 2ºC / min.

Further evidence for the poor reversibility of $LiBH_4$ comes from the IR analysis carried out on recombined samples of $LiBH_4 + 2MgH_2$. The broad peak attributed to the presence of MgH_2 is present for both recombination attempts but has a low intensity suggesting that it did not reform so well (compare Figure 34 and 51). Four of the $LiBH_4$ IR active modes are present but these too have low intensities suggesting poor recombination. The additional IR peak (~2445 cm^{-1}) observed after the recombination attempts made on $2LiBH_4 + MgH_2$ is also weakly present in both the first and second FTIR profiles of $LiBH_4 + 2MgH_2$.

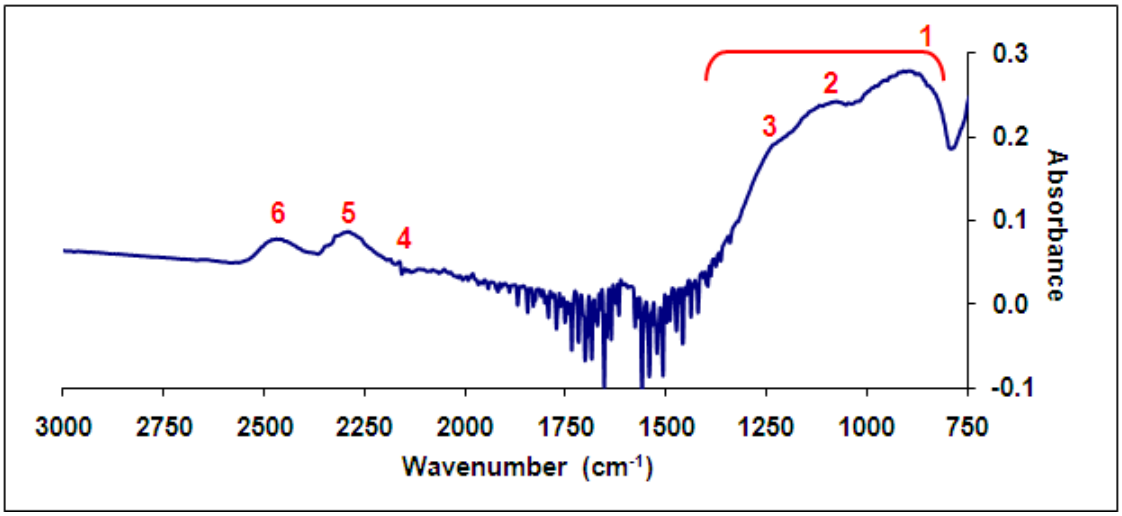

Figure 51) FTIR profile of a recombined $LiBH_4$ + $2MgH_2$ sample. Samples were dehydrogenated on the DSC under 3 bar(g) of Ar flowing at 100 ml/min with heating to 450ºC. Samples were then recombined using 100 bar(g) of H_2 flowing at 100 ml / min with heating up to 450ºC. All heating was at 2ºC / min.

Peak	Wavenumber (cm^{-1})	Assignment [52]	Internal Change	Material
1	790 – 1400		Mg – H Stretch	MgH_2
2	1090	υ_4	B – H Bending	$LiBH_4$
3	1215	$3\upsilon_L$		$LiBH_4$
4	2160	$2^{10}\upsilon_4$	B – H Stretching	
5	2275	υ_3'		$LiBH_4$
6	2450		In phase Breathing	$Li_2B_{12}H_{12}$

Table 24) FTIR table for the first recombination of $LiBH_4$ + $2MgH_2$. Samples were dehydrogenated on the DSC under 3 bar(g) of Ar flowing at 100 ml/min with heating to 450ºC. Samples were then recombined using 100 bar(g) of H_2 flowing at 100 ml / min with heating up to 450ºC. All heating was at 2ºC / min.

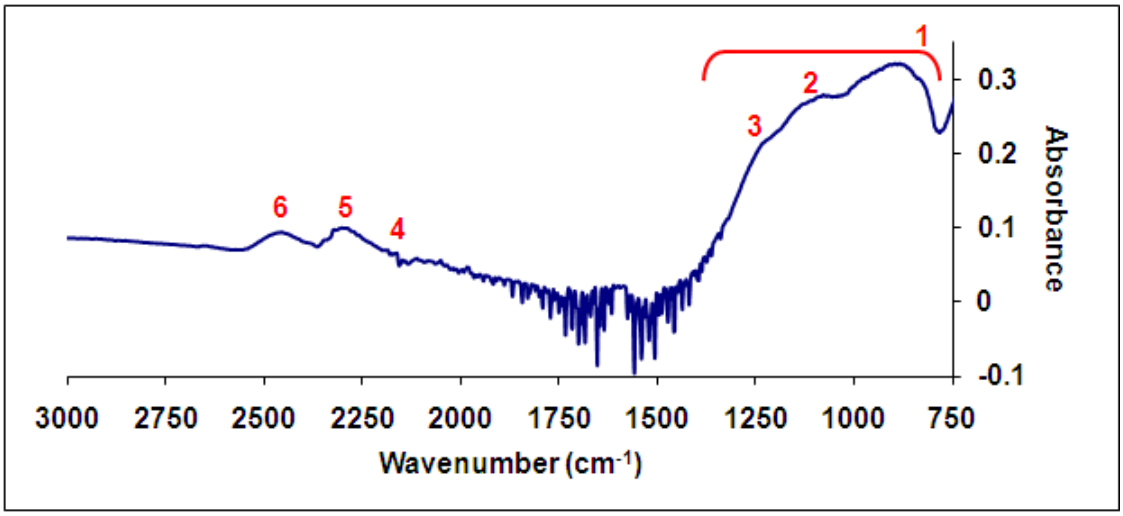

Figure 52) FTIR profile of twice recombined $LiBH_4$ + $2MgH_2$. The sample was dehydrogenated twice on the DSC under 3 bar(g) of Ar flowing at 100 ml / min up to 450ºC and recombined twice using 100 bar(g) of H_2 flowing at 100 ml / min up to 450ºC. All heating was at 2ºC / min.

Peak	Wavenumber (cm^{-1})	Assignment [52]	Internal Change	Material
1	790 – 1400		Mg – H Stretch	MgH_2
2	1085	υ_4	B – H Bending	$LiBH_4$
3	1210	$3\upsilon_L$		$LiBH_4$
4	2160	$2^{10}\upsilon_4$	B – H Stretching	$LiBH_4$
5	2280	υ_3'		$LiBH_4$
6	2440		In phase Breathing	$Li_2B_{12}H_{12}$

Table 25) FTIR for the twice recombined $LiBH_4$ + $2MgH_2$. The sample was dehydrogenated twice on the DSC under 3 bar(g) of Ar flowing at 100 ml / min up to 450ºC and recombined twice using 100 bar(g) of H_2 flowing at 100 ml / min up to 450ºC. All heating was at 2ºC / min.

XRD analysis of the recombined products, reveal a 2θ peak at approximately 25.65º, which is due to the tape that was used to mount the sample. Two small peaks occurring at 2θ values of 44.75° and 50.94° are unassigned but the remaining peaks are due to the reformation of MgH_2 and $Li_{0.184}Mg_{0.816}$ left over from dehydrogenation. There is no evidence in the XRD data to suggest a new phase has formed which could have given rise to the IR peak observed at ~2445 cm^{-1}. The most likely cause of this peak is

the $B_{12}H_{12}^{2-}$ complex which was suggested as the cause for this peak in the $2LiBH_4 + MgH_2$ recombinations (Figure 34 and 35).

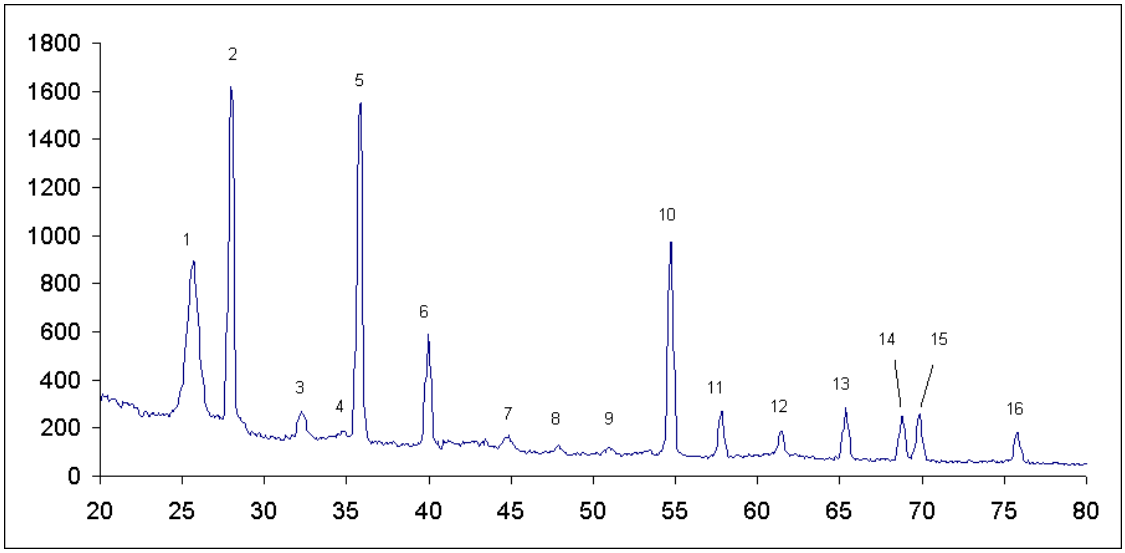

Figure 53) XRD analysis of recombined $LiBH_4$ + $2MgH_2$. The sample was dehydrogenated under 3 bar(g) of Ar flowing at 100 ml / min with heating up to 450ºC and then recombined using 100 bar(g) of H_2 whilst heating to 450ºC. Heating was at 2ºC / min.

Peak number	2θ value	d Spacing (Å)	Assignment
1	25.65	3.47	Tape
2	27.97	3.19	MgH_2
3	32.27	2.77	$Li_{0.184}Mg_{0.816}$
4	34.70	2.59	$Li_{0.184}Mg_{0.816}$
5	35.83	2.51	MgH_2
6	40.03	2.25	MgH_2
7	44.75	2.03	Unassigned
8	47.88	1.90	$Li_{0.184}Mg_{0.816}$
9	50.94	1.79	Unassigned
10	54.72	1.68	MgH_2
11	57.79	1.60	MgH_2
12	61.44	1.51	MgH_2
13	65.37	1.43	MgH_2
14	68.82	1.36	MgH_2
15	69.84	1.35	MgH_2
16	75.80	1.25	MgH_2

Table 26) XRD table for the first recombination attempt on $LiBH_4$ +$2MgH_2$. The sample was dehydrogenated under 3 bar(g) of Ar flowing at 100 ml / min with heating up to 450ºC and then recombined using 100 bar(g) of H_2 whilst heating to 450ºC. Heating was at 2ºC / min.

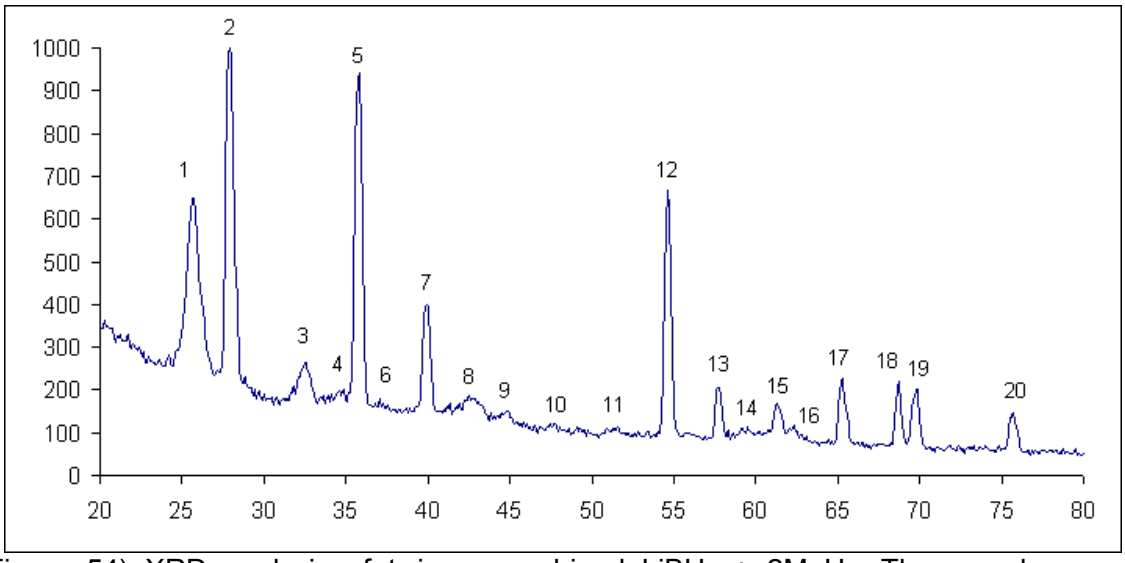

Figure 54) XRD analysis of twice recombined $LiBH_4$ + $2MgH_2$. The samples were dehydrogenated twice on the DSC under 3 bar(g) of Ar flowing at 100 ml / min with heating up to 450ºC and recombined twice under 100 bar(g) of H_2 flowing at 100 ml / min up to 450ºC. All heating was at 2ºC / min.

Peak number	2θ value	d Spacing (Å)	Assignment
1	25.73	3.46	Tape
2	27.90	3.19	MgH_2
3	32.51	2.76	$Li_{0.184}Mg_{0.816}$
4	34.73	2.58	$Li_{0.184}Mg_{0.816}$
5	35.82	2.51	MgH_2
6	37.10	2.42	$Li_{0.184}Mg_{0.816}$
7	39.99	2.25	MgH_2
8	42.68	2.12	MgO
9	44.73	2.03	Unassigned
10	47.76	1.91	$Li_{0.184}Mg_{0.816}$
11	51.39	1.78	Unassigned
12	54.68	1.68	MgH_2
13	57.57	1.60	MgH_2
14	59.37	1.56	Unassigned
15	61.32	1.51	MgO
16	62.35	1.49	Unassigned
17	65.33	1.43	MgH_2
18	68.74	1.37	MgH_2
19	69.80	1.35	MgH_2
20	75.76	1.25	MgH_2

Table 27) XRD table for the twice recombined sample of $LiBH_4$ + $2MgH_2$. The samples were dehydrogenated twice on the DSC under 3 bar(g) of Ar flowing at 100 ml / min with heating up to 450ºC and recombined twice under 100 bar(g) of H_2 flowing at 100 ml / min up to 450ºC. All heating was at 2ºC / min.

5.4 $LiBH_4 + 5MgH_2$

5.4.1 As milled $LiBH_4 + 5MgH_2$

The as milled $LiBH_4 + 5MgH_2$ sample contains a large excess of MgH_2 and therefore like the $LiBH_4 + 2MgH_2$ sample, does not produce very prominent $LiBH_4$ IR and XRD peaks. The IR peak at 1100 cm^{-1} observed in as-received $LiBH_4$ is present with a small intensity in this sample, together with $LiBH_4$ peaks at higher wavenumbers (Figure 55).

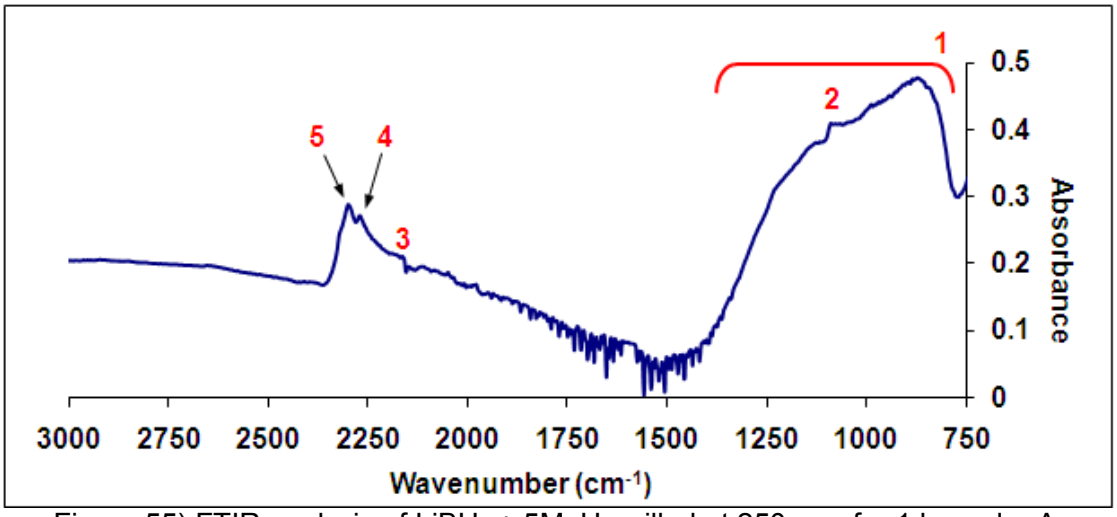

Figure 55) FTIR analysis of $LiBH_4 + 5MgH_2$ milled at 250 rpm for 1 hr under Ar

Peak	Wavenumber (cm^{-1})	Assignment [52]	Internal Change	Material
1	790 – 1400		Mg – H Stretch	MgH_2
2	1100	υ_4	B – H Bending	$LiBH_4$
3	2180	$2^{10}\upsilon_4$	B – H Stretching	$LiBH_4$
4	2290	υ_3		$LiBH_4$
5	2310	υ_3'		$LiBH_4$

Table 28) FTIR table for $LiBH_4 + 5MgH_2$ milled at 250 rpm for 1 hr under Ar

Further structural analysis by XRD of the milled sample shows peaks that can be attributed to $LiBH_4$ and MgH_2 (Figure 56). The XRD analysis of $LiBH_4 + 5MgH_2$ reveals fifteen 2θ peaks the first and largest being due to the tape that was used to mount the samples. The majority of the peaks are due to the presence of MgH_2 as would be expected considering the amount of MgH_2 used to make up these samples. As with the $LiBH_4 + 2MgH_2$ sample there is evidence that milling has induced a reaction between the starting materials to form the $Li_{0.184}Mg_{0.816}$ alloy.

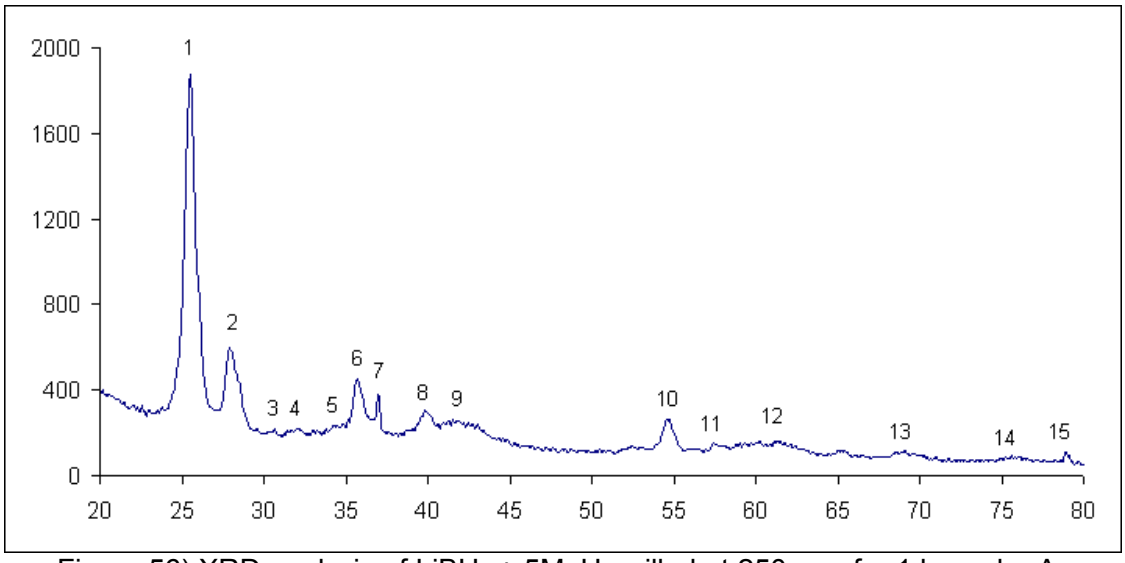

Figure 56) XRD analysis of $LiBH_4$ + $5MgH_2$ milled at 250 rpm for 1 hr under Ar

Peak number	2θ value	d Spacing (Å)	Assignment
1	25.53	3.49	Tape
2	27.94	3.19	MgH_2
3	30.65	2.92	MgH_2
4	32.09	2.79	$Li_{0.184}Mg_{0.816}$
5	34.85	2.58	$Li_{0.184}Mg_{0.816}$
6	35.60	2.52	MgH_2
7	36.99	2.43	$Li_{0.184}Mg_{0.816}$
8	39.91	2.26	MgH_2
9	42.31	2.14	MgO
10	54.70	1.68	MgH_2
11	57.58	1.60	MgH_2
12	65.28	1.43	MgH_2
13	68.85	1.36	MgH_2
14	75.79	1.26	MgH_2
15	78.92	1.21	$Li_{0.184}Mg_{0.816}$

Table 29) XRD table for $LiBH_4$ + $5MgH_2$ milled at 250 rpm for 1 hr under Ar

5.4.2 First Dehydrogenation of $LiBH_4$ + $5MgH_2$

Dehydrogenations carried out on this sample with a TGA and revealed that $LiBH_4$ + $5MgH_2$ releases 7.5 wt% upon heating to 450ºC (Figure 57). This 7.5% loss in mass is only 0.5 wt% less than that which was observed during the dehydrogenation of

$LiBH_4$ + $2MgH_2$ on the TGA. The maximum, theoretical amount of hydrogen which can be stored by this system is 9.13 wt% H_2 which is reduced to a figure of 8.48 wt% when it is assumed that LiH is produced as a product of dehydrogenation.

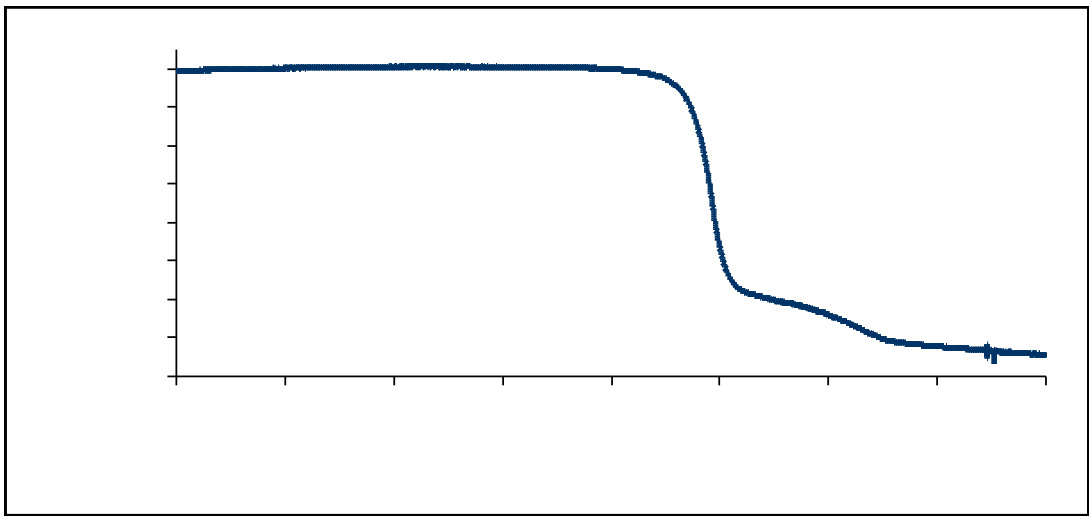

Figure 57) TGA analysis for the first dehydrogenation of $LiBH_4$ + $5MgH_2$. The sample was dehydrogenated under 0.5 bar(g) of Ar flowing at 40 ml / min while heating up to 450ºC at 2ºC / min

Just as with $2LiBH_4$ + MgH_2 and $LiBH_4$ + $2MgH_2$ (Figures 22 and 40), mass loss from this sample occurred in two stages, the first beginning at approximately 260ºC and the second occurring at approximately 310ºC. The first loss of mass was recorded as 6 wt% while the second produced a loss of 1.5 wt%. These figures again suggest that the constituent materials have released their hydrogen at separate times rather than together because the mass loss expected from MgH_2 for this sample is 6.52 wt% and the loss in mass expected due to $LiBH_4$ is 1.96 wt% (theoretical maximum).

Mass spectrometry data gained for this sample confirms that the sample loses hydrogen in two stages (Figure 58). The first mass spectrometry signal is a sharp peak which

occurs at the same temperature the TGA recorded the first loss of mass from the sample. The second mass spectrometry signal is very small in comparison to the first and much broader but appears in a position that would be expected if hydrogen were being released during the second loss of mass. As with the $LiBH_4$ + $2MgH_2$ sample the mass spectrometry showed no evidence for the production of diborane gas during dehydrogenation.

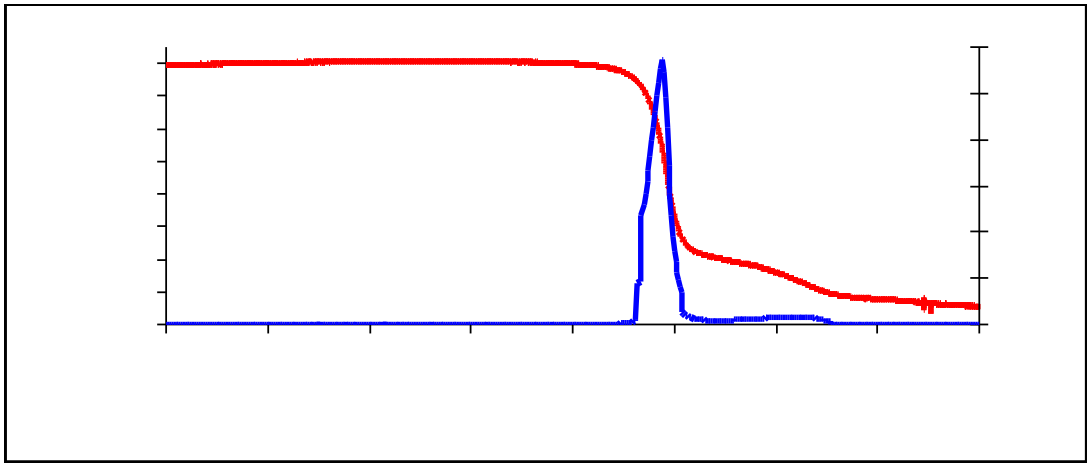

Figure 58) TGA and Hydrogen mass spectroscopy data for $LiBH_4$ + $5MgH_2$. The sample was dehydrogenated under 0.5 bar(g) of Ar flowing at 40 ml / min while heating up to 450ºC at 2ºC / min

DSC analysis of $LiBH_4$ + $5MgH_2$ (Figure 59) produces a profile very similar to that seen for as received MgH_2 (Figure 15), because of the reduced amount of lithium borohydride. The phase change of $LiBH_4$ which accounts for the first DSC peak is recorded at 121ºC, which is ~5ºC higher than that recorded for $2LiBH_4$ + MgH_2 and $LiBH_4$ + $2MgH_2$ samples (Figures 25 and 42). The DSC peak produced by the melting of $LiBH_4$ can be observed as a small shoulder on the left of the MgH_2 peak at 283ºC. The MgH_2 peak itself begins at a temperature of approximately 260ºC.

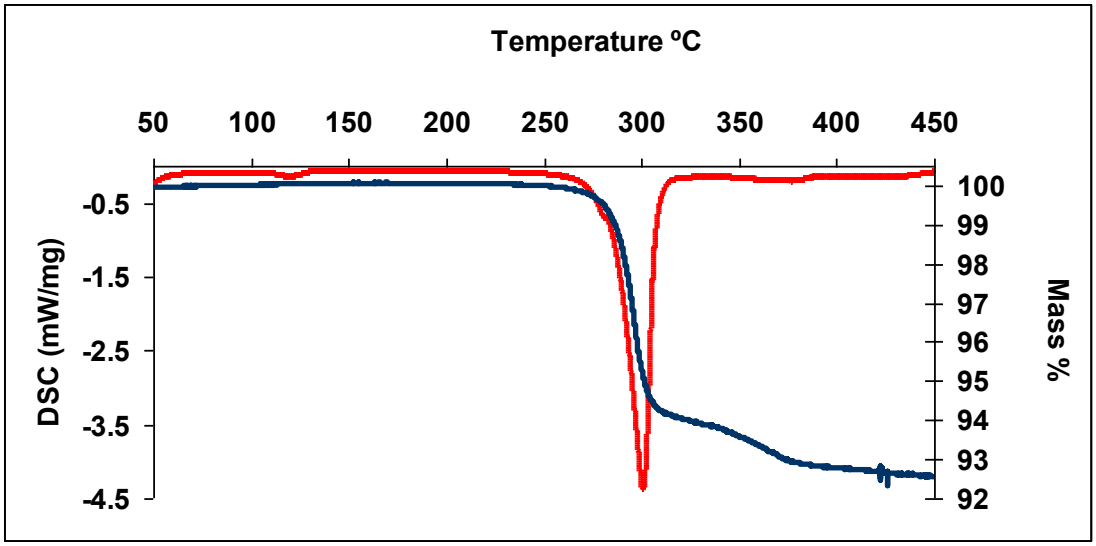

Figure 59) DSC and TGA data obtained for $LiBH_4$ + $5MgH_2$. TGA data was obtained by dehydrogenating under 0.5 bar(g) Ar flowing at 40 ml / min while heating up to 450ºC at 2ºC / min. DSC data was recorded while dehydrogenating into 3 bar(g) of Ar flowing at 100 ml / min whist heating to 450ºC at a heating rate of 2ºC / min

The final borohydride signal is still present, occurring after the large MgH_2 peak but has become much flatter. Closer inspection of the final $LiBH_4$ peak (Figure 60) reveals that it is in fact composed of what appears to be two endothermic peaks, which were also observed for both $2LiBH_4$ + MgH_2 and $LiBH_4$ + $2MgH_2$ (Figure 26 and 43).

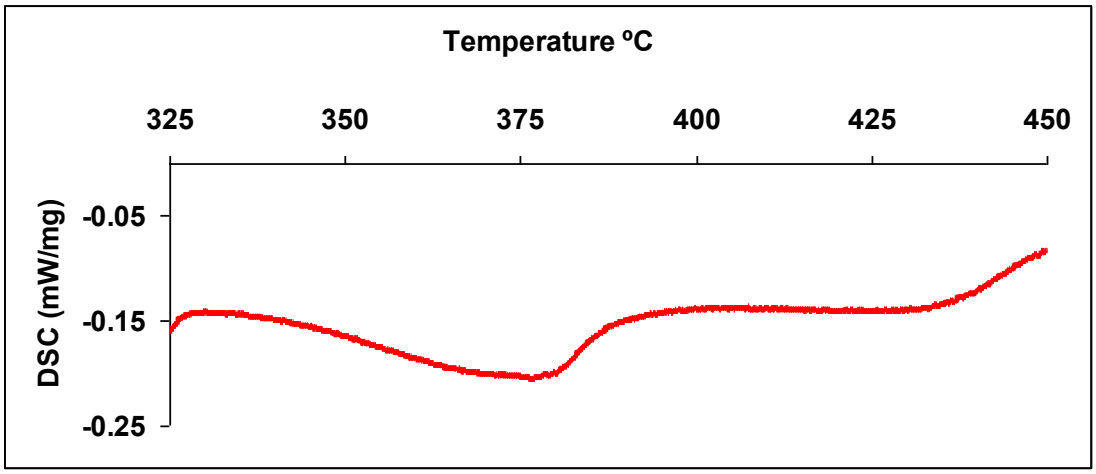

Figure 60) Expanded view of the fourth endothermic peak produced by dehydrogenating a $LiBH_4$ + $5MgH_2$ sample. Taken from Figure 59.

The energy for these endothermic processes have been calculated from the DSC experiments (Table 30), however the melting point figures are absent due to the difficulty in distinguishing this peak from that of the magnesium hydride peak. As carried out for the $LiBH_4 + 2MgH_2$ sample, because the phase change value is lower than expected and wouldn't be expected to change the average value obtained during this investigation (3.01 kJ / mol $LiBH_4$) and the expected value (4.18 kJ / mol $LiBH_4$) can be used to evaluate how much $LiBH_4$ is unaccounted for within the sample. From these figures it is approximated that 27.99% of the $LiBH_4$ we started with in this sample is either left in the sample unreacted, dehydrogenated during the milling process or a combination of the two.

Sample Mass (mg)	12.15	10.95	13.67	10.72	**Average**
Phase Change (kJ / mol $LiBH_4$)	3.29	2.66	3.04	3.04	**3.01**
MgH_2 Dehydrogenation (kJ / mol H_2)	47.82	44.31	49.06	49.92	**47.78**
$LiBH_4$ Dehydrogenation (kJ / mol H_2)	2.87	3.63	2.35	3.86	**3.18**
kJ / mol H_2 (7.5 wt.% H_2)	51.23	48.38	51.91	54.27	**51.45**

Table 30) Enthalpy values calculated for the first dehydrogenation of $LiBH_4 + 5MgH_2$. Calculated from DSC data obtained under 3 bar(g) of Ar flowing at 100 ml / min whilst heating up to 450ºC at 2ºC / min.

The energy required to remove hydrogen from $LiBH_4$, is lower for this sample than that obtained for both the $LiBH_4 + 2MgH_2$ and $2LiBH_4 + MgH_2$ sample. The enthalpy of decomposition for MgH_2 is largest for this sample and due to the large amount of MgH_2

present within this sample it creates the largest overall enthalpy of dehydrogenation for all of the samples studied.

FTIR analysis of the dehydrogenated $LiBH_4$ + $5MgH_2$ samples revealed no trace of IR activity as was observed for the dehydrogenated sample of $LiBH_4$ + $2MgH_2$.

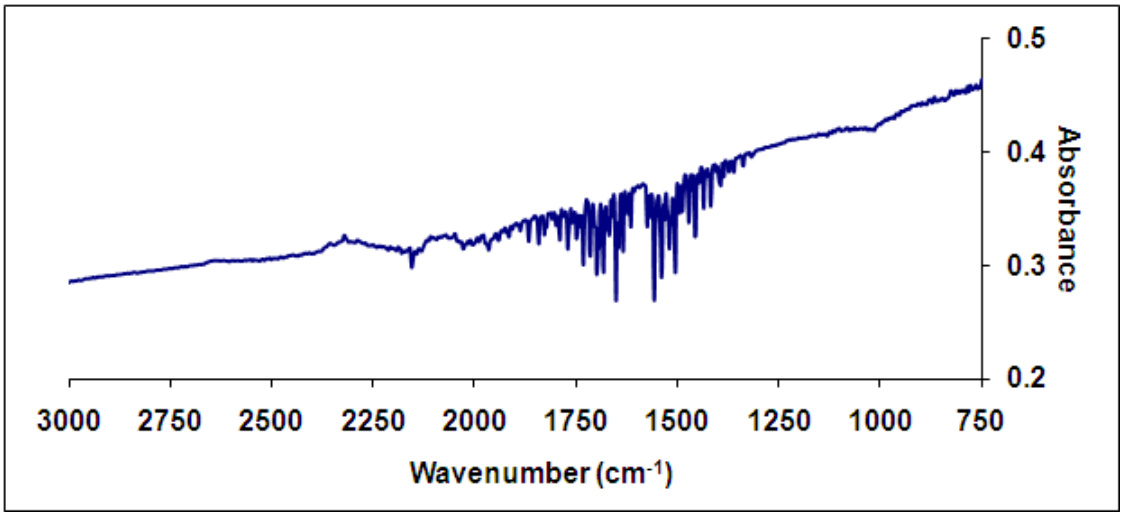

Figure 61) FTIR spectra produced by a dehydrogenated sample of $LiBH_4$ + $5MgH_2$. Dehydrogenated under 3 bar(g) of Ar flowing at 100 ml / min whilst heating up to 450ºC at 2ºC / min.

Wavenumber (cm^{-1})	Assignment
No Peaks	NA

Table 31) FTIR table for the dehydrogenation of $LiBH_4$ + $5MgH_2$. Dehydrogenated under 3 bar(g) of Ar flowing at 100 ml / min whilst heating up to 450ºC at 2ºC / min.

XRD analysis of the dehydrogenated $LiBH_4$ + $5MgH_2$ sample reveals a large 2θ peak at 25.61º which arises due to the tape used when preparing the sample for XRD. Three of the peaks can be attributed to residual MgH_2 left over within the sample producing peaks at 2θ values of 27.95°, 35.82° and 39.88°. The remaining ten peaks are due to the formation of a $Li_{0.184}Mg_{0.816}$ alloy.

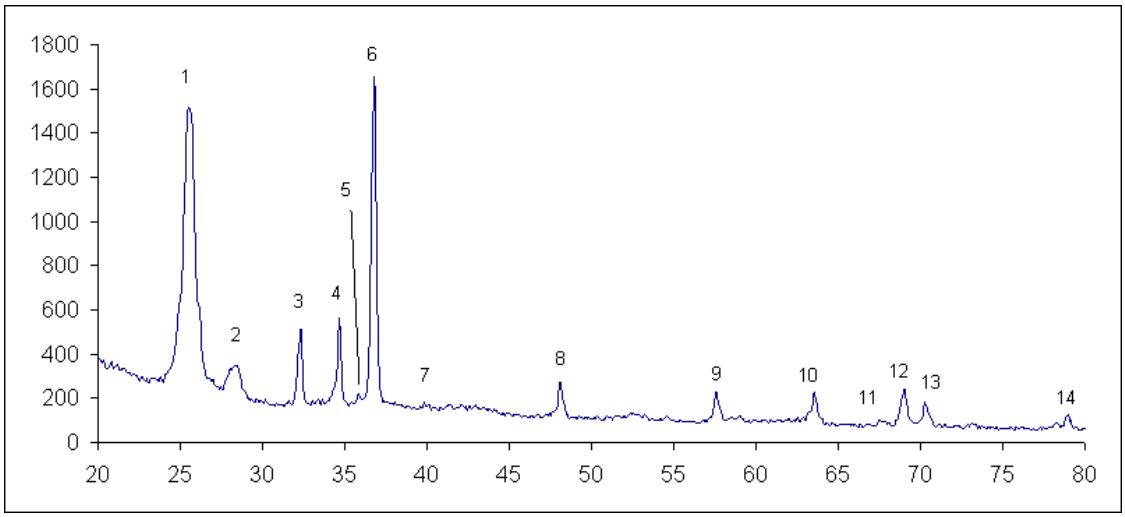

Figure 62) XRD analysis of dehydrogenated $LiBH_4$ + $5MgH_2$. Dehydrogenated under 3 bar(g) of Ar flowing at 100 ml / min whilst heating up to 450ºC at 2ºC / min.

Peak number	2θ value	d Spacing (Å)	Assignment
1	25.76	3.46	Tape
2	27.95	3.19	MgH_2
3	32.28	2.77	$Li_{0.184}Mg_{0.816}$
4	34.62	2.59	$Li_{0.184}Mg_{0.816}$
5	35.82	2.51	MgH_2
6	36.78	2.44	$Li_{0.184}Mg_{0.816}$
7	39.88	2.26	MgH_2
8	48.09	1.89	$Li_{0.184}Mg_{0.816}$
9	57.60	1.60	$Li_{0.184}Mg_{0.816}$
10	63.49	1.46	$Li_{0.184}Mg_{0.816}$
11	67.49	1.39	$Li_{0.184}Mg_{0.816}$
12	68.96	1.36	$Li_{0.184}Mg_{0.816}$
13	70.25	1.34	$Li_{0.184}Mg_{0.816}$
14	78.91	1.21	$Li_{0.184}Mg_{0.816}$

Table 32) XRD table for dehydrogenated $LiBH_4$ + $5MgH_2$. Dehydrogenated under 3 bar(g) of Ar flowing at 100 ml / min whilst heating up to 450ºC at 2ºC / min.

5.4.3 Cycling of $LiBH_4$ + $5MgH_2$

The TGA profile for the second dehydrogenation of this sample (Figure 63) is similar to that for the second dehydrogenation of $LiBH_4$ + $2MgH_2$ (Figure 46) with a loss from MgH_2 still occurring but the borohydride component is now missing. After recombination $LiBH_4$ + $5MgH_2$ samples release just a third of the hydrogen (2.5 wt%) they did during the first dehydrogenation (7.5 wt%). The 2.5 wt% lost from these samples during their second dehydrogenations is less than half that obtained for the second dehydrogenations of $LiBH_4$ + $2MgH_2$ samples, indicating that the reversibility is much harder to induce in these samples (under these conditions).

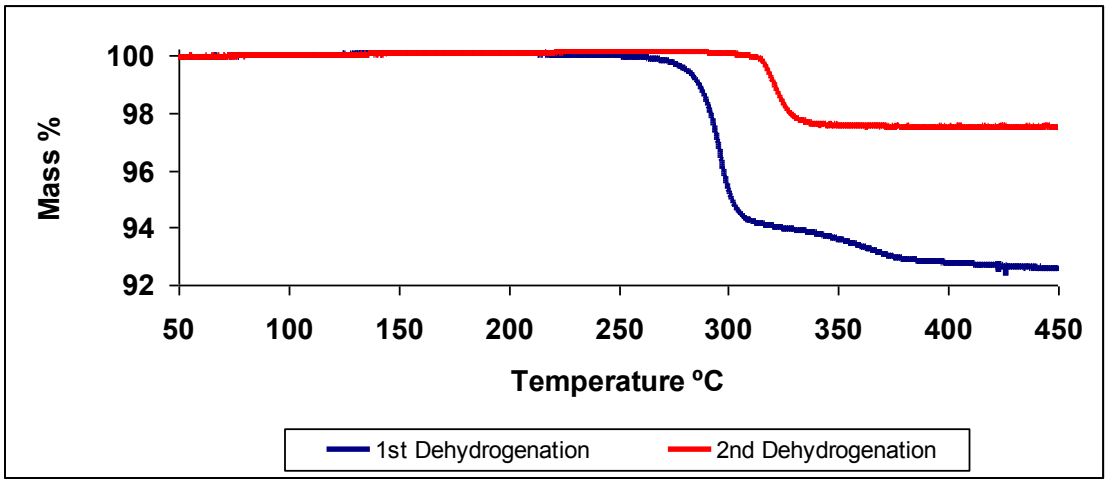

Figure 63) First and second TGA profiles for $LiBH_4$ + $5MgH_2$. First decomposition was obtained by dehydrogenating under 0.5 bar(g) of Ar flowing at 40 ml / min whilst heating up to 450ºC. The second decomposition was then obtained by dehydrogenating a sample on the DSC under 3 bar(g) of Ar flowing at 100 ml / min up to 450ºC, then recombining it under 100 bar(g) of H_2 flowing at 100 ml / min up to 450ºC on the DSC. After recombination the sample was then dehydrogenated again but this time on the TGA under 0.5 bar(g) of Ar flowing at 40 ml / min up to 450ºC. All heating was at 2ºC / min.

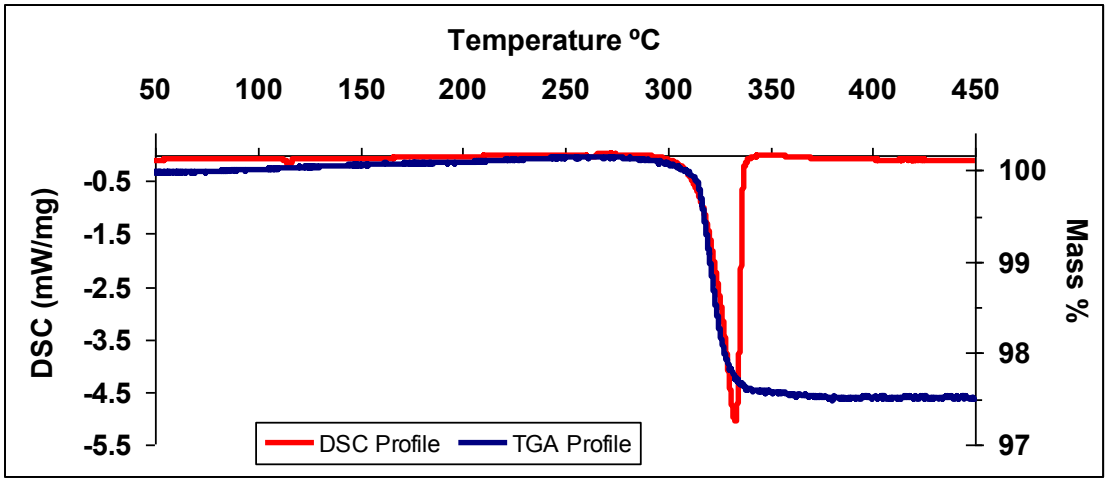

Figure 64) TGA and DSC data for the second dehydrogenations of $LiBH_4$ + 5MgH_2. Two samples were firstly dehydrogenated on the DSC under 3 bar(g) of Ar flowing at 100 ml / min while heating up to 450ºC, these two samples were then recombined on the DSC under 100 bar(g) of H_2 flowing at 100 ml / min while heating up to 450ºC. One of these samples was then dehydrogenated on the TGA under 0.5 bar(g) of Ar flowing at 40 ml / min whilst heating up to 450ºC and the other was dehydrogenated on the DSC using 3 bar(g) of Ar flowing at 100 ml / min while heating up to 450ºC. All heating was at 2ºC / min.

The melting point of $LiBH_4$ is reduced by 19ºC during the second dehydrogenation, to 264ºC (Figure 66). Another difference between the DSC profiles for the first and second dehydrogenations is that the phase change now occurs at 116ºC, which is the approximate temperature at which it was observed for the first and second dehydrogenations of 2$LiBH_4$ + MgH_2 and $LiBH_4$ + 2MgH_2 (Figure 32 and 48). The DSC peak produced by MgH_2 occurs a lot later during the second dehydrogenation (280ºC) suggesting that the kinetics of dehydrogenation has suffered. The exact difference in onset temperature between the first and second MgH_2 DSC peak is difficult to analyse because the melting point of $LiBH_4$ was incorporated into this peak during the first dehydrogenation (Figure 66). The $LiBH_4$ peak at the end of the DSC run also occurs later than it did for the first dehydrogenation (Figure 67), but at approximately the same temperature as it did for the second dehydrogenation of $LiBH_4$ + 2MgH_2 (Figure 48).

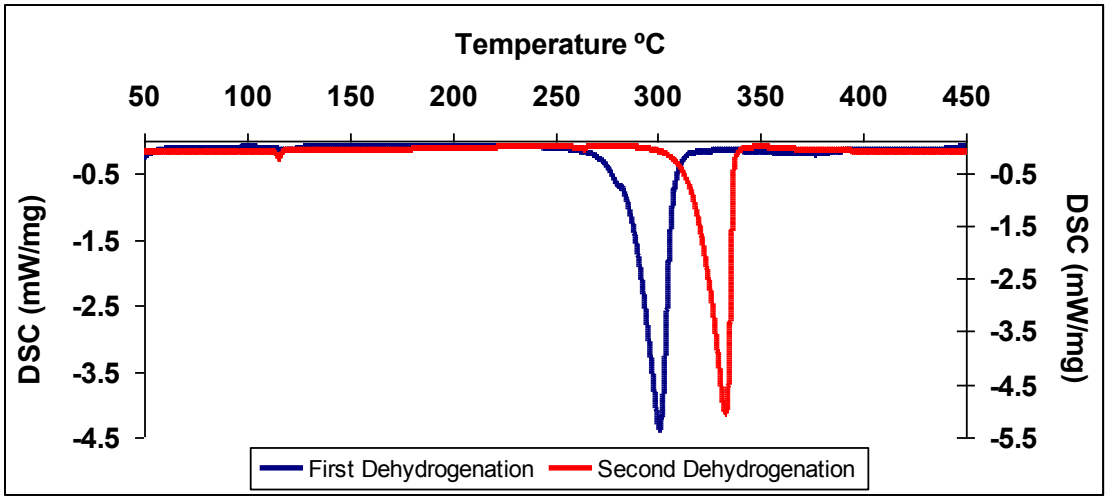

Figure 65) DSC profile of the first and second dehydrogenations of $LiBH_4$ + $5MgH_2$. Samples were firstly desorbed on the DSC under 3 bar(g) of Ar flowing at 100 ml / min while heating up to 450ºC. The dehydrogenated samples were then recombined on the DSC with 100 bar(g) H_2 flowing at 100 ml / min whilst heating to 450ºC. The sample was then dehydrogenated again on the DSC under 3 bar(g) of Ar flowing at 100 ml / min to 450ºC to yield the second dehydrogenation profile. All heating was at 2ºC / min.

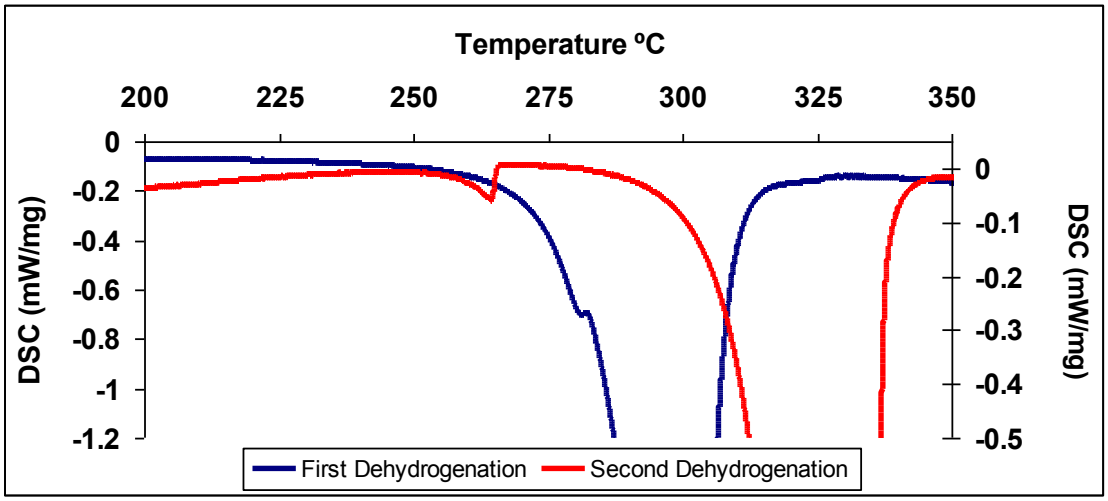

Figure 66) Expanded views (200 – 350ºC) of the DSC profiles produced by the first and second dehydrogenations of $LiBH_4$ + $5MgH_2$. Taken from Figure 65.

The DSC profile for the decomposition of $LiBH_4$ appears to be comprised of two endothermic peaks (Figure 67), which were also observed for the first dehydrogenations of $2LiBH_4$ + MgH_2 and $LiBH_4$ + $2MgH_2$ (Figure 32 and 48). These two endothermic peaks change shape after the second dehydrogenations of $2LiBH_4$ + MgH_2 and $LiBH_4$ + $2MgH_2$.

Even though this sample contains the least amount of $LiBH_4$, a double endothermic peak was observed, which again was also seen for the first dehydrogenations of $2LiBH_4 + MgH_2$ and $LiBH_4 + 2MgH_2$. It is similar to the signal produced at the end of a second dehydrogenation for $LiBH_4 + 2MgH_2$ (Figure 68) but has larger peaks.

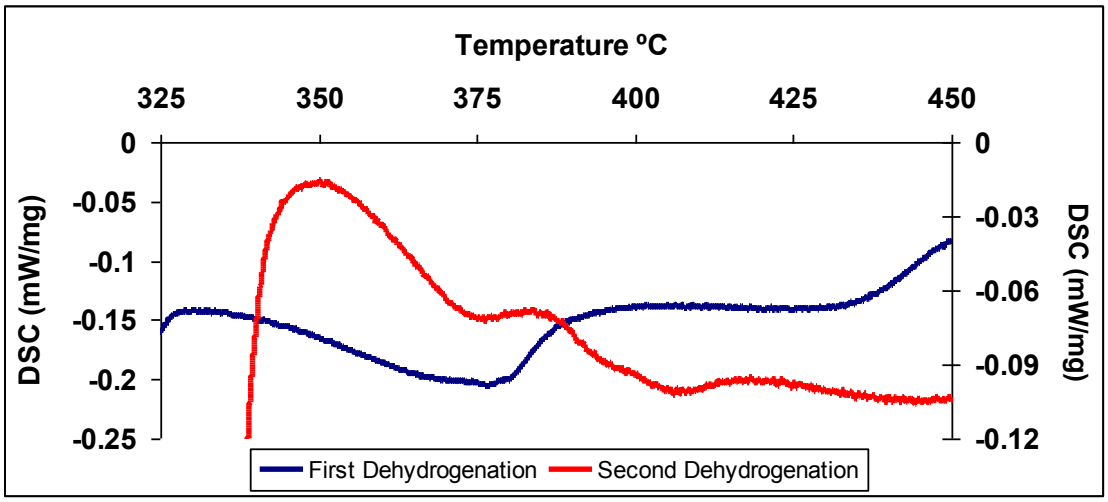

Figure 67) Expanded views (325 – 450ºC) of the DSC profiles produced by the first and second dehydrogenations of $LiBH_4 + 5MgH_2$. Taken from Figure 65.

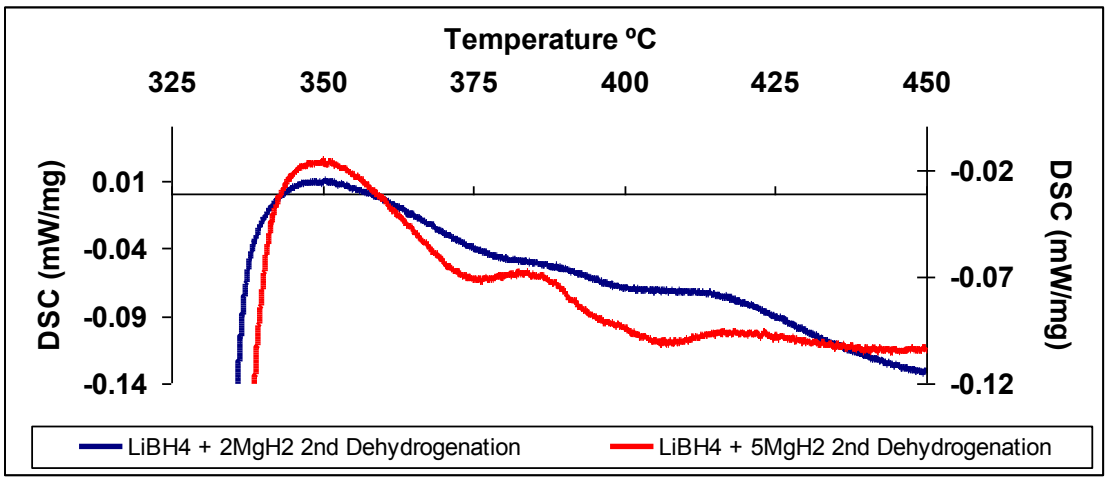

Figure 68) Expanded views (325 – 450ºC) of the DSC profiles produced by the second dehydrogenations of $LiBH_4 + 2MgH_2$ and $LiBH_4 + 5MgH_2$. Both samples were dehydrogenated twice on the DSC under 3 bar(g) Ar flowing at 100 ml / min with heating up to 450ºC and recombined twice under 100 bar(g) of H_2 flowing at 100 ml / min up to 450ºC. All heating was at 2ºC / min.

The energy required for the various processes of dehydrogenation are calculated (Table 33) and also includes enthalpy data for the melting of $LiBH_4$ now it is separated from the MgH_2 peak. Calculations made from data recorded during the second dehydrogenations revealed that the phase change of $LiBH_4$ requires less energy than it did during the first dehydrogenation.

The removal of hydrogen from $LiBH_4$ during the second decomposition (4.54 kJ / mol H_2) requires more energy than it did during the first dehydrogenation (3.18 kJ / mol $LiBH_4$). The energy required to remove H_2 from MgH_2 also increases from the first decomposition to the second. Due to the small amount of hydrogen released from this sample the reaction enthalpy for these second dehydrogenations has dramatically increased, requiring over three times the amount of energy to release one mole of hydrogen when compared to the first dehydrogenation.

As with the previous two samples we can use the enthalpy data obtained for the phase change of $LiBH_4$ from the second decompositions (1.75 kJ / mol $LiBH_4$) to estimate the amount of $LiBH_4$ material that reformed during the first recombination. From these figures it's estimated that 58.14% of the $LiBH_4$ we started with gets reformed during the first recombination effort. This value is much higher than the recombination estimates obtained for the $2LiBH_4 + MgH_2$ (15%) and $LiBH_4 + 2MgH_2$ samples. No such comparison can be made with the melting point enthalpy data obtained from $LiBH_4$ because the melting point wasn't observed during the first dehydrogenation.

Sample Mass (mg)	10.72	10.95	**Average**
Phase Change (kJ / mol $LiBH_4$)	1.75	1.74	**1.75**
Melting Point (kJ / mol $LiBH_4$)	1.94	1.95	**1.93**
MgH_2 Dehydrogenation (kJ / mol H_2)	155.306	152.37	**153.94**
$LiBH_4$ Dehydrogenation (kJ / mol H_2)	4.66	4.41	**4.54**
kJ / mol H_2 (2.5 wt.% H_2)	161.80	158.59	**160.20**

Table 33) Enthalpy values calculated from DSC data obtained for the second dehydrogenations of $LiBH_4$ + $5MgH_2$. The samples were dehydrogenated twice on the DSC under 3 bar(g) Ar flowing at 100 ml / min with heating up to 450ºC and recombined twice under 100 bar(g) of H_2 flowing at 100 ml / min up to 450ºC. All heating was at 2ºC / min.

Recombination attempts were also carried out on the dehydrogenated samples of $LiBH_4$ + $5MgH_2$ (Figure 69) and these behaved in a similar manner to the $LiBH_4$ + $2MgH_2$ samples (Figure 50). Single peaks were observed for both the first and second recombinations but they occurred at temperatures lower than those observed for the first and second recombinations of $LiBH_4$ + $2MgH_2$. The first recombination peak occurs at a temperature 11.5ºC lower than the first $LiBH_4$ + $2MgH_2$ recombination peak and the second recombination peak occurs 17ºC lower than the second recombination peak of $LiBH_4$ + $2MgH_2$.

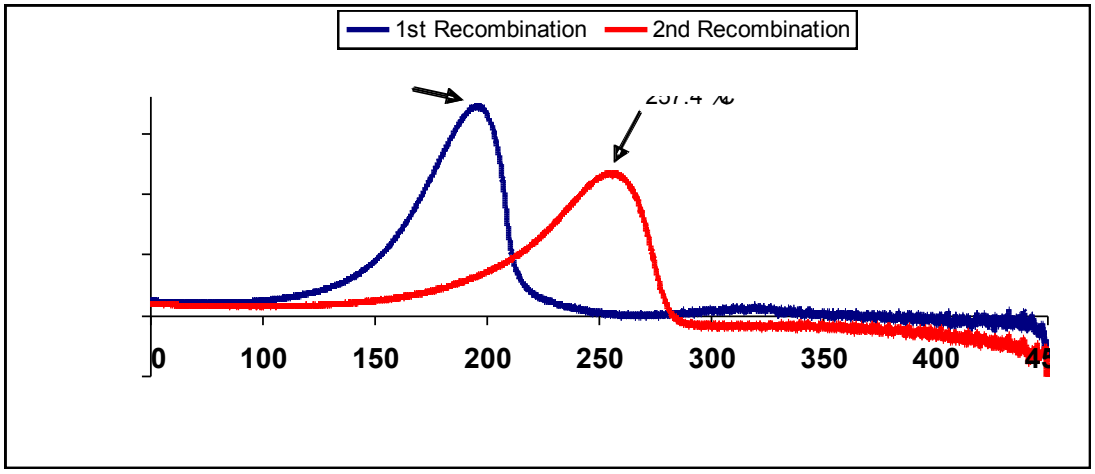

Figure 69) DSC data for first and second recombinations of $LiBH_4$ + $5MgH_2$. For the first recombination samples were dehydrogenated on the DSC up to 450ºC then recombined under 100 bar(g) H_2 flowing at 100 ml / min by heating up to 450 ºC. For the second recombination the sample used for the first recombination was dehydrogenated and recombined again using the same conditions employed for the first dehydrogenation and recombination. All heating was done at a rate of 2ºC / min.

FTIR analysis of a recombined $LiBH_4$ + $5MgH_2$ sample revealed a broad area of IR activity between 790 cm^{-1} and 1400 cm^{-1} which was observed for as received MgH_2 suggesting that this material was present within the recombined sample (Figure 70). A small raised area in the middle of the IR activity between 790 cm^{-1} and 1400 cm^{-1}, at 1090 cm^{-1} is also visible which was present in the spectrum of as received $LiBH_4$. Another peak which was present in the spectrum of as received $LiBH_4$ which has reformed during the first recombination effort appears at 2285 cm^{-1} but other peaks observed for $LiBH_4$ are now absent (compare Figure 17 to 70). The “new” IR peak which occurs at approximately 2450 cm^{-1} is present in both the IR spectra of recombined $LiBH_4$ + $5MgH_2$ and the twice recombined material (Figure 71). As this 2450 cm^{-1} peak has reduced in intensity for this sample type (containing the least amount of $LiBH_4$) it would appear that it is $LiBH_4$ that has caused the creation of this peak in the recombined efforts of $2LiBH_4$ + MgH_2 and $LiBH_4$ + $2MgH_2$ supporting evidence to suggest that this peak is due to $Li_2B_{12}H_{12}$.

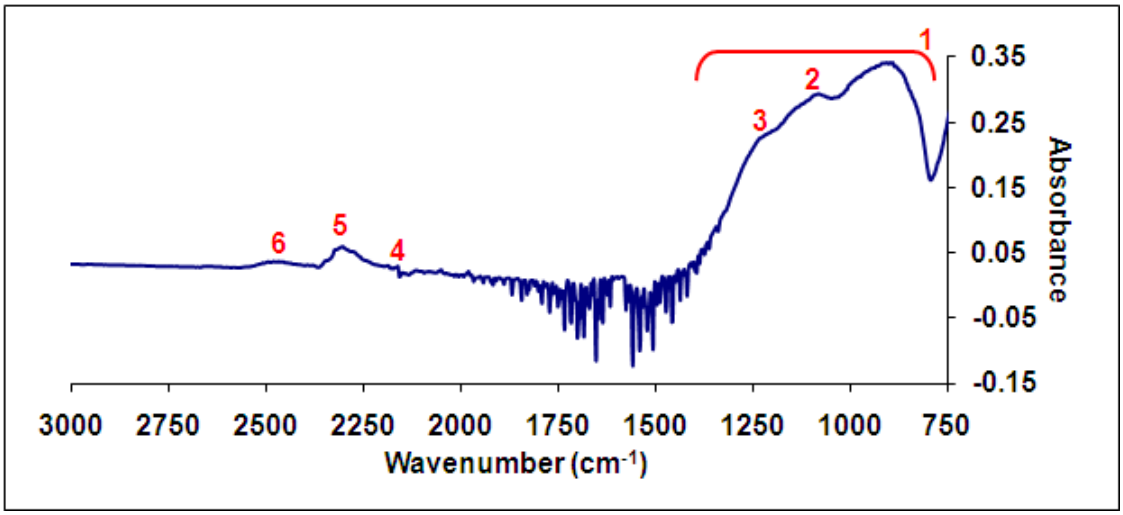

Figure 70) FTIR profile for a recombined $LiBH_4$ + $5MgH_2$. The samples were dehydrogenated on the DSC using 3 bar(g) of Ar flowing at 100 ml / min while heating up to 450ºC at 2ºC / min. The sample was then recombined 100 bar(g) of H_2 flowing at 100 ml / min while being heated to 450ºC at 2ºC / min.

Peak	Wavenumber (cm^{-1})	Assignment [52]	Internal Change	Material
1	790 – 1400		Mg – H Stretch	MgH_2
2	1090	υ_4	B – H Bending	$LiBH_4$
3	1200	$3\upsilon_L$		$LiBH_4$
4	2160	$2^{10}\upsilon_4$	B – H Stretching	$LiBH_4$
5	2285	υ_3'		$LiBH_4$
6	2460		In phase Breathing	$Li_2B_{12}H_{12}$

Table 34) FTIR table for the recombination of $LiBH_4$ + $5MgH_2$. The samples were dehydrogenated on the DSC using 3 bar(g) of Ar flowing at 100 ml / min while heating up to 450ºC at 2ºC / min. The sample was then recombined 100 bar(g) of H_2 flowing at 100 ml / min while being heated to 450ºC at 2ºC / min.

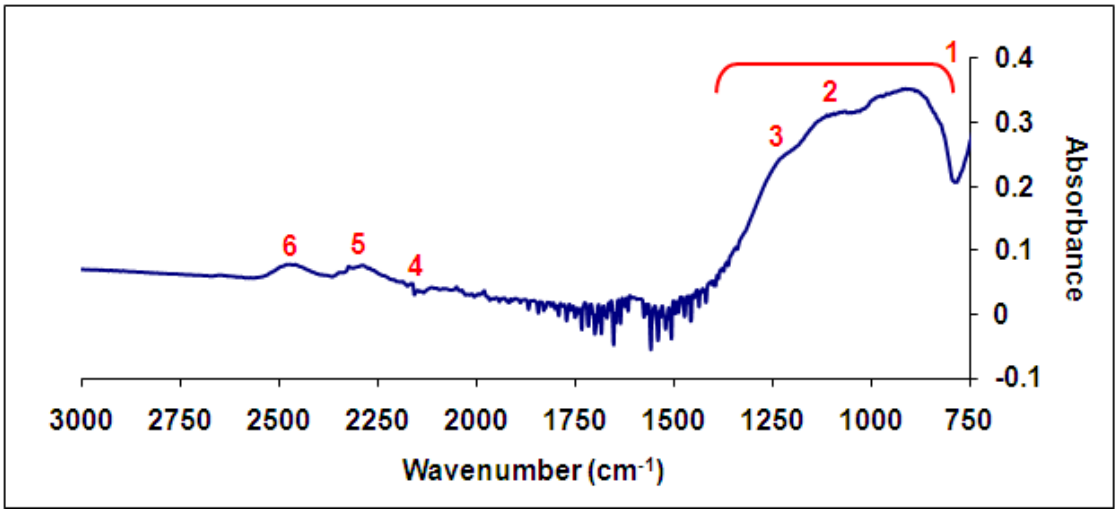

Figure 71) FTIR profile of twice cycled $LiBH_4$ + $5MgH_2$. The sample was dehydrogenated twice on the DSC under 3 bar(g) of Ar flowing at 100 ml / min whilst heating up to 450ºC and recombined twice under 100 bar(g) of H_2 flowing at 100 ml / min whilst heating up to 450ºC. All heating was at 2ºC / min.

Peak	Wavenumber (cm^{-1})	Assignment [52]	Internal Change	Material
1	790 – 1400		Mg – H Stetch	MgH_2
2	1080	υ_4	B – H Bending	$LiBH_4$
3	1200	$3\upsilon_L$		$LiBH_4$
4	2160	$2^{10}\upsilon_4$	B – H Stretching	$LiBH_4$
5	2270	υ_3'		$LiBH_4$
6	2455		In phase Breathing	$Li_2B_{12}H_{12}$

Table 35) FTIR table for twice cycled $LiBH_4$ + $5MgH_2$. The sample was dehydrogenated twice on the DSC under 3 bar(g) of Ar flowing at 100 ml / min whilst heating up to 450ºC and recombined twice under 100 bar(g) of H_2 flowing at 100 ml / min whilst heating up to 450ºC. All heating was at 2ºC / min.

With the FTIR peak which has been observed occurring at ~2450 cm^{-1} more prominent for the twice cycled material than the first recombined sample, XRD analysis of these two states may give some insight into what gave rise to this IR activity. In the recombined XRD pattern (Figure 72) we have the usual peak that occurs at 25.76° which is due to the tape that was used to secure the sample within its holder for analysis and there is one unassigned peak that shows up at 41.25°. The remaining peaks are due to

the presence of MgH_2 and MgO. None of the XRD peaks in Figure 72 are due to any leftover $Li_{0.184}Mg_{0.816}$ alloy formed during dehydrogenation (Figure 62) indicating that this alloy had disappeared upon recombination with H_2.

As with the first recombination, the first XRD peak present in the second dehydrogenation (Figure 73) is due to the tape used in mounting the sample. There are more unassigned peaks in this XRD pattern with three unidentified peaks showing up at 30.07°, 41.15° and 78.88° all with very low intensities. The second of these peaks (41.15°) is very close to the 41.25° peak unassigned in the recombined XRD pattern (Figure 72) and both are very low in intensity. There is a trace of the $Li_{0.184}Mg_{0.816}$ alloy left within the second recombination that wasn't found in the material after the first recombination. The presence of MgO is detected with peaks occurring at 2θ values of 43.02° and 61.43°, the remaining peaks found in Figure 73 are due to the presence of MgH_2.

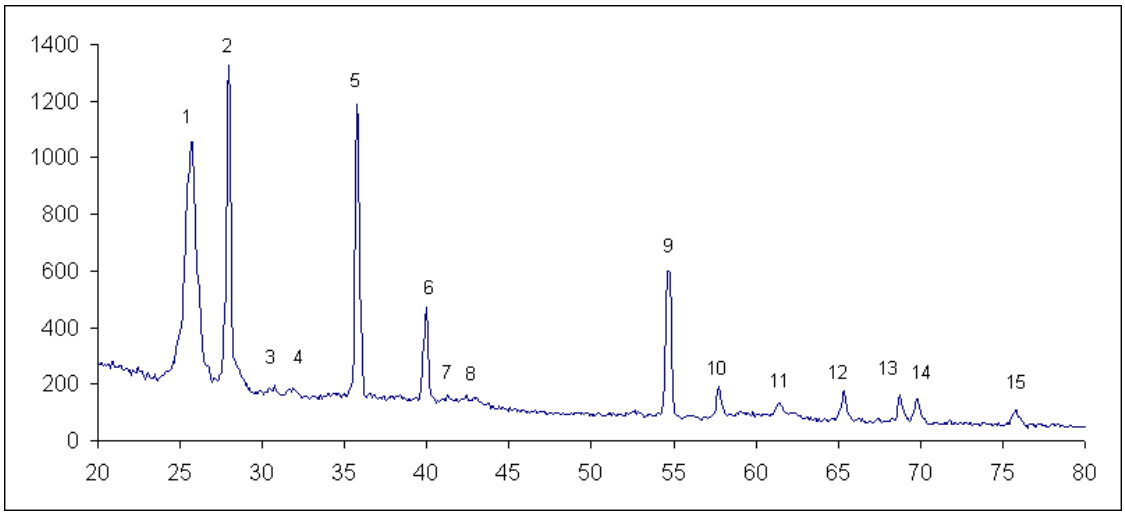

Figure 72) XRD analysis of recombined $LiBH_4$ + $5MgH_2$. The sample was dehydrogenated on the DSC under 3 bar(g) of Ar flowing at 100 ml / min while heating up to 450ºC. The sample was then recombined under 100 bar(g) of H_2 flowing at 100 ml / min while heating up to 450ºC. All heating was at 2ºC / min.

Peak number	2θ value	d Spacing (Å)	Assignment
1	25.76	3.46	Tape
2	27.99	3.19	MgH_2
3	30.65	2.92	MgH_2
4	31.82	2.81	γ – MgH_2
5	35.81	2.51	MgH_2
6	39.89	2.26	MgH_2
7	41.25	2.19	Unassigned
8	43.02	2.10	MgO
9	54.75	1.68	MgH_2
10	57.73	1.60	MgH_2
11	61.43	1.51	MgO
12	65.32	1.43	MgH_2
13	68.74	1.37	MgH_2
14	69.77	1.35	MgH_2
15	75.73	1.26	MgH_2

Table 36) XRD table for the first recombination of $LiBH_4$ + $5MgH_2$. The sample was dehydrogenated on the DSC under 3 bar(g) of Ar flowing at 100 ml / min while heating up to 450ºC. The sample was then recombined under 100 bar(g) of H_2 flowing at 100 ml / min while heating up to 450ºC. All heating was at 2ºC / min.

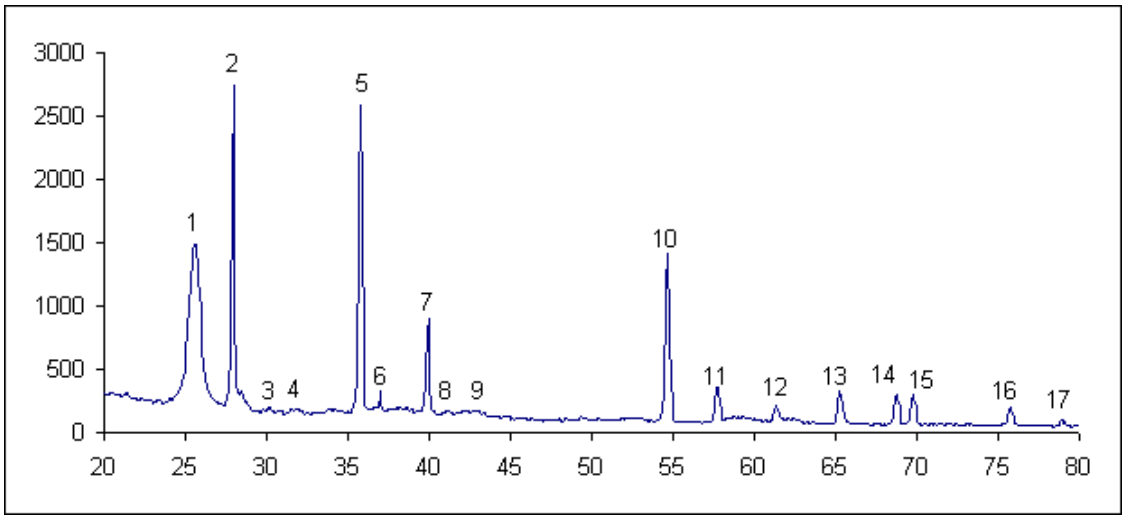

Figure 73) XRD analysis of twice cycled $LiBH_4$ + $5MgH_2$. The sample was dehydrogenated twice on the DSC under 3 bar(g) of Ar flowing at 100 ml / min up to 450ºC and recombined twice under 100 bar(g) of H_2 flowing at 100 ml / min up to 450ºC. All heating was at 2ºC / min.

Peak number	2θ value	d Spacing (Å)	Assignment
1	25.61	3.48	Tape
2	27.96	3.19	MgH_2
3	30.07	2.97	Unassigned
4	31.80	2.81	γ – MgH_2
5	35.79	2.51	MgH_2
6	36.96	2.43	$Li_{0.184}Mg_{0.816}$
7	39.93	2.26	MgH_2
8	41.15	2.19	Unassigned
9	42.91	2.11	MgO
10	54.63	1.68	MgH_2
11	57.67	1.60	MgH_2
12	61.34	1.51	MgO
13	65.27	1.43	MgH_2
14	68.67	1.37	MgH_2
15	69.73	1.35	MgH_2
16	75.70	1.26	MgH_2
17	78.88	1.21	Unassigned

Table 37) XRD table for the second recombination effort of $LiBH_4$ + $5MgH_2$. The sample was dehydrogenated twice on the DSC under 3 bar(g) of Ar flowing at 100 ml / min up to 450ºC and recombined twice under 100 bar(g) of H_2 flowing at 100 ml / min up to 450ºC. All heating was at 2ºC / min.

Although there are more unassigned peaks for the second recombination effort than there were for the first and the ~2450cm^{-1} observed in the FTIR spectra was more

prominent for the second recombination effort than the first (compare Figures 70 and 71) the low number of peaks and the lack of intensity makes them hard to assign with any certainty.

6. Conclusions

- The first conclusion which can be drawn is that the addition of MgH_2 to $LiBH_4$ does induce a reduction in the energy required to remove hydrogen from lithium borohydride. Zuttel recorded the amount of energy required for the removal of hydrogen from $LiBH_4$, and found that after it had been melted, 91.68 kJ / mol $LiBH_4$ was required to produce the decomposition products LiH, B and H_2 [55]. When used as part of a mixed hydride system with MgH_2, the enthalpy of dehydrogenation for $LiBH_4$ was reduced to approximately a fifth of this value for $2LiBH_4 + MgH_2$ indicating that the removal of hydrogen from $LiBH_4$ had been made easier with the presence of MgH_2.

1st Dehydrogenations	Pure MgH_2	Pure $LiBH_4$	$2LiBH_4 + MgH_2$	$LiBH_4 + 2MgH_2$	$LiBH_4 + 5MgH_2$
Phase Change (kJ / mol $LiBH_4$)	___	**4.18** [55]	**4.40**	**3.93**	**3.01**
Melting Point (kJ / mol $LiBH_4$)	___	**7.56** [55]	**6.72**	**4.83**	___
MgH_2 Dehydrogenation (kJ / mol H_2)	**65.91**	___	**14.98**	**31.58**	**47.78**
$LiBH_4$ Dehydrogenation (kJ / mol H_2)	___	**66.7** [41]	**11.59**	**6.92**	**3.18**
Total kJ / mol H_2	**65.91**	**66.7** [41]	**33.09**	**41.30**	**51.45**

Table 38) Summary of the average first dehydrogenation enthalpies

- The enthalpy of decomposition for MgH_2 increases with increased additions of MgH_2 suggesting that the hydrogen is more difficult to remove without the presence of $LiBH_4$. The last sample analysed ($LiBH_4$ + $5MgH_2$) produced a reaction enthalpy much closer to that found for pure MgH_2 than the other two samples. This would suggest that the small amount of $LiBH_4$ present within this sample does not have as much of an effect on the MgH_2 as it did for the previous two samples.

- From the TGA data it can be concluded that increased additions of MgH_2 past the $2LiBH_4$ + MgH_2 stoichiometry, results in a reduction for the onset of dehydrogenation from these mixed hydride systems. This indicates that the presence of $LiBH_4$ may be having an effect on the dehydrogenation mechanism of MgH_2 which loses its hydrogen first, however there is no explanation as to why reduced amounts of $LiBH_4$ appear to have a greater effect on reducing the onset temperature of decomposition.

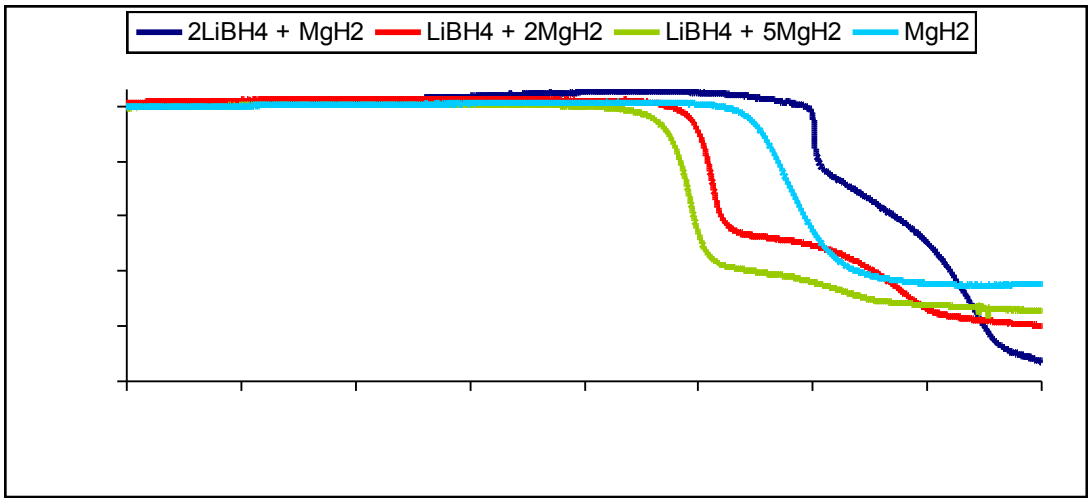

Figure 74) TGA data for pure MgH_2 and the first dehydrogenations of all samples studied. All dehydrogenations were carried out under 0.5 bar(g) of Ar flowing at 40 ml / min while heating to 450ºC / min at a rate of 2ºC / min.

- XRD analysis carried out during this work failed to reveal the presence of any LiH or MgB_2 in the dehydrogenation products of these mixed hydride systems. The reason these materials are not seen in the XRD patterns is because instead of forming these products the Li and Mg present preferentially form a $Li_{0.184}Mg_{0.816}$ instead. X. Yu et al. also failed to find any presence of LiH within their decomposition products of similar samples to the ones studied during this investigation and only found MgB_2 forming at temperatures above approximately 500ºC [45].

- A conclusion which can be drawn from the FTIR analysis of these samples is that a change to the internal bonding in one of the phases occurs somewhere between their first dehydrogenation and the following recombination attempt. This conclusion is made due to the presence of a peak previously unseen in the FTIR analysis of the starting materials, as milled samples or dehydrogenated samples and only appears after recombination attempts have taken place. From

the $LiBH_4$ + $5MgH_2$ sample it can also be concluded that the cause and intensity of this peak increases with successive cycling of the material.

- The molar ratios studied for these mixed hydride systems are reversible and recombination with hydrogen occurred best for the $LiBH_4$ + $2MgH_2$ samples. From the TGA data for the second dehydrogenations, twice as much hydrogen was obtained from the $LiBH_4$ + $2MgH_2$ sample when compared to the other molar ratios. Despite this sample releasing the most hydrogen after recombination, most of it came from the MgH_2 portion of the sample. The $LiBH_4$ component failed to fully recombine for all of the mixed hydride samples with $2LiBH_4$ + MgH_2 losing the most hydrogen from recombined $LiBH_4$ but still losing only a fraction of its potential storage capacity. From this it can be concluded that the reverse reaction of hydrogen with $LiBH_4$ is much harder to induce than the recombination of MgH_2.

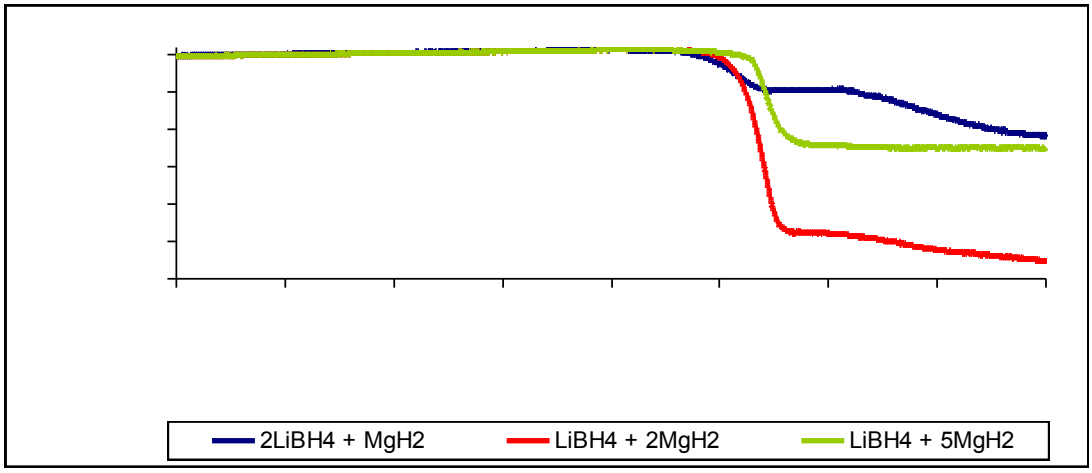

Figure 75) TGA data for the second dehydrogenations of all samples studied. Samples were dehydrogenated in the DSC under 3 bar(g) of Ar while heating to 450ºC. Samples were then recombined under 100 bar(g) of H_2 flowing at 100 ml / min while heating to 450ºC. After this samples were then dehydrogenated on the TGA using 0.5 bar(g) of Ar flowing at 40 ml / min whilst heating to 450ºC. All heating was at 2ºC / min.

7. Future Work

If a Li_xMg_{1-x} alloy is responsible for the destabilization of these mixed hydride systems under Ar, then studying the addition of lithium metal to magnesium hydride or the addition of magnesium to lithium borohydride may provide results which further our understanding of this system. Recombination of these, metal + hydride systems mentioned above may also provide further insight into the production of the IR peak at 2450 cm^{-1} which appears after the recombination of these mixed hydride systems. If the new IR peak appears after recombination for both the $2Li + MgH_2$ and the $Mg + 2LiBH_4$ system then it could be argued that the IR peak arises due to a bond between hydrogen and a new alloy formed between Li and Mg. If the newly formed IR peak only arises during the recombination attempt for $Mg + 2LiBH_4$ or $2Li + MgH_2$ then distortion of the bonding structure of either $LiBH_4$ or MgH_2 is a more likely explanation.

As the mixed hydride systems are dehydrogenating in two stages it would be interesting to do some work with a $LiBD_4 + MgH_2$ sample or even a $LiBH_4 + MgD_2$ sample so that mass spectrometry analysis of the dehydrogenation can exclusively conclude when exactly these individual materials are losing their hydrogen.

The addition of other metals besides Mg and other hydrides are of interest in terms of the destabilization of $LiBH_4$. Some theoretical work has been carried out using first principle calculations and highlights the potential of some materials for this purpose. Two such pieces of work were carried out by Sholl et al. and have indicated that CaH_2 and ScH_2 could be good for the destabilization of $LiBH_4$ [57], [58] It has been suggested that replacing the lithium cation of $LiBH_4$ with one that is less metallic, may reduce the ionic

character of the cation – borohydride bond ultimately weakening the B–H bonds and making dehydrogenation of this material some what easier [47] [48] [49].

From the cycling experiments it was found that the recombination conditions were not sufficient to fully reform the starting materials. It would therefore be beneficial to do more work on this aspect of the project to try and establish the optimum conditions for recombination attempts on these samples. It might be good to experiment with stoichiometries between $2LiBH_4 + MgH_2$ and $LiBH_4 + 2MgH_2$ for this purpose because $2LiBH_4 + MgH_2$ samples possessed the lowest enthalpy of reaction for dehydrogenation and $LiBH_4 + 2MgH_2$ possessed the best cycling properties for this type of mixed hydride system.

It would also be good to conduct some B-NMR analysis on these samples so as to try and identify any boron containing species which could confirm the presence of $B_{12}H_{12}^{2-}$. This could therefore confirm that the IR peak observed at ~2450 cm^{-1} are due to this complex.

8. References

1. International Energy Agency, *World energy outlook 2004*, pg 58 Also available at http://www.iea.org/textbase/nppdf/free/2004/weo2004.pdf

2. Mean central England Temperature Annual Anomalies, 1772 – Oct 2007, Hadley Centre for Climate Change. Available at http://www.metoffice.gov.uk/research/hadleycentre/obsdata/cet.html

3. R. Quadrelli and S. Peterson, *Energy Policy*, **35**, 2007, pg. 5938

4. G. Herbert, S. Iniyan, E. Sreevalsan and S. Rajapandian, *Renewable and Sustainable Energy Reviews*, **11**, 2007, pg. 1117

5. G. Ahmad and E. El Shenawy, *Renewable Energy*, **31**, 2006, pg. 1043

6. J. Falnes, *Marine Structures*, **20**, 2007, pg. 185

7. A. Zuttel and L. Schlapbach, *Nature*, **414**, 2001, pg. 353

8. A. Heinzel, B. Vogel and P. Hubner, *Journal of Power Sources*, **105**, 2002, pg. 207

9. Q. Ming, T. Healey, L. Allen and P. Irving, *Catalysis Today*, **77**, 2002, pg. 51

10. F. Barbir, *Solar Energy*, **78**, 2005, pg. 661

11. S. Goldstein, J. Borgard and X. Vitart, *International Journal of Hydrogen Energy*, **30**, 2005, pg. 619

12. A. Folkesson, C. Anderson, P. Alvfors, M. Alakulka and L. Overgaard, *Journal of Power Sources*, **118**, 2003, pg.349

13. J. Hwang, D. Wang, N. Shih, D. Lai and C. Chen, *Journal of Power Sources*, **133**, 2004, pg. 223

14. C. Wang, Z. Mao, F. Bao, X. Li and X. Xie, *International Journal of Hydrogen Energy*, **30**, 2005, pg. 1031

15. B. Smitha, S. Sridhar and A. Khan, *Journal of Membrane Science*, **259**, 2005, pg .10

16. D. Vallero, *Environmental Contaminants: Assessment and Control*, Academic Press, 2004, pg. 49

17. M. Al – Baghdadi, *Renewable Energy*, **28**, 2003, pg. 1471

18. A. Zuttel, *Materials Today*, **Sept. 2003**, pg. 24

19. A. Zuttel and L. Schlapbach, *Nature*, **414**, 2001, pg. 353

20. S. Satyapal, J. Petrovic, C. Read, G. Thomas and G. Ordaz, *Catalysis Today*, **120**, 2007, pg. 246

21. S. Lynch, *Acta Metallurgica*, **36**, 1988, pg. 2639

22. http://world.honda.com/factbook/auto/fcx/200212/10.html, viewed in July/2007

23. J. Wolf, *MRS Bulletin*, **27**, Sept. 2002, pg. 684

24. J. Zhang, T. Fisher, J. Gore, D. Hazra and P. Ramachandran, *International Journal Of Hydrogen Energy*, **31**, 2006, pg. 2292

25. B. Panella, M. Hirscher and S. Roth, *Carbon*, **43**, 2005, pg. 2209

26. H. Langmi, D. Book, A. Walton, S. Johnson, M. Al – Mamouri, J. Speight, P. Edwards, I. Harris and P. Anderson, *Journal of Alloys and Compounds*, **404 – 406**, 2005, pg. 637

27. B. Panella, M. Hirscher, H. Putter and U. Muller, *Advanced Functional Materials*, **16**, 2006, pg. 520

28. J. Rowsell, A. Millward, K. Park and O. Yaghi, *Journal of the American Chemical Society*, **126**, 2004, pg. 5666

29. A. Zuttel, P. Wenger, P. Sudan, P. Mauron and S. Orimo, *Materials Science and Engineering B*, **108**, 2004, pg. 9

30. J. Fernandez and C. Sanchez, *Journal of Alloys and Compunds*, **340**, 2002, pg. 189

31. J. Huot, G. Liang, S. Boily, A. Van Neste and R. Shulz, *Journal of Alloys and Compounds*, **293 – 295**, 1999, pg. 495

32. N. Hanada, T. Ichikawa, S. Hino and H. Fujii, *Journal of Alloys and Compounds*, **420**, 2006, pg. 46

33. G. Sandrock, *Journal of Alloys and Compounds*, **293 – 295**, 1999, pg. 877

34. M. Au and A. Jurgensen, *Journal of Physical Chemistry B*, **110**, 2006, pg 7062

35. M. Au, A. Jurgensen and K. Zeigler, *Journal of Physical Chemistry B*, **110**, 2006, pg. 26482

36. J. Vajo, S. Skeith and F. Mertens, *The Journal of Physical Chemistry B*, **109**, 2005, pg 3719

37. S. Orimo. Y. Nakamori, N. Ohba, K.Miwa, M. Aoki, S. Towata and A. Zuttel, *Applied Physics Letters*, **89**, 2006, 021920

38. J. Soulie, G. Renaudin, R. Cerny and K. Yvon, *Journal of Alloys and Compounds*, **346**, 2002, pg. 200

39. J. Reilly and R. Wiswall, *Inorganic Chemistry*, **6**, 1967, pg. 2220

40. Vajo, F. Mertens, C. Ahn, R. Bowman and B. Fultz, *Journal of Physical Chemistry B*, **108**, 2004, pg. 13977

41. J. Vajo and G. Olson, *Scripta Materialia*, **56**, 2007**,** pg. 829

42. J. Stampfer, C. Holley and J. Suttle, *Journal of the American Chemical Society*, **82**, 1960, pg. 3504

43. B. Bogdanovic, T. Hartwig and B. Spliethoff, *International Journal of Hydrogen Energy*, **18**, 1993, pg 575

44. U. Bosenberg, S. Doppiu, L. Mosegaard, G. Barkhordarian, N. Eigen, A. Borgschulte, T. Jensen, Y. Cerenius, O. Gutfleisch, T. Klassen, M. Dornheim and R. Bormann, *Acta Materialia,* **55**, 2007, pg. 3951

45. X. Yu, D. Grant and G. Walker, *Chemical Communications*, **2006**, pg. 3906

46. S. Johnson, P. Anderson, P. Edwards, I. Gameson, J. Prendergast, M. Al-Mamouri, D. Book, I. Harris, J. Speight and Allan Walton, *Chemical Communications*, **2005**, pg. 2823

47. K. Miwa, N. Ohba, S. Towata, Y. Nakamori and S. Orimo, *Physical Review B*, **69**, 2004, 245120

48. Y. Nakamori, K. Miwa, A. Ninomiya, H. Li, N. Ohba, S. Towata, A. Zuttel and S. Orimo, *Physical Review B*, **74**, 2006, 045126

49. H. Li, S. Orimo, Y. Nakamori, K. Miwa, N. Ohba, S. Towata and A. Zuttel, *Journal of Alloys and Compounds*, **446 – 447**, 2007, pg. 315

50. F. Gennari, F. Castro and G. Urretavizcaya, *Journal of Alloys and Compounds*, **321**, 2001, pg. 46

51. X. Wang and L. Andrews, *Journal of Physical Chemistry A*, **108**, 2004, pg. 11511

52. K. Harvey and N. McQuaker, *Canadian Journal of Chemistry*, **49**, 1971, pg. 3282

53. Fedneva, *Russian Journal of Inorganic Chemistry*, **9**, 1964, pg. 826

54. E. Jeon and Y. Cho, *Journal of Alloys and Compounds*, **422**, 2006, pg. 273

55. A. Zuttel, A. Borgschulte and S. Orimo, *Scripta Materialia*, **56**, 2007**,** pg. 823

56. E. Muetterties, R. Merriefield, H. Miller, W. Knoth and R. Downing, *Journal of the American Chemical Society*, **84**, 1962, pg. 2506

57. D. Sholl, J. Johnson and S. Alapati, *Journal of Physical Chemistry B*, **110**, 2006, pg. 8769

58. D. Sholl, J. Johnson and S. Alapati, *Journal of Alloys and Compounds*, **446 – 447**, 2007, pg. 23